Acta Pharmaceutica Sinica B 2025;15(9):4511−4542

Chinese Pharmaceutical Association
Institute of Materia Medica, Chinese Academy of Medical Sciences

Acta Pharmaceutica Sinica B

www.elsevier.com/locate/apsb
www.sciencedirect.com

REVIEW

Fibroblast activation protein targeting radiopharmaceuticals: From drug design to clinical translation

Yuxuan Wu[a,b,†], Xingkai Wang[a,†], Xiaona Sun[a,b,†], Xin Gao[a,†], Siqi Zhang[a], Jieting Shen[a], Hao Tian[a], Xueyao Chen[a], Hongyi Huang[a], Shuo Jiang[a], Boyang Zhang[a,b], Yingzi Zhang[f], Minzi Lu[a], Hailong Zhang[c], Zhicheng Sun[b], Ruping Liu[b,*], Hong Zhang[e,*], Ming-Rong Zhang[d,*], Kuan Hu[a,*], Rui Wang[a,c,*]

[a]*State Key Laboratory of Bioactive Substance and Function of Natural Medicines, Institute of Materia Medica, Chinese Academy of Medical Sciences & Peking Union Medical College, Beijing 100050, China*
[b]*School of Printing and Packaging Engineering, Beijing Institute of Graphic Communication, Beijing 102600, China*
[c]*Key Laboratory of Preclinical Study for New Drugs of Gansu Province, School of Basic Medical Sciences & Research Unit of Peptide Science, Chinese Academy of Medical Sciences, 2019RU066, Lanzhou University, Lanzhou 730000, China*
[d]*Department of Advanced Nuclear Medicine Sciences, Institute for Quantum Medical Science, National Institutes for Quantum Science and Technology, Chiba 263-8555, Japan*
[e]*Department of Nuclear Medicine and Positron Emission Tomography Center, The Second Affiliated Hospital of Zhejiang University School of Medicine, Hangzhou 310058, China*
[f]*Department of Orthopaedics, the Second Affiliated Hospital of Soochow University, Suzhou 215031, China*

Received 9 January 2025; received in revised form 20 March 2025; accepted 16 April 2025

KEY WORDS

Tumor microenvironment;
Fibroblast activation protein;

Abstract The activation proteins released by fibroblasts in the tumor microenvironment regulate tumor growth, migration, and treatment response, thereby influencing tumor progression and therapeutic outcomes. Owing to the proliferation and metastasis of tumors, fibroblast activation protein (FAP) is typically highly expressed in the tumor stroma, whereas it is nearly absent in adult normal tissues and

*Corresponding authors.
E-mail addresses: liuruping@bigc.edu.cn (Ruping Liu), hzhang21@zju.edu.cn (Hong Zhang), zhang.ming-rong@qst.go.jp (Ming-Rong Zhang), hukuan@imm.ac.cn (Kuan Hu), wangrui@lzu.edu.cn (Rui Wang).
†These authors made equal contributions to this work.
Peer review under the responsibility of Chinese Pharmaceutical Association and Institute of Materia Medica, Chinese Academy of Medical Sciences.

https://doi.org/10.1016/j.apsb.2025.07.009

Radiopharmaceutical;
Small molecule inhibitors;
Radiotheranostics;
Cancer-associated fibroblasts;
Radionuclide therapy;
Bench-to-bedside

benign lesions, making it an attractive target for precision medicine. Radiolabeled agents targeting FAP have the potential for targeted cancer diagnosis and therapy. This comprehensive review aims to describe the evolution of FAPI-based radiopharmaceuticals and their structural optimization. Within its scope, this review summarizes the advances in the use of radiolabeled small molecule inhibitors for tumor imaging and therapy as well as the modification strategies for FAPIs, combined with insights from structure−activity relationships and clinical studies, providing a valuable perspective for radiopharmaceutical clinical development and application.

1. Introduction

Tumors are heterogeneous diseases that benefit from the microenvironment[1]. They are not only clusters of abnormally proliferating cells in tissues or organs, but also heterogeneous collections of microenvironments[2,3]. The composition and characteristics of the tumor microenvironment (TME) vary significantly across different tumor types, yet hallmark features, including immune cells, stromal cells, blood vessels, and the extracellular matrix, remain constant[2]. There is a dynamic interplay and mutual dependency between cancer cells and the microenvironment[2,4−6]. Remodeling and degradation of the extracellular matrix facilitate cancer cell migration and invasion. Blood vessels provide oxygen to cancer cells, while cancer cells secrete angiogenic factors to promote angiogenesis. The TME is a unique environment for tumors that has a profound impact on tumor progression[7].

Cancer-associated fibroblasts (CAFs) constitute a subset of cells within the cancer microenvironment[8] that participate in cancer progression, including growth, migration, and invasion. The overexpression of fibroblast activation protein (FAP) is observed in more than 90% of epithelial cancers within their microenvironment[9−11], including pancreatic cancer, breast cancer, colorectal cancer, and high-grade glioblastoma[12−14]. The overexpression of FAP offers a promising and stable target for tumor imaging and therapy.

As a widely explored target, FAP has attracted attention for many years. A number of meaningful studies have been conducted by integrating positron emission tomography/computed tomography (PET/CT) imaging. Since the discovery of the pioneering lead compound UAMC-1110[15], research on FAP has flourished. In our previous work, we summarized the development of antibody and peptide-based radiopharmaceuticals targeting FAP[11], from the first FAP-targeting antibody ([^{131}I]mAbF19) in 1994 to the clinical application of FAP-2286, and discussed the advantages and pitfalls of antibody- and peptide-based radiopharmaceuticals targeting FAP from the perspective of clinical applications. To distinguish from reported reviews on FAPIs recently which have focused mainly on clinical applications (disease diagnosis and therapy)[8,16−18], this review takes an alternative aspect. Starting from the discovery of initial FAP inhibitors (FAPIs) and then labeling with multiple radionuclides, we emphasize the varied structures for optimizing the *in vivo* pharmacokinetic properties of FAPI radiopharmaceuticals. In addition, the mechanism of FAPIs is briefly introduced in terms of molecular interactions[19] and downstream signal regulations after binding with FAP[20] (Fig. 1). We provide a comprehensive overview of the discovery of a series of radionuclide-labeled FAP molecules, and summarize their structural features along with their clinical applications.

2. Lead compounds targeting FAP

Early works on the discovery of small molecules targeting FAP provided a fundamental core structure motif that is essential for bioactivity. Notably, Val-boro-Pro, also known as talabostat or PT-100 (**1**, Fig. 2), represents a pioneering advancement in the clinical application of FAP inhibition[21−23]. PT-100 exerts its bioactivity through interacting with bone marrow stromal cells, resulting in the upregulation of specific cytokine production in hematopoietic tissues, thereby promoting the growth and survival of hematopoietic cells[24−26]. In particular, PT-100 strongly inhibits and is specific for FAP, a key orchestrator of peptide bioactivity essential for sustaining cytokine production[27]. Investigations by Adams et al. revealed that while PT-100 exhibits no discernible effect on *in vitro* tumor growth, its oral administration in murine models significantly suppressed the progression of various tumors[27]. Clinical studies have corroborated the inhibitory potential of PT-100 across diverse tumor types (Table 1).

Despite substantial inhibitory effects of PT-100 on FAP, it simultaneously robustly inhibits DPP-IV, DPP8, and DPP9, which is attributed primarily to its dipeptidyl peptidase activity[22]. To increase selectivity toward FAP, Tran et al.[28] synthesized a series of *N*-acyl-Gly-, *N*-acyl-Sar-, and *N*-blocked-boroPro derivatives and systematically explored the structure−activity relationship to optimize selectivity for FAP. Compound **2** (Fig. 2) emerged as a prototypical molecule in this class, distinguished by its cyclic amide structure and potent inhibitory effect on FAP. In addition, Tsai et al.[29] undertook the challenge of developing selective FAPIs, culminating in the discovery of pyroglutamic acid-based FAPIs, marked by higher selectivity for FAP than other dipeptidyl peptidases. Notably, compound **3** (Fig. 2), featuring a fluorine substituent on the pyrrolidone ring, displayed superior targeting selectivity and bioactivity, with an impressive half maximal inhibitory concentration (IC_{50}) value of 0.022 μmol/L for FAP.

Since most reported FAPIs are boronic acid compounds, Ryabtsova et al. diverted their focus toward compounds bearing a carbonitrile warhead[21,28,30], which was recognized as a potent affinity enhancement moiety prevalent in reported inhibitors targeting DPP-IV, DPP8, DPP9, and prolyl oligopeptidase (PREP)[31]. They synthesized FAP-selective compounds based on the structure of *N*-acylated glycyl-(2-cyano) pyrrolidines, which displayed notable selectivity against DPP-IV, DPP9 and DPP-II. Among them, compounds **4**−**8** (Fig. 2) displayed exceptional targeting selectivity against FAP. In addition, they disclosed the effects of the *N*-acyl group and structural modification of the 2-cyanopyrrolidine residue. Notably, compound **5**, characterized by a 1-naphthoyl group, was the most effective inhibitor. The

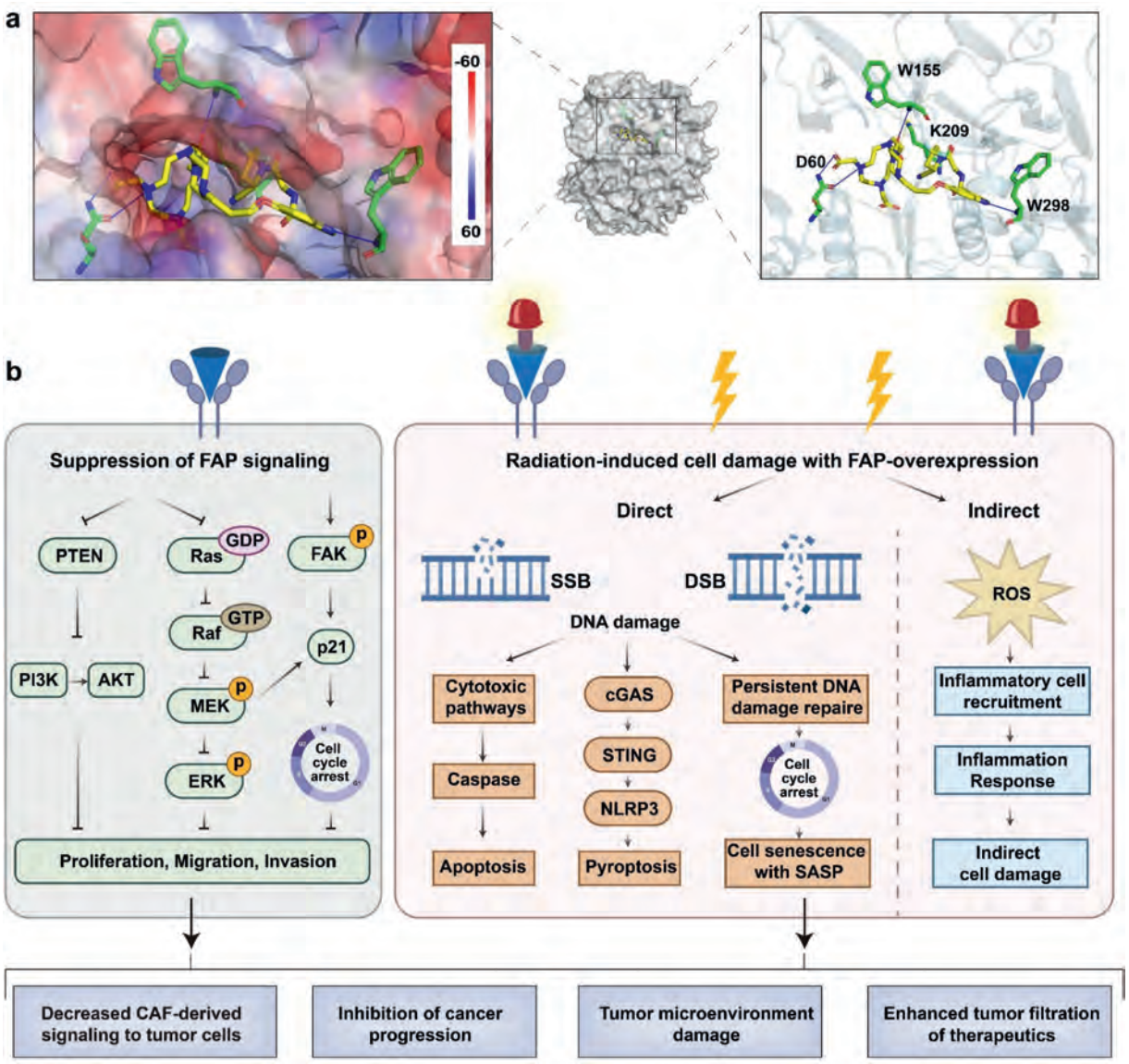

Figure 1 Molecular interactions and biological mechanisms of FAPIs bind with FAP. (A) Docking models of FAPI-04 with FAP (PDB: 1Z68). FAPI-04 serves as a representative FAPI, and the molecular docking is conducted in a similar binding pocket according to the reported literature[19]. Left: electrostatic potential surrounding the interface between FAPI-04 and FAP. Right: detailed interactions between FAPI-04 and FAP. FAPI-04 is shown in yellow, and FAP is shown in grey. The main possible interactions of FAPI-04 with FAP are highlighted with residues of D60, W155, K209, and W298 in the binding position. (B) The proposed biological mechanisms by which FAPIs targeted FAP. In the context of cancer treatment, the mechanisms involve two main pathways. First, FAPIs suppress FAP activity through downstream signaling pathways such as the PI3K/AKT, Ras/ERK, and FAK pathways, leading to the inhibition of tumor cell proliferation, migration, and invasion. Second, FAPI radiopharmaceuticals deliver radiation that directly induces cell damage by causing DNA damage, leading to mitochondrial apoptosis, pyroptosis *via* the STING−NLRP3 axis, and cancer cell senescence. Indirectly, radiation triggers the generation of reactive oxygen species (ROS), enhancing inflammatory responses that further damage cancer cells[20]. Overall, the antitumor effects of FAP targeting involve regulating signals from cancer-associated fibroblasts to tumor cells, inhibition of cancer progression, damaging the tumor microenvironment, and improving infiltration of therapeutic agents into tumors.

introduction of substituents at the 4-position of the (2-cyano) pyrrole alkyl compounds, exemplified by fluoridation inhibitors **6**−**8**, resulted in heightened inhibitory activity compared with that of compounds **4** and **5**, particularly in the presence of mono- or di-fluorinated substituents.

Because of the exopeptidase and endopeptidase activities of FAP, the identification of specific FAPIs concurrently targeting DPPs and PREP posed a formidable challenge[32,33]. Jansen et al.[34,35] used PT-100 and linagliptin (**9**, Fig. 2), an FDA-approved DPP-IV inhibitor exhibiting substantial FAP affinity, as reference compounds to design novel FAPIs. Their synthetic endeavors yielded an *N*-(4-quinolinoyl)-glycyl-(2-cyanopyrrolidine) scaffold, heralding the emergence of the first structure capable of achieving low nanomolar FAP affinity while manifesting a selectivity exceeding 10^3-fold for DPPs and prolyl PREP. Within the framework of structure−activity relationships,

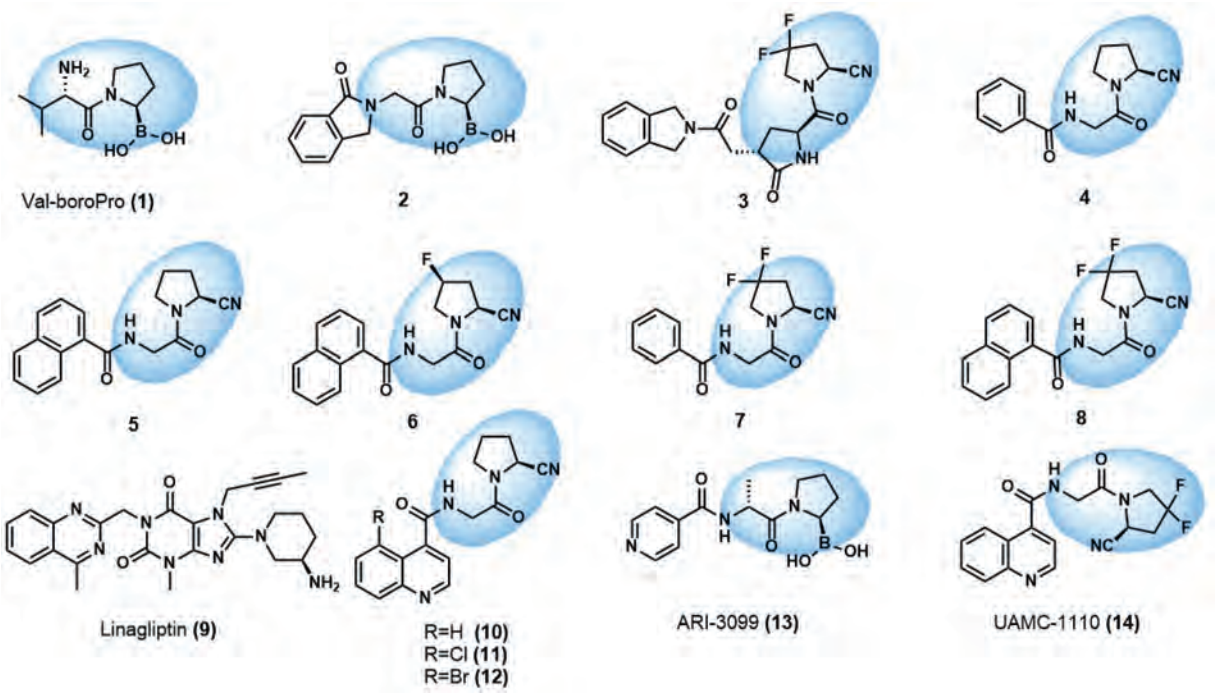

Figure 2 Molecular structures of lead FAPI compounds (blue: bioactive motif targeting FAP).

Table 1 Clinical trials of PT-100. PT100 has been used in treatment of various cancers, such as kidney cancer, lung cancer, brain tumors, and other advanced cancers. It is a pioneering FAPI for developing Val-boro-Pro based molecules. PT-100 has been investigated clinically for cancer therapy without labeling radionuclides despite its lower specificity in targeting FAP compared with its derivatives. However, the discovery of PT-100 inspired researchers to develop more potent FAPIs for targeted diagnosis and therapy for tumor. We summarized the applications and status of clinical studies of PT-100 for cancer therapy. Registration numbers are retrieved from www.clinicaltrials.gov.

Identifier	Phase	Tumor	Purpose	Status
NCT00489710	2	Kidney cancer	Treatment	Terminated for safety reasons
NCT00080080	2	Lung cancer	Treatment	Completed
NCT00116389	2	Pancreatic cancer	Treatment	Terminated (FDA hold May 2007)
NCT00303940	1	Brain tumors or other solid tumors	Treatment	Completed
NCT00290017	3	Non-small cell lung cancer	Treatment	Terminated (FDA hold May 2007)
NCT04171219	2	Advanced malignant solid cancers	Treatment	Not recruiting
NCT00083239	2	Melanoma	Treatment	Completed
NCT00083252	2	Melanoma	Treatment	Completed
NCT00086203	2	Chronic lymphocytic leukemia	Treatment	Completed
NCT00243204	3	Non-small cell lung cancer	Treatment	Terminated (FDA hold May 2007)

the *N*-(4-quinolinoyl) moiety plays a pivotal role in binding affinity with FAP. Compound **10** (Fig. 2), which features this moiety, surpassed compound 5 in terms of FAP affinity[30]. Notably, the introduction of substituents at the 5-position of the quinoline ring with chlorine or bromine resulted in compounds **11** and **12** (Fig. 2), which exerted a minimal effect on FAP binding affinity but maximized selectivity for PREP. In addition, inspired by electrophile-bearing drugs that target serine or threonine proteases available on the pharmaceutical market, Poplawski et al.[36] synthesized ARI-3099 (**13**, Fig. 2), which was characterized by the *N*-(pyridine-4-carbonyl)-D-Ala-boro-Pro motif and demonstrated high selectivity for FAP against both DPPs and PREP.

In 2014, Jansen et al.[15] used compounds **1**, **3**, **9**, **10**, **12**, and **13** as reference compounds to explore the affinity and selectivity of the active structural group of 4-quinolinoyl-Gly-cyanoPro. These findings elucidated that the incorporation of either 4*S*-fluoro or 4,4-difluoro substitutions within the 2-cyanopyrrolidine ring effectively optimized FAP affinity. However, the affinity of FAP was significantly reduced or entirely lost once the motif of glycine or amide bonds was changed. Through kinetic and mechanistic investigations, UAMC-1110 (**14**, Fig. 2) emerged as the most promising FAPI within the spectrum of compounds assessed, distinguished by its prolonged *in vivo* half-life.

In this section, lead compounds are introduced. PT-100, which is characterized by a Val-boro-Pro motif, plays a significant role in FAPIs development. Through structural−activity relationship studies, novel FAPIs with high binding affinity and specificity were designed and evaluated. By replacing boronic acid with a cyan group and then introducing fluorine and quinoline groups, UAMC-1110 was developed and has high biological activity and

proper pharmacokinetics, which offers profound significance for radiopharmaceuticals that target FAP.

3. Radiolabeled small molecule FAPIs

On the basis of the structure of UAMC-1110, FAPIs are modified on the quinoline side chain and then conjugated with DOTA, NOTA or other chelators for radionuclide labeling. Radiopharmaceuticals are faced with unprecedented opportunities for deciphering clinical challenges in disease diagnosis and therapy and demonstrating great potential in clinical translations[37−40]. Multiple targets, such as PD-L1 and $\alpha_5\beta_1$, have been proven effective in tumor imaging[41−44]. FAP is overexpressed in tumor tissue and is an ideal target for radiotheranostics. In this section, we introduce the development of radiolabeled FAPIs with proper chemical modifications of linkers, chelators, multimerizations, and heterodimerizations. In addition, the biodistributions and pharmacokinetics of modified FAPIs are included as summarized in Table 2[45−75].

3.1. FAPIs with varied linkers

As a hallmark of cancer imaging, FAP targeted radiopharmaceuticals outperform conventional tracers (such as [^{18}F]FDG)[76]. To develop effective radiolabeled FAPIs, modifications conducted on linkers have been demonstrated promising methods. In 2018, Loktev et al.[45] refined quinoline-based FAPIs, yielding radioiodine-labeled FAPI-01 (**15**, Fig. 3). The synthesis of FAPI-01 involved a bromine/lithium exchange on 5-bromoquinoline 4-carboxylic acid using the palladium-catalyzed bromine/tin exchange method. In parallel, the synthesis of FAPI-02 (**16**, Fig. 3) was conducted in a well-orchestrated five-step process, and DOTA was incorporated into the foundational FAPI scaffold. This modification strategy facilitated subsequent radiolabeling through the introduction of radioactive metals. Notably, experimental evidence underscored the susceptibility of [^{125}I]FAPI-01 to deiodinase-induced loss of inhibitory activity. To circumvent this challenge, the non-halogenated derivative FAPI-02 emerged, with its FAP-binding moiety thoughtfully coupled with DOTA. This ingenious design not only enhanced the stability but also extended the potential applications of FAPI-02 as both a diagnostic and therapeutic agent. The specificity, tumor uptake characteristics, and minimal background activity of FAPI-02 were validated through PET/CT imaging in xenograft mouse models. In a case involving locally advanced lung adenocarcinoma, comparisons with the widely employed clinical radiotracer [^{18}F]FDG revealed that [^{68}Ga]FAPI-02 provided superior imaging contrast, accompanied by increased uptake in metastatic lesions, which collectively enhanced contrast and lesion visibility. This comparative assay demonstrated that FAPI-02 possesses an exceptional potential for precise FAP targeting, making it a formidable tool for rapid, high-contrast imaging within mesenchyme-rich tumor environments.

Nevertheless, the therapeutic potential of FAPI-02 may be constrained by its limited retention time in tumors. In response, Lindner et al. designed 13 new FAPIs to investigate potential therapeutic applications[46]. Within this distinguished cohort, FAPI-04 (**17**, Fig. 3) was identified as the most valuable tracer for clinical conversion. FAPI-04, distinguished by its 4,4-difluoroproline structure, exhibited enhanced stability, heightened affinity, and a more deliberate *in vitro* tracer excretion profile. Subsequent PET imaging in mice and patients revealed the elevated uptake and extended retention of FAPI-04 within tumor sites. Remarkably, PET/CT imaging conducted on two patients with metastatic breast cancer confirmed the rapid accumulation of [^{68}Ga]FAPI-04 in the metastatic lesions and its clearance from the bloodstream, primarily through the kidney. Moreover, these patients were treated with [^{90}Y]FAPI-04, resulting in alleviated pain symptoms, and a noteworthy absence of adverse effects was observed, particularly in terms of hematotoxicity.

Comparative studies involving FAPI-04 juxtaposed against alternative tracers have further contributed to a deeper comprehension. In a preliminary dosimetric evaluation, Giesel et al.[76] compared [^{68}Ga]FAPI-02 and [^{68}Ga]FAPI-04. This inquiry involved the examination of two patients at different intervals after tracer injection. It was determined that tumor uptake exhibited a greater decrease for [^{68}Ga]FAPI-02 at 1−3 h after injection. However, both tracers resulted in similar tumor-to-background ratios at 1 h after injection (Fig. 4A). In addition, a comparison of tumor uptake between [^{18}F]FDG and [^{68}Ga]FAPI-02 revealed a noteworthy finding: the mean standardized uptake value maximum (SUV_{max}) for [^{68}Ga]FAPI-02 in the brain, liver, and oral/pharyngeal mucosa was significantly lower than that for [^{18}F]FDG. This disparity enhances imaging contrast within the context of pancreatic cancer and colorectal cancer liver metastases while improving the delineation of esophageal cancer. In the case of all other organs, no substantial differences were observed.

FAPI-04 has been subjected to examination across diverse tumor types. In a study conducted by Kratochwil et al.[77] [^{68}Ga]FAPI-04 was administered to 80 cancer patients, allowing for the quantitative assessment of tracer uptake across various tumor categories, thereby shedding light on potential future indications. PET imaging showed that patients with sarcoma, esophageal cancer, breast cancer, and cholangiocarcinoma presented the highest tumor uptake, with an average SUV_{max} greater than 12 at 1 h post-injection. These findings provided invaluable insights into the detection and treatment of tumors characterized by increased tracer uptake. In addition to investigations into tumor uptake, other researchers had investigated the diagnostic accuracy and temporal sensitivity of FAPI-04. Chen et al.[78] compared [^{68}Ga]FAPI-04 with [^{18}F]FDG PET/CT in 75 patients, which represented diverse cancer types. The results revealed that [^{68}Ga]FAPI-04 was more sensitive and precise than [^{18}F]FDG in detecting primary and metastatic lesions (Fig. 4B). However, [^{68}Ga]FAPI-04 PET had a greater number of false positives, which made it less specific for detecting metastatic lesions. Additionally, Ding et al.[79] assessed the potential of these two tracers in the early-stage diagnosis of tumor metastasis. PET imaging of tumor-bearing mice revealed the increased sensitivity of [^{68}Ga]FAPI-04 and its increased uptake in lung and lymph node metastases, facilitating early-stage detection of lung and lymph node metastases in the cancer milieu.

Furthermore, researchers have investigated the radiolabeling of FAPI-04 with different radionuclides. Watabe et al.[80] performed a series of experiments involving the radiolabeling of FAPI-04 with ^{64}Cu and ^{225}Ac, which have long half-lives. These radiolabeled tracers were subsequently administered to mice for PET scans and the results of these investigations showed similar physiological accumulation patterns, characterized by notable accumulation in the liver and kidneys. Specifically, [^{64}Cu]FAPI-04 exhibited rapid renal clearance and a gradual tumor washout profile. Notably, compared with [^{68}Ga]FAPI-04, [^{64}Cu]FAPI-04 displayed enhanced accumulation in both tumor and normal organ tissues and reduced urinary excretion. In addition, [^{225}Ac]FAPI-04

Table 2 Categories of small molecule FAPIs. According to our research, FAP-targeting radiopharmaceuticals have achieved great success in tumor imaging and therapy. To optimize tumor uptake and *in vivo* biodistributions, novel chemical modifications have been introduced. Researchers have reported multiple radiopharmaceuticals based on modified linkers, chelators, and FAP-multimers with quinoline-Val-boro-Pro motif. The preclinical properties (such as bioactivity, *in vivo* tumor uptake and clearance patterns) of reported radiopharmaceuticals are listed here.

Category	Name, year	IC_{50}	Tumor model	Tumor uptake, Time	Clearance pattern	Advantage	Ref.
FAPIs with varied linkers	[^{68}Ga]FAPI-02, 2018	21.0 nmol/L	HT-1080-FAP	4.7[b], 2 h	Rapid clearance from the bloodstream and elimination primarily *via* the kidney.	Fast imaging.	45
	[^{68}Ga]FAPI-04, 2018	6.5 nmol/L (EC_{50})	HT-1080-FAP	1.2[a], 1 h	Rapid clearance from the bloodstream and elimination primarily *via* the kidney.	Rapid and high tumor uptake.	46
	[^{177}Lu]FAPI-46, 2022	−	HT-1080-FAP	12.35 ± 6.25[b], 1 h	Rapid clearance by the kidneys.	High accumulation in the tumor.	47
	[^{68}Ga]DOTA.SA.FAPi, 2021	0.8−1.4 nmol/L	HT-29	0.75 ± 0.09[a], 1 h	A slightly higher accumulation at the bones and small intestine	Improved pharmacology.	48
	[^{177}Lu]OncoFAP-DOTAGA, 2022	−	SK-RC52.hFAP	>30, 1 h	Fast wash out from blood and kidneys.	Excellent tumor-to-organ ratios.	49
	[^{111}In]QCP02, 2021	16.20 nmol/L (K_i)	U87	18.16 ± 11.67[b], 30 min	Clearance through the gastrointestinal tract.	Favorable PK and biodistribution.	50
	[^{68}Ga]FAPtp, 2021	1.20 nmol/L	U87MG	1[a], 10 min	Excreted mainly by the liver.	Higher tumor contrast imaging than [^{68}Ga]FAPI-04.	51
	[^{18}F]AlF−P-FAPI, 2022	0.073 nmol/L (K_d)	A549-FAP	7.0 ± 1.0[b], 1 h	Predominant liver excretion and non-specific uptake in the gallbladder and intestine.	High tumor uptake and retention.	52
FAPIs with different chelators	[^{18}F]FGlc-FAPI, 2020	167 ± 110 nmol/L	HT1080-FAP	4.6[b], 10 min	Pronounced uptake in the liver and intestine, suggesting a hepatobiliary elimination pathway.	High uptake in tumor.	53
	[^{18}F]AlF-FAPI-74, 2021	4.2 nmol/L (EC_{50})	HT-1080-FAP	1.91[a], 57 min	Rapidly clearance and elimination predominantly *via* the kidney.	Excellent early time point imaging.	54
	[^{18}F]AlF-NOTA-FAPI, 2021	1.73 ± 0.93 nmol/L	A549 U87MG	0.87[a], 1 h 3.53[a], 1h	Rapid clearance through the kidney and the highest uptake was observed in the gallbladder at 1 h post-injection.	Excellent imaging quality and tumor detection efficacy.	55
	[^{18}F]AlF-NOTA-FAPI-04, 2022	−	U87MG	15.48 ± 1.82[b], 1 h	Rapid clearance through the kidney, with extremely low uptake in most normal organs.	Fast imaging.	56
Albumin binder conjugated FAPIs	[^{68}Ga]Alb-FAPtp-01, 2021	25.80 nmol/L	U87MG	1.775 ± 0.179[a], 1 h	Much faster washout rate in kidney and liver than that of [^{68}Ga]FAPI-04.	Prominent tumor uptake.	51,57
	[^{68}Ga]/[^{177}Lu]RPS-309, 2021	7.3 ± 1.4 nmol/L	SW872	5.0 ± 0.3[b], 3 h	Significant clearance from all normal tissues except liver and stomach.	High affinity targeting FAP.	58
	[^{177}Lu]TEFAPI-06, 2022	10.16 ± 2.56 nmol/L	Pancreatic cancer PDX	4.8 ± 0.6[b], 4 h	Clear slowly from kidney.	Prolonged tumor retention.	59
	[^{177}Lu]TEFAPI-07, 2022	7.81 ± 2.28 nmol/L	Pancreatic cancer PDX	7.87 ± 2.08[b], 24 h	No obvious clearance of TEFAPI-07 from the kidneys over time.		59
	[^{177}Lu]EB-FAPI-B1, 2022	16.5 nmol/L	U87MG	12.42 ± 1.54[b], 96 h	Eliminated mainly through the kidney.	Enhanced tumor uptake and retention.	60

	[^{68}Ga]FSDD$_0$I, 2022	14.21 ± 11.55 nmol/L	HCC-PDX	18.50 ± 0.50[b], 4 h	Accumulated in the blood, muscle, liver, and kidneys.	Improved tumor uptake and retention.	61
	[^{177}Lu]TE-FAPI-03, 2022	34.89 ± 5.02 nmol/L	HT-1080-FAP	2.84 ± 1.19[b], 24 h	Fast elimination mainly through the liver, and kidneys.	Enhanced tumor uptake and retention.	62
	[^{177}Lu]TE-FAPI-04, 2022	9.43 ± 0.93 nmol/L	HT-1080-FAP	3.86 ± 1.15[b], 24 h			
	[^{86}Y]FAPI-C16, 2022	5.06 ± 0.69 nmol/L	HT-1080-FAP	0.91 ± 0.04[a], 12 h	Mainly enriched in the heart and blood vessels, resulting in the much slower clearing out than [^{86}Y]FAPI-C12.	Higher tumor uptake.	63
FAPI multimers	[^{68}Ga]DOTA-2P(FAPI)$_2$, 2022	–	HCC-PDX	8.97 ± 0.32[b], 1 h	High initial kidney uptake and rapid renal clearance.	High tumor uptake and long retention time.	64
	[^{99m}Tc][Tc−(CN−C$_5$-FAPI)$_6$]$^+$, 2022	2.01 ± 0.53 nmol/L (Kd)	U87MG	1.85 ± 0.88[b], 4 h	Elimination by the liver, kidneys and bladder.	High tumor uptake and tumor/organ ratio.	65
	[^{99m}Tc][Tc−(CN−PEG$_4$-FAPI)$_6$]$^+$, 2022	3.90 ± 0.65 nmol/L (Kd)	U87MG	11.02 ± 1.59[b], 4 h		Specifically binds to FAP.	65
	[^{177}Lu]ND-bisFAP, 2022	0.25 ± 0.05 nmol/L	A549-FAP	32.6 ± 3.1[b], 24 h	Rapid clearance from the kidney leading to high-quality PET images.	High tumor uptake and retention time.	66
Heterodimer of FAPIs	[^{18}F]AlF-PSMA-FAPI-01, 2022	1.7 nmol/L	A549-FAP	6.40 ± 0.32[b], 1 h	Rapid clearance from non-target organs *via* the kidneys.	High tumor uptake.	67,68
	[^{18}F]AlF-PSMA-FAPI-02, 2022	5.8 nmol/L	A549-FAP	6.47 ± 0.76[b], 1 h			
	[^{64}Cu]FP-L1, 2022	0.31 nmol/L (Ki)	U87	23.84 ± 3.46[b], 4 h	Low pancreatic uptake and high renal uptake.	High and specific binding affinities targetin both FAP and PSMA.	69
	[^{68}Ga]FAPI-RGD, 2022	–	Panc02	6.16 ± 0.46[b], 30 min	The physiological biodistribution of [^{68}Ga]FAPI-RGD involved the thyroid glands, salivary glands, pancreas, kidneys, liver, heart content, spleen, and urinary bladder.	Improved tumor uptake and retention time.	70
Other FAPIs	FL-L3-^{99m}Tc, 2020	10.5 nmol/L (Kd)	MDA-MB231	2.23[b], 2 h	Metabolized mainly by the kidney.	Enabled facile detection of tumor xenografts with little off-target uptake.	71
	[^{68}Ga]MHLL1, 2021	212 nmol/L (hFAP)	MI	1.3 ± 0.4[b], 21 day	Rapid clearance from blood and wash out mainly through the kidney.	Imaging the MI area.	72
	[^{131}I]FAPI-02, 2021	142 nmol/L (mFAP)	U87MG	4.78 ± 1.34[b], 30 min	Mainly excreted through the kidneys as well as the hepatobiliary pathway.	Higher accumulation, longer dwell time, and increased tumor-to-organ ratios.	73
	[^{131}I]FAPI-04, 2021	12.8 nmol/L	U87MG	6.16 ± 1.21[b], 30 min			
	[^{99m}Tc]iFAP, 2022	–	Hep-G2	7.05 ± 1.13[b], 30 min	Rapid renal elimination.	High tumor uptake and fast kidney elimination.	74
	[^{11}C]RJ1101, 2022	–	U87MG	1.34 ± 0.10[b], 30 min	Significant hepatobiliary excretion	High specific tumor uptake.	75
	[^{11}C]RJ1102, 2022	–	U87MG	1.71 ± 0.08[b], 30 min			

[a]Tumor uptake evaluation presented by SUV.
[b]Tumor uptake evaluation presented by %ID/g.

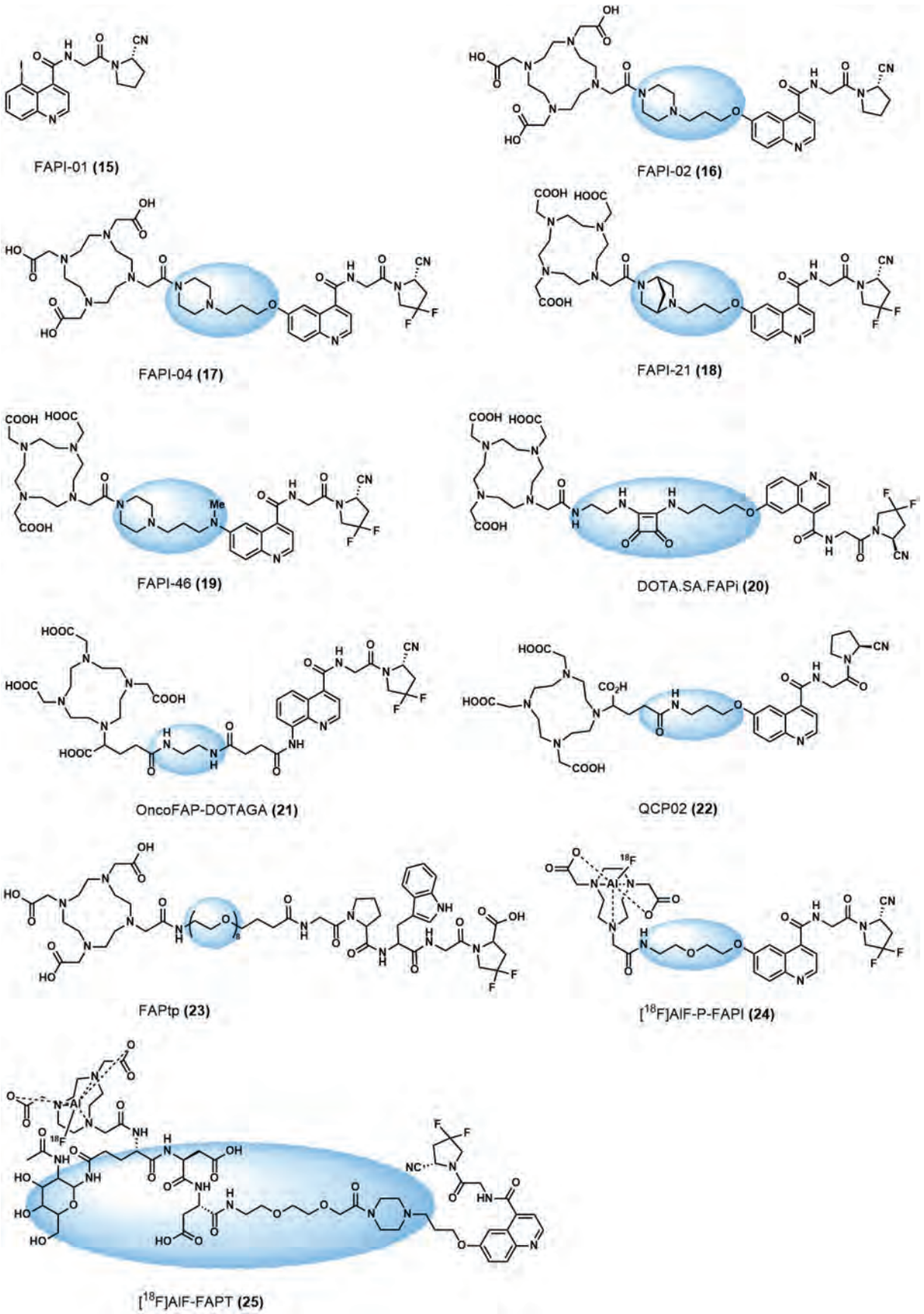

Figure 3 Chemical structures of FAPIs with various linkers (blue: various functional linkers used for radiolabeling or optimizing *in vivo* pharmacokinetic properties).

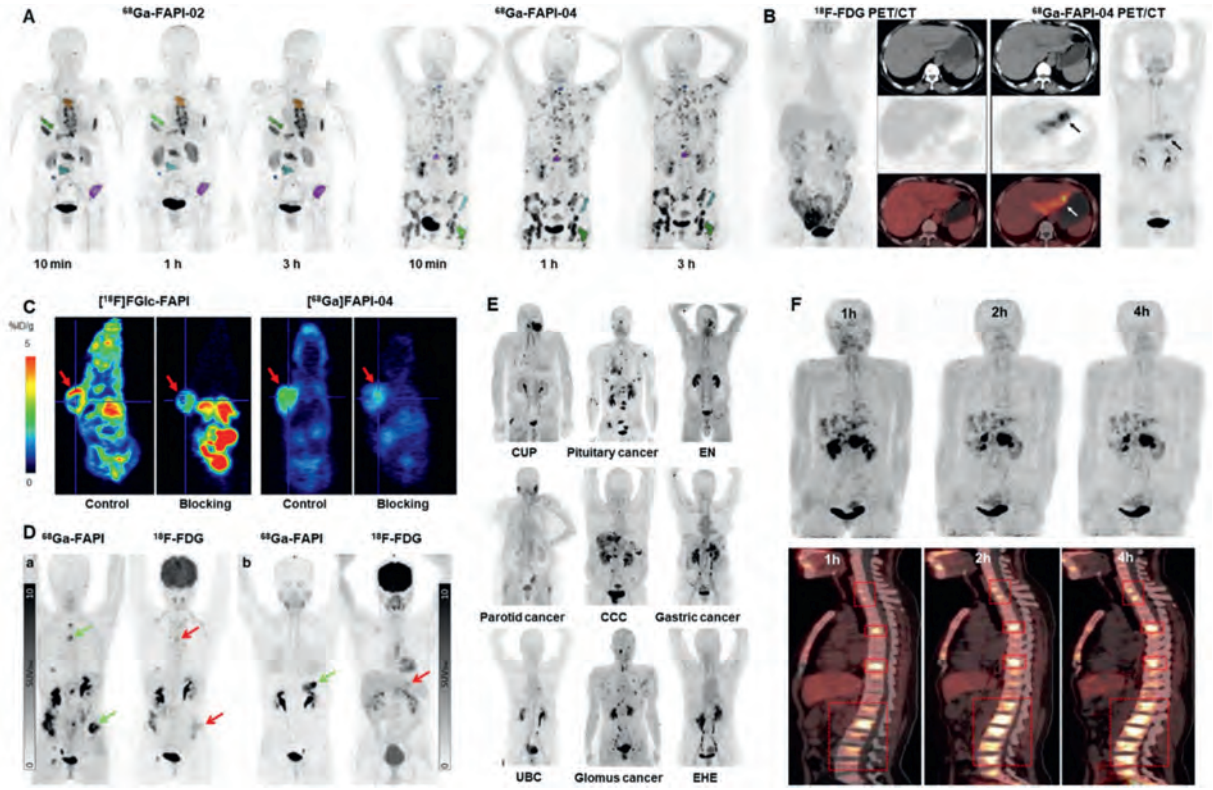

Figure 4 PET/CT comparisons of different FAPIs used in preclinical and clinical studies. (A) Comparison of PET imaging between [^{68}Ga]FAPI-02 and [^{68}Ga]FAPI-04 in patients at various time points. Reproduced with permission from Ref. 76. Copyright © 2019 SNMMI. (B) Comparison of [^{18}F]FDG and [^{68}Ga]FAPI-04 PET/CT *in vivo*. Left: [^{18}F]FDG PET/CT revealed no tumor. Right: [^{68}Ga]FAPI-04 PET/CT clearly revealed the position of tumor. Reprinted with the permission from Ref. 78. Copyright © 2020 Springer Nature. (C) PET images of HT1080hFAP xenografts generated *via* [^{18}F]FGlc-FAPI and [^{68}Ga]FAPI-04. Reprinted with the permission from Ref. 125. Copyright © 2020 SNMMI. (D) PET/CT images of [^{68}Ga]FAPI and [^{18}F]FDG in ovarian cancer (a) and pancreatic cancer (b) patients, with the tumors indicated in green ([^{68}Ga]FAPI) and red ([^{18}F]FDG). Reprinted with the permission from Ref. 161. Copyright © 2021 Springer Nature. (E) PET/CT images of [^{68}Ga]FAPI in nine different rare malignancies (CUP = Cancer of unknown primary, EN = Esthesioneuroblastoma, CCC = Cholangiocarcinoma, UBC = Urinary bladder cancer, EHE = Epithelioid hemangioendothelioma). Reprinted with the permission from Ref. 162. Copyright © 2022 Springer Nature. (F) PET/CT images of [^{18}F]AlF-NOTA-FAPI-04 in cancer patients. Reprinted with the permission from Ref. 56. Copyright © 2022 Springer Nature.

substantially inhibited tumor growth in xenografted human pancreatic tumor-bearing mice. These findings support the potential utility of these two radiotracers in pancreatic cancer therapy, particularly in cases characterized by FAP overexpression.

Among FAPI-based radiopharmaceuticals, FAPI-04 exhibited high uptake in FAP-positive tumors in clinical settings[80–82]. To improve its therapeutic efficacy, increase tracer uptake in tumors, and prolong intratumoral retention, Loktev et al.[10] synthesized 15 novel FAPIs by modifying the structure of the quinoline moiety and the linker region between the quinoline and the chelator. All of these new compounds exhibited higher affinities for FAP, with binding affinities similar to or greater than those of FAPI-04. Based on the results of the *in vitro* experiments, ten compounds were selected for PET imaging in mice. These studies showed that all compounds rapidly accumulated in the tumors and were primarily excreted *via* the kidneys. Remarkably, FAPI-21 and FAPI-46 (**18** and **19**, Fig. 3) showed even greater tumor uptake than FAPI-04, leading to significantly higher tumor-to-normal ratios. Therefore, these two tracers were selected for initial diagnostic applications in the clinical setting. Subsequent PET/CT imaging confirmed their ability to accumulate rapidly in both primary and metastatic tumors while exhibiting low uptake in normal tissues, with predominant renal excretion. Notably, contrasted with FAPI-21, FAPI-46 demonstrated superior suitability as a therapeutic agent in clinical studies because of its lower uptake in normal tissues and superior tumor uptake (Table 2).

Additionally, the optimal timing for FAPI-based imaging remains under investigation. Ferdinandus et al.[83] conducted a comprehensive review of FAPI-46, which systematically investigated its utility in early- and late-stage imaging among a diverse cohort of cancer patients. This study included 69 patients who underwent imaging at two different time points, resulting in the detection of a total of 400 lesions, with an almost equiprobable distribution between early and late detection cases. Nevertheless, two lesions were exclusively identified at the early time-point imaging. In addition, a reduction in inflammatory uptake from the early to late imaging stages endowed this temporal disparity with the potential to discriminate between inflammatory and malignant uptake. Compared with late-stage imaging, early-stage imaging featured streamlined procedures, increased scan volumes, and reduced waiting time and proved feasible for clinical implementation. Furthermore, FAPI-46 labeled with different radionuclides had been studied. Liu et al.[47] evaluated the efficacy of α-based therapy [^{225}Ac]FAPI-46 and β-based therapy [^{177}Lu]

FAPI-46 in pancreatic cancer models. The results displayed a dose-dependent increase in tumor inhibition in both groups. While [^{177}Lu]FAPI-46 exhibited a comparatively prolonged therapeutic response, [^{225}Ac]FAPI-46 displayed a more rapid onset of therapeutic effects. In conclusion, radiotracers hold promise as potential therapeutic modalities for treating pancreatic cancer. However, future research efforts are essential to determine the optimal radionuclide for prospective therapeutic applications.

Following the success of UAMC-1110, a novel FAP-targeted radiopharmaceutical, DOTA.SA.FAPi (**20**, Fig. 3), was synthesized by Moon et al.[84] using DOTA as a chelator and square amide (SA) as a linker. SA, a cyclic aromatic diacid, constitutes the backbone of the linker structure, forming the essential squaramide moiety[85−89]. The incorporation of SA into the chelator and target vector was achieved *via* a straightforward chemical process, which imparted favorable pharmacological properties to the resulting compounds[86,90−92]. Notably, previous studies on SA-containing inhibitors, particularly those targeting prostate-specific membrane antigen (PSMA), have demonstrated high tumor uptake and commendable *in vivo* kinetics[93−95]. DOTA.SA.FAPi displayed remarkable inhibitory potency against FAP, exhibiting a low nanomolar affinity akin to that of UAMC-1110. This underscored the notion that the introduction of additional structural elements in the quinoline ring did not compromise its FAP-targeting affinity. Furthermore, [^{68}Ga]DOTA.SA.FAPi demonstrated exceptional stability, resisting transmetallation and transchelation processes. Subsequent PET/CT imaging validated its ability to achieve rapid accumulation in tumors while maintaining minimal uptake in normal tissues[84]. The tracer was primarily cleared through the kidneys. Notably, compared with FAPI-04 in multiple tumor models, consistent results were observed despite variations in experimental series and tumor models[80].

Interestingly, a comparative analysis conducted by Ballal et al.[48] included [^{68}Ga]DOTA.SA.FAPi and [^{18}F]FDG PET/CT scans in 54 patients representing 14 different cancer types. This investigation revealed the consistent uptake of [^{68}Ga]DOTA.SA.FAPi, coupled with rapid clearance from normal organs. Of particular note, [^{68}Ga]DOTA.SA.FAPi exhibited distinctive behavior in scenarios involving brain metastases, lung nodules, and lymph nodes, presenting minimal uptake within normal brain parenchyma, thereby enhancing its diagnostic utility for conditions that are not clearly detectable by [^{18}F]FDG.

Additionally, Millul et al.[96] introduced OncoFAP, a novel FAP-specific ligand with a submillimolar-level affinity for human FAP. The chemical structure of OncoFAP incorporated a carboxylic acid segment that facilitates conjugation with various payloads through amide coupling. Radiolabeling with ^{177}Lu led to the synthesis of OncoFAP-DOTAGA (**21**, Fig. 3), which was evaluated for its tumor-targeting capabilities in mice. The results showed the selective accumulation of [^{177}Lu]OncoFAP-DOTAGA in FAP-positive tumors, with uptake increasing proportionally to the injection dose until it reached saturation above 500 nmol/kg.

Notably, the versatility of OncoFAP-DOTAGA had versatility extended to radiolabeling with ^{68}Ga. Backhaus et al.[49] synthesized and assessed [^{68}Ga]OncoFAP, revealing its compelling affinity (IC_{50} = 0.51 ± 0.11 nmol/L) for FAP, low lipophilicity, and excellent stability. In comparison with [^{68}Ga]FAPI-46, [^{68}Ga]OncoFAP exhibited significantly greater uptake in FAP-positive tumors in mice. On the basis of promising preclinical results, clinical imaging employing [^{68}Ga]OncoFAP in 12 cancer patients underscored its exceptional affinity for primary tumors, lymph nodes, and distant metastases, positioning it as a potential alternative to existing FAP tracers, although further evaluation in clinical contexts is warranted.

In parallel, Slania et al.[50] synthesized QCP01 and QCP02 (**22**, Fig. 3), small molecule FAPIs based on the (4-quinolinoyl)-glycyl-2-cyanopyrrolidine scaffold. These compounds shared structural similarities with FAPI-02 but deviated by employing a flexible linear linker group instead of semirigid piperazine moieties, potentially enhancing binding to the target site. Employing ^{111}In, known for its dual emitted photons and extended physical half-life, as an imaging radionuclide, these tracers achieved robust tumor uptake[97−99], which was attributed to the strong affinity of ^{111}In with the carboxylate group on DOTAGA, the chelating group of QCP02[100−102]. Of note, [^{111}In]QCP02 demonstrated robust binding in all the FAP-positive cell lines while displaying negligible binding in FAP-negative cell lines. In addition, comparative uptake evaluations alongside FAPI-02 and FAPI-04 revealed higher [^{111}In]QCP02 accumulation in tumors and normal organs. Strikingly, optimal imaging results were achieved 30 min after injection. This research has been patented under the U.S. Patent and Trademark Office (Patent No. 20200330624A1)[103].

Generally, the introduction of polyethylene glycol (PEG) group can prolong the *in vivo* drug half-life[52,104−114], Lin et al.[51] synthesized [^{68}Ga]FAPtp (**23**, Fig. 3), a novel FAPI tracer distinguished by a short PEGylating linker and peptide amide core structures for the diagnosis and treatment of FAP. Compared with the reference FAPI tracer, [^{68}Ga]FAPI-04 demonstrated similar tumor uptake levels in U87MG tumor bearing mice. Notably, [^{68}Ga]FAPtp outperformed its counterpart by increasing tumor uptake and accelerating renal and hepatic clearance kinetics. The pronounced hepatic clearance of [^{68}Ga]FAPtp was threefold greater than that of [^{68}Ga]FAPI-04, which was attributed to the hydrophilic nature of the polyethylene glycol linker. This expedited excretion presents a potential advantage of [^{68}Ga]FAPtp for clinical translation.

To further explore the utilization of PEG in FAPI tracer development, Hu et al.[52] applied PEG to develop a new FAPI, denoted [^{18}F]AlF−P-FAPI (**24**, Fig. 3). The synthesis of the tracer involved the introduction of a PEG linker between the chelating agent NOTA and the pharmacophore-targeted FAP, followed by chelation with Al^{18}F. The chelator NOTA was instrumental in facilitating efficient Al^{18}F radiolabeling of the peptides, ensuring a high labeling yield and enabling automated production[115−119]. In this context, PEGylation served to prolong the *in vivo* half-life of the tracer[105,120]. [^{18}F]AlF−P-FAPI displayed notable characteristics, including high hydrophilicity, robust stability and specific binding to FAP. Comparative assessments with [^{18}F]FAPI-42 revealed lower efflux and heightened *in vivo* stability for [^{18}F]AlF−P-FAPI. PET/CT imaging substantiated its superior tumor uptake and enhanced tumor-to-background ratios compared with [^{18}F]FAPI-42 and [^{68}Ga]FAPI-04. These promising attributes prompted a preliminary clinical study in patients with nasopharyngeal cancer, where PET/CT imaging with [^{18}F]AlF−P-FAPI highlighted strong radioactive uptake in lymph node metastases and primary tumors. Importantly, the tracer exhibited renal excretion with minimal brain uptake, ensuring clear delineation of primary tumor lesions and lymph node metastases. The combined evidence underscores the favorable characteristics of [^{18}F]AlF−P-FAPI in preclinical evaluation, indicating its potential translation into clinical practice[52].

In parallel, Huang et al.[121] synthesized [^{18}F]AlF-FAPT (**25**, Fig. 3), another innovative PEGylated FAPI tracer. The incorporation of amino acids and hydrophilic linkers into [^{18}F]AlF-FAPT,

contributed to heightened hydrophilicity and reduced lipophilicity, consequently minimizing hepatobiliary metabolism. Comparative PET/CT imaging studies in tumor-bearing mice revealed the tracer's predominant urinary excretion pathway. Furthermore, [^{18}F]AlF-FAPT demonstrated enhanced stability, maintained elevated tumor uptake and was stable for up to 120 min. In contrast, [^{18}F]FAPI-42 exhibited decreased tumor uptake over time. Most importantly, [^{18}F]AlF-FAPT exhibited lower hepatobiliary uptake than did [^{18}F]FAPI-42, indicating that [^{18}F]AlF-FAPT is a valuable tool for abdominal tumor imaging.

This section provides a collection of various radiolabeled FAPIs developed early. The majority of these compounds share the quinoline-Val-Pro motif to maintain binding affinity and a chelator linked with different linkers. Among them, FAPI-04 and FAPI-46 demonstrated high binding affinity and specificity. Ga-68-labeled FAPIs are more sensitive in the diagnosis of tumors. Lu-177-labeled FAPI-04 and FAPI-46 are effective therapeutic radiopharmaceuticals that have been studied in the clinic. Through chemical modification of the side chains of FAPIs, many radionuclides, such as Ga-68, F-18 and Lu-177, are capable of labeling these ligands. To develop more potent radiopharmaceuticals targeting FAP, researchers have also synthesized FAPIs conjugated with more functional chelators.

3.2. Advances in chelator-modified FAPI tracers

In the quest for optimizing FAPI performance, researchers have explored the modification of chelators, recognizing their crucial role in radiotracer dynamics. When ^{68}Ga-labeled FAPIs were applied for PET/CT imaging, a recurring challenge emerged: the high internalization rate of the tracer but with significant efflux, leading to relatively short internal tumor half-lives[10,46]. To enhance the therapeutic potential of FAPIs, it became imperative to align the physical half-life of the radionuclide for labeling with the biological half-life of the ligand. Given the rapid elimination rate of FAPIs within tumors, ^{188}Re is a better choice than ^{177}Lu and ^{225}Ac[122,123]. Building upon this premise, Lindner et al.[124] designed and evaluated specific FAPI variants for labeling with ^{99m}Tc and ^{188}Re. Their initial efforts led to the development of the first ^{99m}Tc-labeled derivative, FAPI-19. While FAPI-19 displayed specificity and high affinity for FAP-positive cells, a significant portion of its radioactivity was observed to accumulate in the liver rather than in tumor sites. In pursuit of enhanced tumor uptake, the research team introduced hydrophilic amino acids into the chelating moiety. Encouragingly, the inclusion of glutamic acid promoted tumor uptake. Subsequent structural refinements yielded FAPI-34 (**26**, Fig. 5), featuring carboxyglutamic acid, notable for its robust *in vivo* stability and substantial tumor accumulation. Consequently, [^{99m}Tc]FAPI-34 was selected for use in monitoring [^{90}Y]FAPI-46 treatment in cancer patients when PET detection is not available.

Moreover, Toms et al.[125] synthesized alkyne-bearing FAPI-04, employing click chemistry-based ^{18}F-fluoroglycosylation to construct the novel FAPI glycoconjugate [^{18}F]FGlc-FAPI (**27**, Fig. 5) as a promising FAP ligand (FL) for preclinical evaluation. The introduction of ^{18}F-labeled glycosylated moieties holds

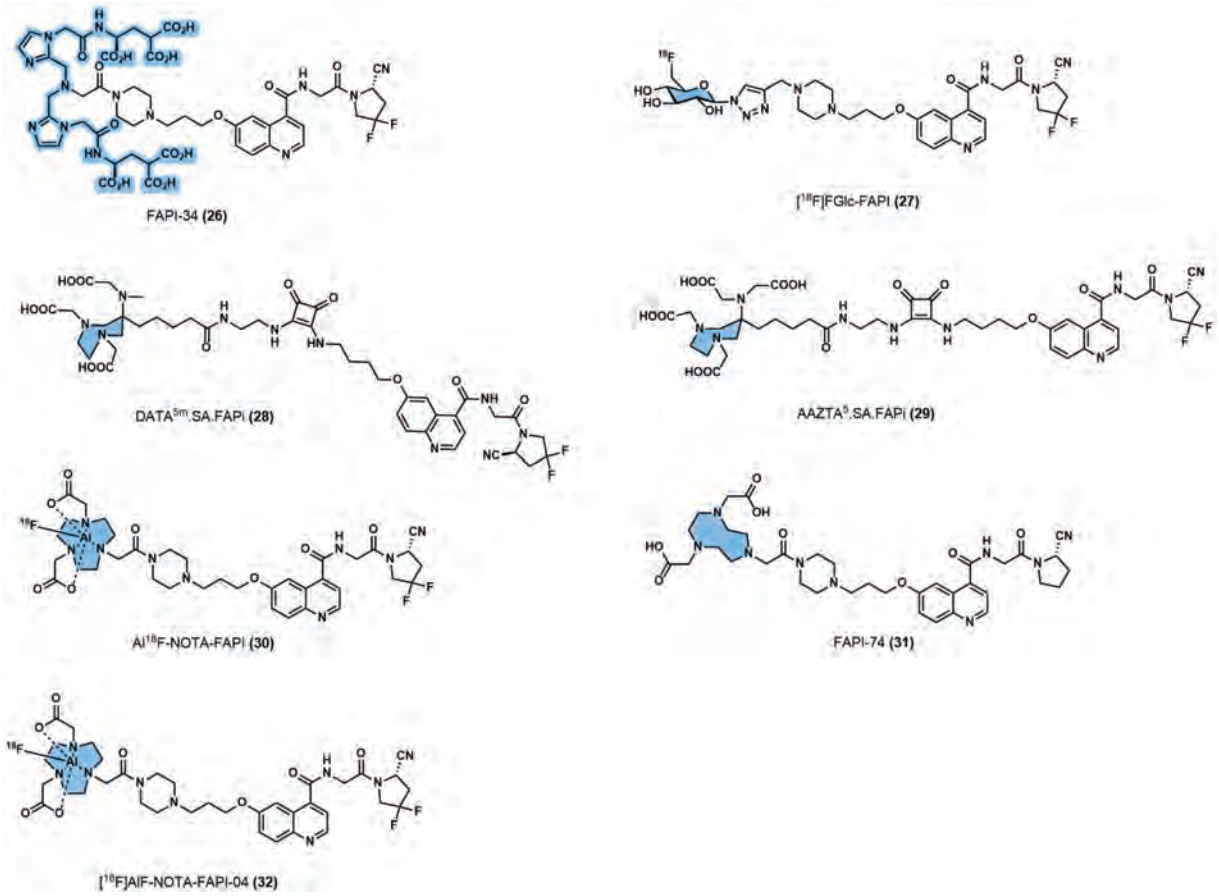

Figure 5 Structures of FAPIs with different chelators (blue: various chelators for labeling with multiple radionuclides).

promise for enhancing radioactive tracer clearance dynamics, with glycosylated molecules demonstrating stability in the bloodstream and optimized active drug delivery[53,126,127]. [^{18}F]FGlc-FAPI, which had slightly less affinity for FAP than FAPI-04, still maintained an IC_{50} value within the nanomolar concentration range and exhibited high stability. PET/CT imaging in mice indicated that this tracer was predominantly involved in hepatobiliary excretion, distinguishing it from the almost exclusive bladder and kidney excretion of [^{68}Ga]FAPI-04. Both tracers displayed specific tumor uptake within 60 min after injection during small animal PET imaging (Fig. 4C). They also found greater tumor uptake of the tracer than [^{68}Ga]FAPI-04. Moreover, [^{18}F]FGlc-FAPI had a lower tumor-to-background ratio and showed lower blood clearance because of higher plasma protein binding. Notably, [^{18}F]FGlc-FAPI demonstrated elevated uptake in bone tissues, making it a prospective tool for monitoring conditions such as arthritis.

Building upon the synthesis of DOTA.SA.FAPi, Moon et al.[84] synthesized the novel FAP-targeting radiotracer, DATA^{5m}.SA.FAPi (**28**, Fig. 5), using the bifunctional DATA^{5m} chelator. Similarly, DATA^{5m}.SA.FAPi also showed inhibitory efficacy against FAP, exhibiting a low nanomolar FAP affinity range similar to that of UAMC-1110. The DATA^{5m} chelator, a bifunctional derivative of DATA, afforded unique capability of ^{68}Ga labeling at room temperature[128−133]. Radiolabeling with ^{68}Ga yielded [^{68}Ga]DATA^{5m}.SA.FAPi with high yield, characterized by remarkable stability *in vivo* and *in vitro*. A significant milestone was achieved with the initiation of the first clinical trial in collaboration with the University Medical Center Bonn, where [^{68}Ga]DATA^{5m}.SA.FAPi was administered to a patient with metastatic cancer, yielding promising PET/CT images that distinctly highlighted tumor-specific uptake[134].

Meanwhile, Kreppel et al.[135] investigated the correlation between [^{68}Ga]DATA^{5m}.SA.FAPi and Ki-67, a marker of tumor aggressiveness in patients with neuroendocrine tumor (NET) liver metastases. PET imaging studies involving 13 patients with NET liver metastases, revealed a correlation between the tracer and Ki-67 in NETs. Notably, [^{18}F]FDG PET/CT and [^{68}Ga]DATA^{5m}.SA.FAPi, while correlated with Ki-67, were grounded in fundamentally different imaging principles that [^{18}F]FDG uptake hinged on the glucose metabolism of tumor cells and manifested predominantly at the lesion center[136−139]. Conversely, [^{68}Ga]DATA^{5m}.SA.FAPi PET signals primarily emanated from FAP expression in CAFs in the tumor stroma, resulting in a more localized imaging pattern around the lesion. This difference had implications for diagnosing NET patients with dedifferentiation. In addition, Greifenstein et al.[140] demonstrated the feasibility and repeatability of the automated synthesis of [^{68}Ga]DATA^{5m}.SA.FAPi. Moreover, they embarked on the first application of this tracer in patients with multiple solid tumors, confirming its diagnostic potential for detecting CAFs across a spectrum of cancers, including liposarcoma, soft tissue tumors, and bone metastases.

In addition, Moon et al.[141] explored the integration of the AAZTA^5 chelator, 1,4-bis-(carboxylmethyl)-6-[bis-(carboxymethyl)-amino-6-pentanoic-acid]-perhydro-1,4-diazepine to fashion the squalamine-containing compound AAZTA^5.SA.FAPi (**29**, Fig. 5) targeting FAP. In the same manner as DATA^{5m}.SA.FAPi, SA was coupled to the terminal carboxyl group of AAZTA^5 and subsequently bound to the FAP-targeting part[84]. AAZTA^5.SA.FAPi exhibited subnanomolar FAP affinity, akin to the FAP affinity profile of DOTA.SA.FAPi and DATA^{5m}.SA.FAPi. In addition, AAZTA^5.SA.FAPi was highly selective for PREP and DPPs. AAZTA, renowned for its capacity to complex under mild conditions and maintain high stability[142,143], enables rapid complexation with ^{44}Sc and ^{177}Lu, both of which were vital for achieving high coordination[144,145]. Compared with the DOTA derivatives, AAZTA^5.SA.FAPi labeled with ^{68}Ga, ^{44}Sc, and ^{177}Lu exhibited elevated radiochemical yields. Notably, [^{44}Sc]AAZTA^5.SA.FAPi necessitated fewer precursors and yielded higher specific activity. Intriguingly, all radioactive complexes showcased impeccable stability.

While ^{68}Ga-labeled tracers have shown high tumor uptake rates and image contrast[76,77], their utility is often hampered by limited remote supply owing to the short half-life and minimal elution from generators[54,146]. In contrast, ^{18}F, which is characterized by a longer half-life, limited positron range, and superior spatial resolution for PET/CT imaging[147−154], emerges as an enticing alternative[155]. Given these advantages, Wang et al.[55] synthesized [^{18}F]AlF-NOTA-FAPI (**30**, Fig. 5), a novel tracer for FAP-targeted tumor imaging. [^{18}F]AlF-NOTA-FAPI exhibited robust stability and specific binding to FAP. Compared with [^{68}Ga]DOTA-FAPI-04, this tracer demonstrated a higher clearance rate and lower uptake in normal organs. PET/CT imaging in cancer patients revealed the capability of [^{18}F]AlF-NOTA-FAPI to detect more tumor lesions than [^{18}F]FDG and to differentiate between benign and malignant lesions. While it was imperative to temper enthusiasm, as [^{18}F]FDG imaging outperformed [^{18}F]AlF-NOTA-FAPI in select patients, it remained pivotal that [^{18}F]AlF-NOTA-FAPI evinced lower uptake in the spleen and brain than [^{18}F]FDG, thereby engendering a superior tumor-to-background ratio. These findings collectively positioned [^{18}F]AlF-NOTA-FAPI as a prospective candidate and adjunctive tool for clinical imaging.

Based on previous studies, [^{18}F]AlF-NOTA-FAPI ([^{18}F]FAPI-42) demonstrated favorable performance in terms of both tumor uptake and detection. The optimal timing for PET imaging remained unclear, prompting Hu et al.[156] to investigate the kinetics of [^{18}F]FAPI-42 in different cancer patients. The PET/CT imaging results were striking, revealing that [^{18}F]FAPI-42 exhibited remarkable tumor uptake, rendering the lesions conspicuously visible. A noteworthy characteristic of this tracer was its swift accumulation in tumors, attaining significant levels at just 18 min post-injection. Furthermore, a comparison was made between [^{18}F]FAPI-42 and [^{68}Ga]FAPI-04 revealing that both tracers exhibited equivalent proficiency in detecting positive lesions, indicating that substituting DOTA with NOTA and chelating with Al^{18}F did not compromise the affinity of the tracer for FAP. In fact, [^{18}F]FAPI-42 outperformed [^{68}Ga]FAPI-04 in terms of uptake in liver and bone lesions, underscoring its potential in detecting such lesions.

As discussed above, the use of ^{68}Ga-labeled FAPIs is constrained in clinic use because of limited production batch sizes and the short half-life of the radionuclide[157,158]. Lindner et al.[159] synthesized seven new radiofluorinated FAPI ligands in 2021. All of these compounds demonstrated high binding affinities for FAP. Notably, [^{18}F]FAPI-74 (**31**, Fig. 5) and [^{18}F]FAPI-75 emerged as particularly promising radiotracers, demonstrating high tumor uptake and efficient renal excretion. PET imaging confirmed that their tumor accumulation and contrast mirrored those of [^{68}Ga]FAPI-04. Of particular note, [^{18}F]AlF-FAPI-75, featuring a difluoro substitution on cyanopyrrolidine, exhibited heightened tumor uptake owing to its enhanced affinity. However, from the time activity curves, [^{18}F]AlF-FAPI-74 exhibited lower uptake in nontarget tissues and expeditious clearance. Consequently, FAPI-74 was selected for PET/CT imaging in a cancer patient, yielding images predominantly concentrated in primary and metastatic

tumors and virtually absent in normal tissues, thus producing high-contrast images.

The NOTA group in FAPI-74 accommodates facile labeling with ^{68}Ga and ^{18}F at ambient temperature, conferring versatility for routine use. Leveraging this advantage, Giesel et al.[54] evaluated the biological distribution and absorbed dose of PET scans utilizing ^{18}F-labeled and ^{68}Ga-labeled FAPI-74. The results illuminated that the optimal contrast for primary tumors, lymph nodes, and distant metastases was achieved 1 h post-injection. In PET/CT imaging of lung cancer patients, [^{18}F]Al-FAPI-74 outperformed diagnostic CT scans by identifying more distant metastases, akin to the efficacy of [^{18}F]FDG PET. In essence, as a pragmatic and versatile tracer, FAPI-74 is ideally labeled with Al^{18}F, facilitating mass production and distribution *via* satellite concepts, an advantage over previous ligands in terms of production capacity.

Additionally, Giesel et al.[160] compared PET imaging utilizing [^{68}Ga]FAPIs (FAPI-02, FAPI-04, FAPI-46, and FAPI-74) in 71 cancer patients juxtaposed with [^{18}F]FDG. Compared with [^{18}F]FDG, [^{68}Ga]FAPI showed lower uptake in most normal tissues while maintaining comparable or superior tumor-to-background ratios. Importantly, there was no significant difference in the mean SUV_{max} between these tracers in primary tumors or total metastases. However, as shown in Fig. 4D, [^{68}Ga]FAPI PET/CT displayed robust tumor uptake, whereas [^{18}F]FDG PET/CT exhibited only mild to moderate uptake in select patients. This underlines the potential utility of [^{68}Ga]FAPI for enhancing the diagnosis of tumors characterized by high physiological uptake of [^{18}F]FDG.

Dendl et al.[161] performed [^{68}Ga]FAPI (FAPI-04, FAPI-46, and FAPI-74) PET/CT scans in 55 patients afflicted with rare tumors to evaluate their applicability in the context of uncommon malignancies. The outcomes of these investigations revealed minimal tracer uptake within the majority of normal organs. Across various rare malignancies, [^{68}Ga]FAPI PET/CT exhibited outstanding tumor visualization capabilities, yielding a high tumor-to-background ratio (Fig. 4E), which underscored the potential of [^{68}Ga]FAPI PET/CT as an indispensable imaging tool for evaluating diverse malignancies.

Wei et al.[56] introduced a new tracer, [^{18}F]AlF-NOTA-FAPI-04 (**32**, Fig. 5), which was a product of the chelation of Al^{18}F-labeled FAPI-04 with NOTA. This tracer exhibited a robust FAP binding affinity and rapid uptake in U87MG tumors, with peak uptake recorded at 1 h post-injection and sustained retention at 2 h. Notably, the tracer exhibited extremely low uptake in most normal organs. The utility of this tracer was further explored through PET/CT imaging in different cancer patients. The scans revealed the substantial accumulation of [^{18}F]AlF-NOTA-FAPI-04 in primary tumors, lymph nodes, and liver and bone metastases (Fig. 4F). Additionally, uptake in other normal organs remained low, resulting in high-contrast images. Furthermore, radioactive metabolites were mainly excreted *via* the kidney. To demonstrate diagnostic efficacy, dual-tracer imaging was performed using [^{18}F]AlF-NOTA-FAPI-04 and [^{18}F]FDG in seven patients with advanced lung cancer. Compared with [^{18}F]FDG, [^{18}F]AlF-NOTA-FAPI-04 exhibited superior capabilities in identifying metastatic lesions when compared with [^{18}F]FDG, suggesting its potential contribution to tumor staging.

In addition, Wei et al.[162] investigated the discriminatory potential of [^{18}F]AlF-NOTA-FAPI-04 in distinguishing various subtypes of lung cancer based on varying levels of radiotracer uptake. While no appreciable differences were observed in tracer uptake between primary tumors and the combined entity of primary and metastatic tumors of the same pathological type, variations were evident in the uptake of metastatic tumors with different pathological characteristics. This intriguing finding suggested that [^{18}F]AlF-NOTA-FAPI-04 may serve as a valuable tool for discerning different pathological subtypes of lung cancer through PET/CT imaging of metastatic lung cancer lesions.

To expand the horizons of its clinical application, FAP-targeted tracers have been explored for the diagnosis of rheumatoid arthritis (RA)[163–165]. Ge et al.[166] conducted preclinical and preliminary clinical investigations into RA by employing [^{18}F]AlF-NOTA-FAPI-04. In stark contrast to [^{18}F]FDG, this tracer exhibited high uptake in inflamed joints in the early phase of RA, and its uptake was positively correlated with RA severity scores. However, [^{18}F]FDG exhibited negligible accumulation in inflamed joints and pronounced uptake in the brain, chest, and muscle tissues. In addition, PET/CT imaging was performed in two RA patients, revealing conspicuously elevated uptake of the radiotracer within the synovial tissue of affected arthritic joints. These findings underscored the potential of [^{18}F]AlF-NOTA-FAPI-04 as a valuable diagnostic tool for RA imaging.

This section focuses on chelators used for FAP/PET imaging. Ga-68 is generally the most used radionuclide and chelated by DOTA. To improve tumor uptake and reduce normal organ accumulation, various chelators, such as DATA^{5m} and AAZTA^{5}, have been introduced into the side chain of FAPIs. NOTA-conjugated FAPIs have been well developed for F-18 labeling to optimize diagnostic accuracy. The effects of various linkers and chelators on the pharmacokinetics and binding affinity between FAPIs and FAP are illustrated in Table 3.

3.3. Albumin binder-conjugated FAPIs

Owing to the limited retention time of radiolabeled FAPIs within tumors[76], strategies aimed at modulating their pharmacokinetics (PK) through increased binding to serum albumin have been gained prominence[167–171]. This approach, which improves the uptake and retention of radiolabeled ligands within tumors, is founded upon the established concept that albumin binding alters drug distribution a phenomenon initially demonstrated with paclitaxel in chemotherapy[172–176]. This strategy has been successfully applied to increase the uptake of radioligands targeting receptors such as the folate receptor and PSMA[177–184], and recent investigations have extended its applicability to FAP inhibitors.

In 2021, Kelly et al.[185] designed a PSMA-targeting trifunctional ligand that integrated an albumin-binding group, a chelator, and a targeting moiety through a flexible linker. The PK of this ligand was determined by the interplay of targeting affinity, serum albumin affinity, and linker geometry. This ligand demonstrated substantial uptake in xenograft tumors while exhibiting rapid clearance from normal tissues. Building upon this foundational work, Kelly et al.[58] leveraged a comparable scaffold to design RPS-309 (**33**, Fig. 6), a trifunctional small molecule ligand that targeted FAP. RPS-309 incorporated the FAP-targeting motif, chelator, albumin-binding moiety, and a flexible PEG linker. This agent evinced specific binding to FAP and was amenable to radiolabeling with either ^{68}Ga or ^{177}Lu, yielding highly purified radioactive compounds. Notably, [^{68}Ga]RPS-309 substantially accumulated in SW872 xenograft tumors, and the uptake of [^{68}Ga]RPS-309 in tumors was 5.0 $\pm$ 0.3 %ID/g, while there is no significant clearance ($P = 0.31$) from tumors was observed.

Table 3 Various linkers and chelators used in FAPIs. To improve tumor binding affinity and *in vivo* pharmacokinetics, different functional linkers have been developed. For labeling with different radionuclides or making them more stable *in vivo*, various chelators have been introduced into FAPI structures. We summarize representative structures of linkers and chelators in FAPIs and highlight their features.

Representative linker	Feature	Representative chelator	Feature
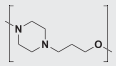 Piperazine moiety[45,46]	Increasing the tumor uptake; Increasing tumor-to-normal ratios; Improving the *in vivo* stability of the molecule.	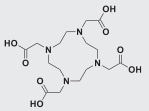 DOTA[45,64,84]	Labeling with various radionuclides.
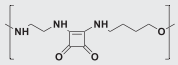 Square amide[84]	Conjugation with two chemical structures; Mild conjugation conditions.	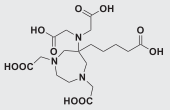 Bifunctional DATA[5m84,142]	Mild labeling conditions; High stability *in vivo*.
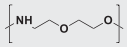 Polyethyleneglycol group[52]	Increasing the tumor uptake; Increasing tumor-to-normal ratios; Improving the *in vivo* stability of the molecule; Rapid clearance from normal organs.	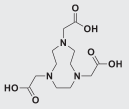 NOTA[55]	Labeling with various radionuclides; Metabolized mainly by liver/kidney.
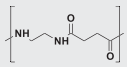 Flexible linear linker group[96]	Modulating the molecular properties; Being conjugated with functional chemical groups.	 ^{18}F-fluoroglycosylation[126]	Enhanced blood stability; Increasing the tumor uptake; Metabolized mainly by liver.
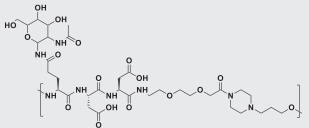 Amino acids and hydrophilic linkers[122]	Enhancing the tumor uptake; Improving the molecular hydrophilicity.	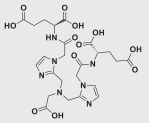 Carboxyglutamic acid chelating moiety[125]	Improved *in vivo* stability; Substantial tumor accumulation.

Conversely, [^{177}Lu]RPS-309 exhibited a relatively high clearance rate, maintaining tumor retention. Although RPS-309 exhibited a relatively prolonged blood residence time relative to previously reported FAP-targeting radiolands, it did not result in progressive tumor growth over time. The observed tumor clearance kinetics observed between 4 and 24 h aligned with those of preliminary studies involving other FAPI radioligands.

It has been suggested that the difluorinated proline residue has higher lipophilicity and a better fit, which decreases the K_m value of [^{68}Ga]FAPtp binding to FAP. However, difluorine substitution on pyrrolidine can significantly improve the potency of nitrile-based inhibitors[29,57]. Capitalizing on the potential impact of the difluorinated proline residue on FAP targeting and informed by prior research on FAPtp, Lin et al.[51] synthesized [^{68}Ga]Alb-FAPtp-01 (**34**, Fig. 6), an albumin-binding FAPI featuring an albumin-binding moiety, 4-*p*-chlorophenyl butyric acid. This structural modification aimed to optimize PK, extend tracer circulation, and prolong the tumor retention time. The mean standard uptake values (SUVs) of tumor uptake were 1.775 ± 0.179, 1.533 ± 0.222, and 1.425 ± 0.204 at 1, 2, and 3 h, respectively. In contrast to the low tumor uptake and rapid renal clearance characteristic of the non-albumin-binding FAPI tracers ([^{68}Ga]FAPI-04 and [^{68}Ga]FAPtp), [^{68}Ga]Alb-FAPtp-01 displayed rapid tumor uptake and prolonged retention. This effect stemmed not only from the tracer's FAP-targeting ability but also from its ability to bind to albumin. Albumin binding facilitated stable tracer diffusion and transport into tumors by intrinsic blood vessels or internal fluid pressure. Overall, the prolonged retention of [^{68}Ga]Alb-FAPtp-01 may increase tumor uptake and bolster imaging contrast.

Two frequently employed albumin binders, 4-(*p*-iodophenyl) butyric acid (IPBA)[171,179,180,195,196] and truncated Evans blue (EB)[186−194], have shown promise in enhancing tumor uptake and retention time, thereby amplifying therapeutic effects[57]. In 2022, Xu et al.[59] capitalized on the synergistic potential of these two albumin binders to refine FAPI-04, yielding two novel albumin-binding FAPI tracers, TEFAPI-06 and TEFAPI-07 (**35** and **36**, Fig. 6). The analysis confirmed the stability and high specificity of these tracers for FAP binding. Radiolabeling with ^{68}Ga and ^{86}Y corroborated their robust tumor-targeting capabilities and prolonged retention. In comparison with [^{177}Lu]FAPI-04, the ^{177}Lu-labeled variants of these tracers demonstrated superior tumor uptake and retention time, primarily attributable to their FAP-targeting attributes. Moreover, in terms of radiation therapy, both tracers elicited substantial tumor growth inhibition, surpassing the modest inhibition observed with [^{177}Lu]FAPI-04. These findings underscore the potential of TEFAPI-06 and TEFAPI-07 for further clinical translational research.

EB has a high affinity for serum albumin, and its derivatives combined with targeted molecules can prolong drug circulation[197−200]. Except TEFAPI-07 mentioned above, Wen et al.[60] synthesized a series of albumin-binding FAPIs based on FAPI-02, named EB-FAPI-B1, B2, B3, and B4 (**37**−**40**, Fig. 6). These compounds incorporated four components: a FAP-targeting moiety, a radionuclide labeling DOTA group, a PEG linker, and a truncated EB. Upon radiolabeling with ^{177}Lu, the resulting tracers

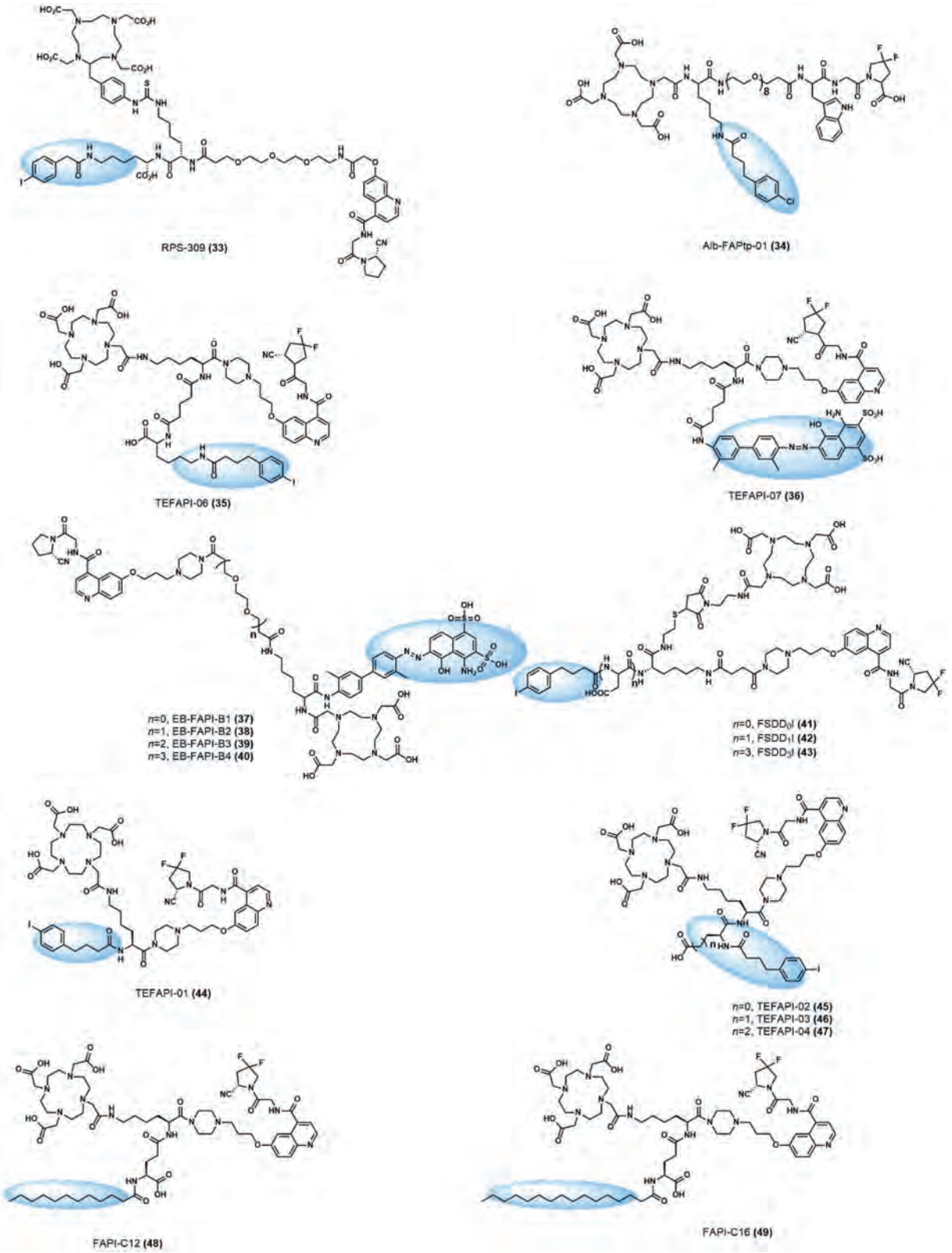

Figure 6 Structures of albumin binder-conjugated FAPIs (blue: albumin-binding motif).

displayed excellent stability and specific binding to FAP *in vitro*. SPECT imaging results demonstrated that [^{177}Lu]EB-FAPI-B1 exhibited low uptake in most organs, whereas the other three tracers showed prolonged radioactivity in the liver and kidneys, suggesting potential toxicity to normal organs. This outcome indicated that PEG-modified EB-FAPI-Bn may not improve FAP targeting, possibly due to blocked cellular uptake of macromolecules that affected drug delivery to cancer cells[201]. Additionally,

these researchers examined the uptake and retention of these tracers in tumors. Among the four tracers, [^{177}Lu]EB-FAPI-B1 displayed significant tumor uptake and prolonged retention, maintaining high uptake even at 96 h post-injection. Consequently, treatment studies using three different doses of [^{177}Lu]EB-FAPI-B1 revealed that all the tested doses effectively inhibited tumor growth, with no significant differences in therapeutic effect.

Chen's group[113,186,193] synthesized a series of tracers incorporating the radioactive 4-(*p*-iodophenyl) butyric acid moiety, capitalizing on its straightforward synthesis and strong albumin-binding capabilities. Consequently, Meng et al.[61] synthesized a series of albumin-binding FAPI ligands derived from FAPI-04, namely $FSDD_0I$, $FSDD_1I$, and $FSDD_3I$ (**41**−**43**, Fig. 6), by coupling IPBA with a bifunctional chelator. These studies showed that the introduction of IPBA did not compromise the binding affinity of these three FAPI ligands for FAP and emphasized the significant role of IPBA in albumin binding. PET imaging demonstrated that [^{68}Ga]$FSDD_nI$ had significant tumor uptake compared with [^{68}Ga]FAPI-04. Notably, [^{68}Ga]$FSDD_0I$ exhibited significantly higher tumor uptake and retention than the other two tracers, which might be attributed to its enhanced albumin-binding properties or relatively weak hydrophilicity. In addition, [^{68}Ga]$FSDD_3I$ displayed shorter blood retention and faster renal clearance, possibly due to the insertion of repetitive peptide sequences that improved hydrophilicity.

Ding et al.[62] synthesized four albumin-bound FAPIs, namely TE-FAPI-01, TE-FAPI-02, TE-FAPI-03, and TE-FAPI-04 (**44**−**47**, Fig. 6). These compounds exhibited excellent stability and strong binding affinity for FAP both *in vitro* and *in vivo*. Differences in the side chains of the introduced IPBA moiety were identified as key factors contributing to the differences in their PK profiles, including blood circulation and tumor uptake. Of particular significance, TE-FAPI-04 outperformed other radiopharmaceutical tracers, characterized by a longer blood half-life and higher tumor uptake. Furthermore, compared with FAPI-04, TE-FAPI-04 exhibited superior tumor retention capabilities compared with FAPI-04. At 24 h after administration, the tumor uptake of [^{177}Lu]TE-FAPI-04 was 10-fold greater than that of [^{177}Lu]FAPI-04. This observation indicated that TE-FAPI-04 held promise for prolonging the diagnostic timeframe and facilitating subsequent diagnostic analyses.

In addition to conventional albumin binders, fatty acids, such as palmitic acid (C16), have been explored as albumin-binding moieties[202−205]. C16 has been associated with longer blood circulation than other fatty acids[206]. Zhang et al[63]. conjugated lauric acid (C12) and C16 to FAPI-04 to yield two albumin-binding FAPI derivatives, FAPI-C12 and FAPI-C16 (**48** and **49**, Fig. 6). Both radiopharmaceutical tracers exhibited exceptional stability and high specificity for FAP. While radiolabeled FAPI-C12 exhibited greater tumor uptake within the first hour after injection, it displayed a subsequent rapid decline and lower uptake at subsequent time points. Conversely, [^{177}Lu]FAPI-C16 resulted in a significantly prolonged tumor retention compared with [^{177}Lu]FAPI-C12. Extended retention and elevated uptake were critical factors for effective tumor therapy. In comparative therapeutic assessments with [^{177}Lu]FAPI-04, both FAPI-C12 and FAPI-C16 demonstrated superior therapeutic effects, and [^{177}Lu]FAPI-C12 exhibited a greater capacity to inhibit tumor growth, despite achieving median survival outcomes similar to those of [^{177}Lu]FAPI-04.

FAPI based cancer therapy has been proven to be effective preclinically and clinically. To maintain high tumor uptake, chemical strategies such as covalently linked IPBA and Evans blue, have been used to prolong FAPIs' *in vivo* half-lives. These methods are able to bind FAPIs with albumin, thus prolonging the tumor retention time. In addition to the albumin-binding strategy, multimerization is also an effective method for enhancing tumor uptake and retention time.

3.4. *FAPI multimers*

Although FAPIs have shown promise in preclinical and clinical studies[10,15,45,46], they are often challenged by shorter tumor retention time and faster renal clearance. To overcome this challenge, researchers have developed dimer derivatives, a strategy that has been demonstrated to enhance tumor accumulation and retention[207−210]. Dimeric molecules, as evidenced in various studies including those involving arginine-glycine-aspartate (RGD) dimers[211−214], have consistently exhibited enhanced tumor uptake when compared to their monomeric counterparts[215−218].

Zhao et al.[64] synthesized a FAPI dimer, DOTA-2P$(FAPI)_2$ (**50**, Fig. 7), leveraging the foundation laid by FAPI-46. The dimer incorporates two FAPI motifs interlinked by two miniature polyethylene glycols in a homodimeric peptide scaffold. This structural augmentation introduces amphiphilic polyethylene glycol linkers, a widely recognized enhancement strategy for optimizing *in vivo* PK properties[219−224]. In-depth *in vitro* binding experiments that conducted with synthesized [^{68}Ga]DOTA-2P$(FAPI)_2$ revealed not only remarkable stability but also profound and specific affinity for FAP. This robust performance underscored the fact that the polyvalent strategy did not compromise the intrinsic FAP-binding affinity of the ligand. Indeed, the polyvalent strategy can enhance tumor targeting ability while concurrently increasing the caliber of *in vivo* imaging outcomes[220,225].

Based on the advantages of dimers, Zhao's group[227] conducted extensive PET imaging investigations in mice and cancer patients. Compared with [^{68}Ga]FAPI-46, the dimeric tracer exhibited a notably greater degree of tumor uptake, substantiating the enhanced propensity for rapid tumor accumulation in two hepatocellular carcinoma patient-derived xenograft (HCC-PDX) models. Furthermore, quantified measurements at 1 and 4 h post-injection revealed a high tumor-kidney ratio. Complementary PET imaging of mouse models revealed rapid renal elimination. Specifically, the uptake of the tracer was high in the kidney and liver at 30 min after injection, and this uptake was rapidly eliminated at 60 min after injection, which may be attributed to the improved hydrophilicity of PEG groups[219,220]. These encouraging outcomes from murine studies served as a springboard for clinical investigations involving patients with undifferentiated nasopharyngeal carcinoma, papillary thyroid carcinoma, and HCC. Patients received intravenous infusions of both [^{68}Ga]FAPI-46 and [^{68}Ga]DOTA-2P$(FAPI)_2$, followed by PET/CT imaging sessions. Impressively, clinical imaging results mirrored findings from animal experiments, reaffirming the accelerated accumulation of dimers within tumor lesions and consistently outperforming [^{68}Ga]FAPI-46. Notably, however, in the clinical context, tracer retention in the blood pool remained high at 4 h after injection, contrary to observations from animal studies. The clinical results provided compelling evidence that DOTA-2P$(FAPI)_2$ had potential as a prominent tracer for the diagnosis and targeted treatment of FAP-positive malignancies.

A comparison between [^{177}Lu]DOTA-2P$(FAPI)_2$ (experimental group) and [^{177}Lu]FAPI-46 (control group) by Zhao et al.[227]

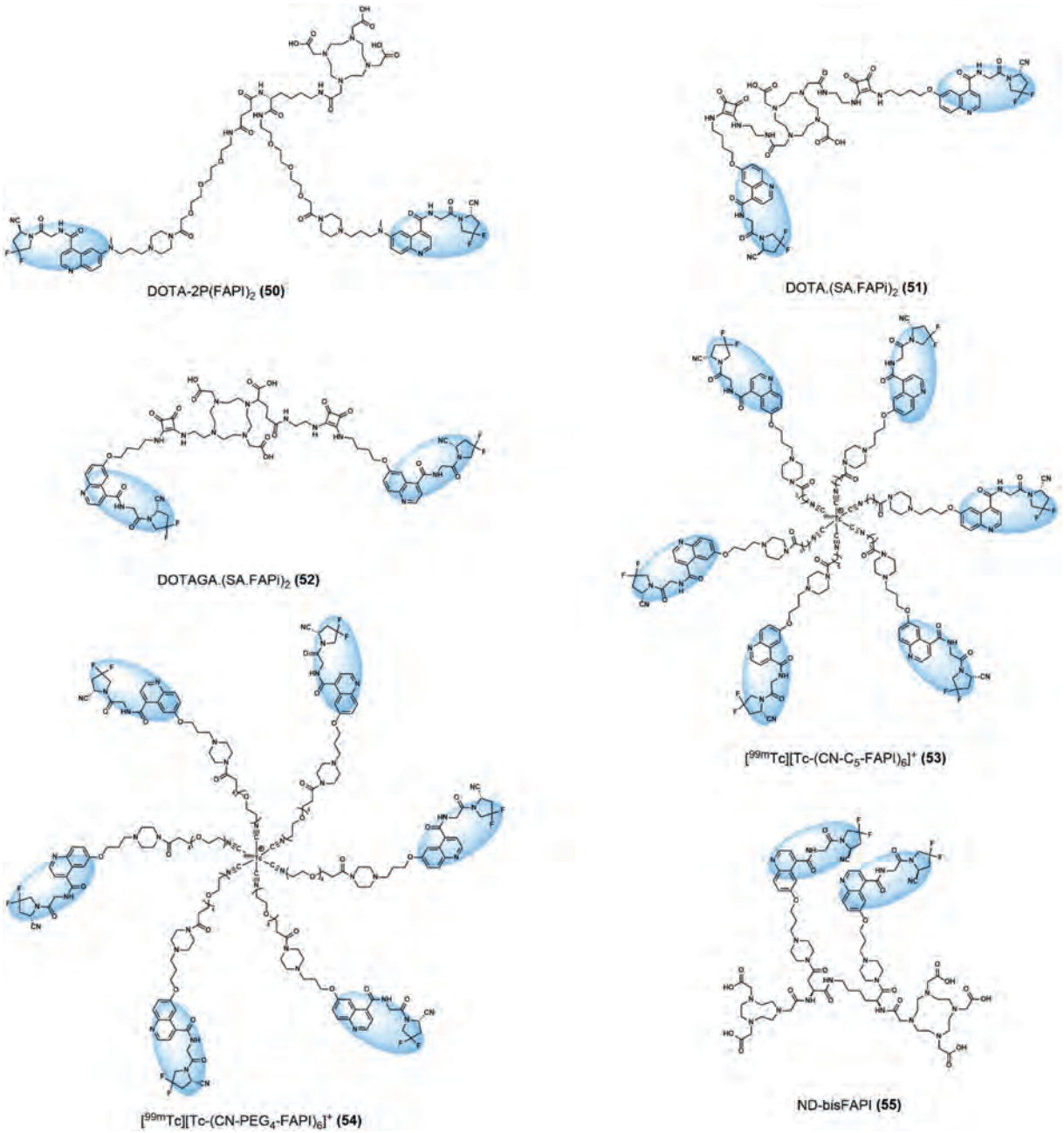

Figure 7 Structures of FAPI multimers (blue: bioactive structures targeting FAP).

further confirmed the efficacy of the dimer in FAP-targeted radionuclide therapy. In both HCC-PDXs and HT-1080-FAP cell-derived xenografts[226], biological distribution studies revealed that the dimer demonstrated heightened tumor uptake and prolonged tumor retention than its monomeric counterpart [^{177}Lu]FAPI-46. *In vivo*, both the control group and experimental group showed a significant reduction in tumor progression. However, the control group exhibited tumor recurrence in more than half of the patients, whereas the experimental group remained free of tumor recurrence, demonstrating the effectiveness and safety of [^{177}Lu]DOTA-2P(FAPI)$_2$ in treating FAP-positive malignancies.

Leveraging the attributes of dimers for bolstering tumor accumulation and protracted retention, Moon et al. engineered two amide-conjugated FAPIs, DOTA.(SA.FAPi)$_2$ and DOTAGA.(SA.FAPi)$_2$ (**51** and **52**, Fig. 7)[141]. Compared with the reference compound UAMC-1110 and the monomeric tracer DOTA.SA.FAPi, the IC_{50} values of the dimeric tracer for FAP were in the subnanomolar to low nanomolar range, and the affinity for PREP was in the micromolar range, resulting in a high FAP/PREP selectivity index, which favored FAP targeting. In clinical studies employing PET/CT, [^{68}Ga]DOTAGA.(SA.FAPi)$_2$ displayed higher tumor uptake and longer tumor retention than its monomeric counterpart. Nevertheless, in patients with papillary thyroid cancer and type III pancreatic NETs, while the dimeric tracer exhibited preserved retention, it also exhibited retention in normal organs such as blood pool. Intriguingly, when [^{177}Lu]DOTAGA.(SA.FAPi)$_2$ was used for SPECT imaging and blood pool activity as recorded at remarkably low levels. These observations suggested

that inherent limitations may be associated with this tracer, which was related to high radiation exposure of normal organs and variable distribution patterns among patients. Therefore, monomer-guided dimer treatment may be more suitable for clinical applications.

In a parallel investigation, Ballal et al.[228] evaluated and compared [^{177}Lu]DOTA.SA.FAPi and [^{177}Lu]DOTAGA.(SA.FAPi)$_2$ in patients with solid tumors. This study encompassed two groups: the control group, which included three patients who were injected with the monomer tracer, and the experimental group, which incorporated seven patients subjected to the dimeric tracer. Strikingly, the experimental group showcased a higher average absorbed dose in nontarget organs than the control group. Significantly, the dimeric tracer exhibited strong uptake, a characteristic that persisted even 168 h post-treatment. In stark contrast, the monomeric counterpart experienced rapid clearance and demonstrated limited uptake within a relatively short interval after treatment. Moreover, the median absorbed dose in the tumors in the experimental group was 5.16 times higher than that observed in the control group. This phenomenon, which was characterized by long tumor retention and rapid clearance from nontarget organs, offered a promising prospect for the therapeutic landscape for patients with advanced cancer.

In addition to the aforementioned dimeric constructs, alternative multimeric approaches have been harnessed. Ruan et al.[65] synthesized two isocyanide-containing monomers (CN-PEG$_4$-FAPI and CN-C$_5$-FAPI) as FAPIs. These endeavors capitalized on the distinct nuclear attributes of ^{99m}Tc, coupled with its cost-effectiveness. Both of these monomeric entities demonstrated low nanomolar IC_{50} values for FAP, attesting to their unwavering specific affinity for FAP even in the context of structural refinements to FAPI. These research endeavors culminated in the generation of high radiochemical purity of multimers, specifically [^{99m}Tc][Tc-(CN-C$_5$-FAPI)$_6$]$^+$ and [^{99m}Tc][Tc-(CN-PEG$_4$-FAPI)$_6$]$^+$ (**53** and **54**, Fig. 7). The radiolabeling of CN-C5-FAPI and CN-PEG4-FAPI with ^{99m}Tc further enhanced their sound *in vitro* stability.

In mouse tumor models, compared with multimer **53**, **54** showed a 6-fold increase in tumor uptake at just 1 h after intravenous injection. Notably, kidney uptake of **54** proved lower than that of **53**, whereas no significant difference in uptake was observed in other organs. These findings suggested that the presence or absence of the PEG$_4$ linker affected the uptake in noncancerous organs, as well as the uptake of tracers in tumors. An increase in the PEG content emerged as a pivotal strategy for enhancing the tumor-to-organ ratio. Substantiating these observations, SPECT imaging in nude mice confirmed that **54** exhibited higher tumor uptake and yielded clearer background images than **53**. Within 30 min post-injection, **54** produced a robust tumor signal, resulting in continued escalation and sustained tumor accumulation for at least 4 h, thereby yielding high-contrast images. However, after excretion, **54** also exhibited some uptake in the intestinal biliary tract and kidneys. In conclusion, these results collectively suggested a promising future for **54** as a candidate for imaging FAP-targeted tumors.

Employing bivalent structures as a pharmaceutical design strategy to increase tumor uptake has garnered substantial interest. Notably, Hu's group[229] reported on a bivalent PSMA radioligand ([^{18}F]AlF-Bi-PSMA), which demonstrated higher tumor uptake and longer retention than its monomeric counterpart. Building upon this paradigm, Li et al.[66] synthesized a bivalent ligand, denoted ND-bisFAPI (**55**, Fig. 7), that incorporates NOTA and DOTA chelators, thereby targeting FAP. The NOTA chelator in this ligand can form complexes with Al^{18}F for PET imaging[118,230−232], while the DOTA chelator can be labeled with ^{177}Lu to facilitate radiotherapy[233−235]. Both radiotracers exhibited robust stability and specific binding to FAP. PET imaging results of A549-FAP and U87MG xenograft models unveiled that [^{18}F]AlF-ND-bisFAPI displayed higher tumor uptake than its monomeric counterpart. PET imaging of this tracer at 6 h post-injection in A549-FAP tumor-bearing mice revealed swift tumor uptake and exceptional retention, accompanied by a favorable tumor-to-nontargeted ratio. Furthermore, their investigation delved into the therapeutic effect of ^{177}Lu-labeled dimers. Specifically, [^{177}Lu]FAPI-04 and [^{177}Lu]ND-bisFAPI were administered to A549-FAP tumor-bearing mice. At 24 h post-injection, the bivalent ligand exhibited 4-fold greater radiation accumulation within tumors than the monomeric ligand. However, the bivalent ligand exhibited higher uptake in nontargeted tissues and organs than the monomeric ligand, which may potentially result in increased *in vivo* toxicity. In the dose−response analysis, the administration of the bivalent ligand at 37 MBq demonstrated superior tumor-suppressive effects, whereas the monomeric ligand exhibited a slightly longer median survival at equivalent doses, likely attributable to some degree of toxicity incurred by the bivalent ligand in nontarget organs. Notably, when the administered dose was halved, the median survival between the two groups became comparable. Importantly, no long-term toxicity-related issues were observed within the 30-day period following the administration of both radioinhibitors, and both significantly impeded tumor growth. These findings collectively underscored the superior tumor-suppressive effects of 37 MBq [^{177}Lu]ND-bisFAPI treatment in contrast to 37 MBq [^{177}Lu]FAPI-04. Hence, in light of this comprehensive analysis, bivalent ligand emerged as a promising radiopharmaceutical for applications targeting FAP.

FAPI multimers are composed of two or more FAPIs conjugated by linkers. Radiopharmaceuticals based on multivalent FAP ligands can bind more strongly than monomers and reduce the off-target effect. This is an effective method to prolong the tumor retention time. In addition to FAPI multimers, PSMA or integrin targeted molecules can also be conjugated with FAPIs, which are heterodimers.

3.5. *Heterodimers of FAPIs*

Dimeric radiotracers offer advantages over monomeric radiotracers, primarily by increasing targeted receptor engagement, elevating local ligand concentration, and optimizing PK. While homodimeric radiotracers have shown promise in improving tumor uptake and retention[66,141], addressing the intricate tumor−stromal interactions and heterogeneity in multicellular systems requires a fresh perspective. Heterodimers, which are covalently fused with linkers connecting two monospecific ligands, offer a means to further enhance efficacy[236−238]. Various heterodimeric radiotracers can improve tumor targeting ability, reduce patients' treatment costs, relieve their discomfort, and alleviate their radiation burden[239−243].

FAP, which is characteristically overexpressed in CAFs, and PSMA, which is prevalent in the endothelium of neovascularized regions across diverse solid tumor types, have garnered increasing attention[67,244−249]. Their co-expression in numerous malignancies, spanning colorectal, gastric, lung, thyroid, prostate, and pancreatic cancers[77,249−258], underscores the potential of developing heterodimers to simultaneously target FAP and PSMA

receptors, which holds promise for both diagnosis and treatment. Here, three kinds of PSMA/FAP heterodimers are introduced.

Hu et al. designed ^{18}F-labeled bispecific PSMA/FAP heterodimers by conjugating a linker and NOTA to a quinoline-based pharmacophore for FAP targeting and a lysine-ureido-glutamate pharmacophore for PSMA targeting[68]. Modulating the molecular weight and PK of these heterodimers was achieved by introduction of specific altered linkers. The resulting [^{18}F]AlF-PSMA-FAPI-01 and [^{18}F]AlF-PSMA-FAPI-02 (**56** and **57**, Fig. 8) exhibited double the receptor binding affinities for both PSMA and FAP, displaying specific affinity for each receptor. These heterodimers exhibited high hydrophilicity and good stability, rendering them multifunctional agents for precise receptor targeting.

Comparative assessments against corresponding monomeric tracers in tumor-bearing mice demonstrated significantly heightened tumor uptake by the heterodimeric tracers. PET images of nude mice revealed swift tumor uptake, prolonged retention in tumors, and renal clearance of these agents from nontarget organs. Crucially, these heterodimeric tracers exhibited superior tumor uptake compared with [^{18}F]FAPI-42 and [^{18}F]AlF-PSMA-BCH.

Boinapally et al. synthesized FP-L1 and FP-L2 (**58** and **59**, Fig. 8) as heterodimers concurrently targeting FAP and PSMA[69]. Utilizing "click chemistry", these compounds were skillfully crafted to ensure robust stability and potent FAP-binding affinity *in vitro*. Biological distribution studies, employing [^{64}Cu]FP-L1 and [^{64}Cu]FP-L2 in mouse xenograft models harboring PSMA-positive PC3 PIP and FAP-positive U87MG tumors revealed substantially heightened tumor uptake of [^{64}Cu]FP-L1 and decreased kidney uptake in both tumor types. Notably, these heterodimers exhibited substantial clearance (5.34 ± 0.29 % ID/g at 48 h) yet retained prolonged tumor retention compared with [^{111}In]QCP02 (0.58 ± 0.03 % ID/g at 28 h)[50]. In a small tumor model, tumor uptake of [^{64}Cu]FP-L1 mirrored that of [^{64}Cu]FAPI-04 at 2 h after injection. Nevertheless, it should be noted that this approach might necessitate tissue sampling for lesion detection.

Inspired by the concept of enhancing tumor uptake and retention through heterodimeric PET probes targeting distinct tumor markers, Zang et al.[70,242] designed and synthesized FAPI-RGD (**60**, Fig. 8), a bispecific heterodimeric radiotracer that simultaneously targets FAP and $\alpha_v\beta_3$. Coupled with FAPI-02 for FAP targeting, RGDfK peptide for $\alpha_v\beta_3$ targeting, a polyethylene glycol linker and NOTA, this tracer displayed compelling binding affinity and specificity. Cyclic RGD peptides exhibited high binding specificity for integrin $\alpha_v\beta_3$, a receptor highly expressed in angiogenic endothelial cells and most types of tumor cells[211,259]. The results of their study underscored the favorable binding affinity and specificity of [^{68}Ga]FAPI-RGD. Notably, this tracer demonstrated significantly elevated tumor uptake and prolonged retention compared with both monomeric [^{68}Ga]FAPI-02 and [^{68}Ga]RGDfK at all observed time points. Furthermore, the initial human imaging findings from their study indicated that they

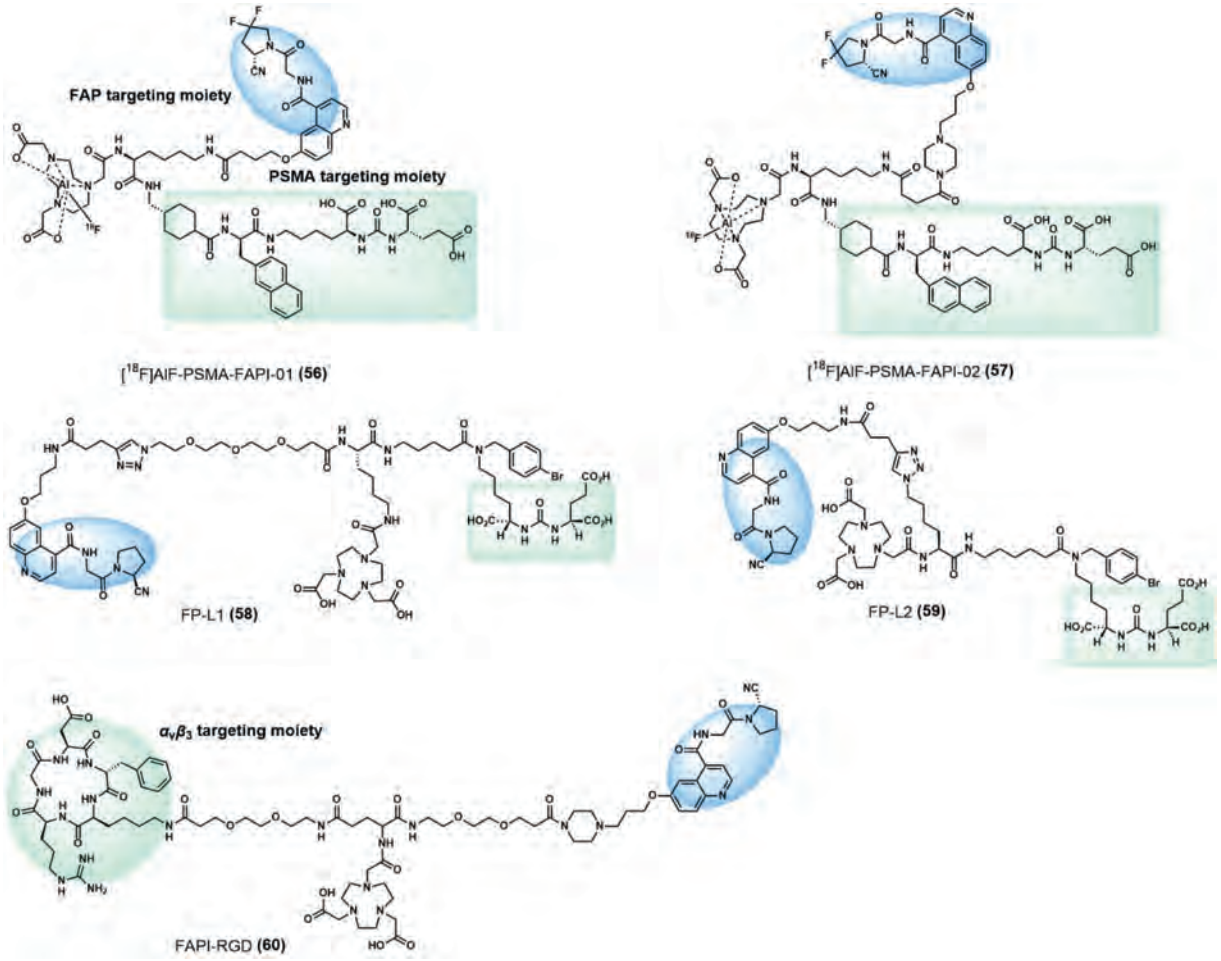

Figure 8 Structures of heterodimers of FAPIs (blue: FAP-binding moiety; green: PSMA/$\alpha_v\beta_3$-binding moiety).

were well-tolerated by patients, demonstrating rapid tumor uptake. Within the first 2 h post-injection, this tracer exhibited rapid and high tumor uptake, long retention, and a high tumor-to-background ratio. High radioactivity in the urinary tract was observed, indicating its predominant renal excretion, which was consistent with findings from other reported [^{68}Ga]FAPI tracers. While no substantial difference was noted between this tracer and [^{18}F]FDG in primary and metastatic tumors. Among six patients, one renal cancer patient exhibited improved tumor uptake with [^{68}Ga]FAPI-RGD than [^{18}F]FDG. Therefore, further investigations into [^{68}Ga]FAPI-RGD are warranted to evaluate its uptake in different cancer types in the future.

The dual-targeting approach is gaining more interest in cancer imaging and treatment. FAP/$\alpha_v\beta_3$ and FAP/PSMA show higher binding affinity and tumor uptake compared to FAPI monomers. Different chemical linkers are used to create dual-targeting molecules through "clicking" or other reactions. By labeling with radionuclides, heterodimeric radiotracers hold promise for precise tumor diagnosis and therapy.

3.6. *Alternative FAPI structures*

In addition to the above FAPIs, which are characterized by a classical structure in which the FAP-targeting moiety is tethered to the chelator *via* a linker, alternative chemical structures have demonstrated inhibitory activity against FAP. In chronological progression, these compounds have been introduced, offering various avenues for FAP-targeted imaging and therapy.

In 2015, Meletta et al.[260] synthesized MIP-1232, a boronic acid-based FAPI, which was subsequently radiolabeled with ^{125}I to yield [^{125}I]MIP-1232 (**61**, Fig. 9) with a radiochemical purity of more than 90% and the tracer was evaluated for potential use in plaque imaging. Evaluation through *in vitro* autoradiography in mouse xenograft models revealed slightly higher radioactivity signals within vulnerable plaques compared with those of stable plaques. This nuanced difference arises from the higher binding affinity of radioactive tracers in atherosclerotic plaques than in normal arteries. However, meticulous correction for tissue sample size demonstrated no significant variance in the mean specific binding between different plaques or between plaques and normal arteries. Therefore, targeting FAP with [^{125}I]MIP-1232 demonstrated a limited correlation with atherosclerosis imaging. Autoradiography of xenograft tissue revealed that, compared with NCI-H69 xenografts with low FAP levels, FAP + SK-Mel-187 xenografts exhibited a notably distinct radioactive signal. The saturability of [^{125}I]MIP-1232 binding upon excess MIP-1232 confirmed its target specificity, suggesting its potential utility in FAP imaging.

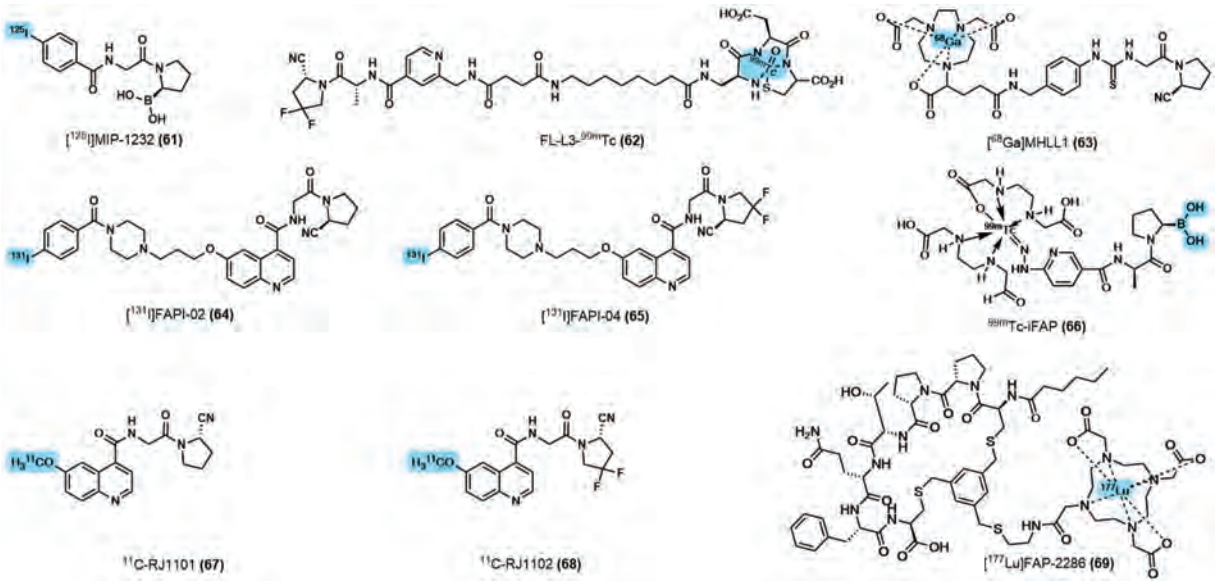

Figure 9 Alternative FAPI structures (blue: unique structures with boronic acid or ^{11}C/^{131}I/^{99m}Tc labeled FAPIs).

Table 4 Alternative structures of FAPIs. Boronic acid-based FAPIs, ^{11}C- and ^{131}I-labeled FAPIs, and cyclic peptide-based FAPIs are illustrated. In addition, we summarize their unique structural features and applications.

Agent	Radionuclide	Structural feature	Application
[^{125}I]MIP-1232	^{125}I	Boronic acid-based FAPIs	Atherosclerosis imaging
[^{99m}Tc]iFAP	^{99m}Tc	Boronic acid-based FAPIs	Tumor imaging
[^{99m}Tc]-FL-L3	^{99m}Tc	FL-containing for ^{99m}Tc labeling	Tumor imaging
[^{131}I]FAPI-02	^{131}I	Aromatic ring modified FAPIs for ^{131}I labeling	Tumor imaging and therapy
[^{131}I]FAPI-04	^{131}I	Aromatic ring modified FAPIs for ^{131}I labeling	Tumor imaging and therapy
[^{11}C]RJ1101	^{11}C	Quinoline-modified FAPIs for ^{11}C labeling	Tumor imaging
[^{11}C]RJ1102	^{11}C	Quinoline-modified FAPIs for ^{131}I labeling	Tumor imaging
[^{68}Ga]/[^{177}Lu]FAP-2286	^{68}Ga/^{177}Lu	Cyclic peptide conjugated DOTA	Tumor imaging and therapy
[^{68}Ga]MHLL1	^{68}Ga	Small molecule conjugated NOTA	Imaging the MI area

In 2020, Roy et al.[71] synthesized [^{99m}Tc]-FL-L3 (**62**, Fig. 9), a FAP-targeting radioactive conjugate formed by conjugating the FL with the chelator ^{99m}Tc. *In vitro* assessments confirmed the robust specific affinity of this conjugate for FAP-transduced HEK293 cells. Tumor uptake (2.23 %ID/g) was observed in MDA-MB231 mice injected with the tracer. Importantly, the high kidney uptake remained unaffected by the co-administration of unlabeled FL, demonstrating renal excretion of the tracer *in vivo*.

The expanding utility of FAP-targeted radiotracers extends beyond oncology and has permeated fields such as cardiology[261−264]. A preliminary study revealed pronounced FAP expression in focal zones *via* targeted imaging of mice with myocardial infarction (MI)[82]. To dynamically monitor fibrosis after MI in mice noninvasively, Langer et al.[72] obtained a novel FAP-targeted radiotracer [^{68}Ga]MHLL1 (**63**, Fig. 9) by one-step chemical synthesis in 2021. Owing to its stability and specific binding to FAP, the tracer's *in vivo* PET imaging in mice revealed favorable properties, including low blood pool retention and efficient renal clearance. Subsequent PET imaging of [^{68}Ga]MHLL1 in mouse models of MI revealed that the tracer specific bind to FAP in the infarct and peri-infarct areas, as well as in remote non-infarct areas after MI. This tracer holds promise for noninvasively characterizing early FAP after MI.

While therapeutic isotopes such as ^{90}Y, ^{177}Lu, and ^{225}Ac boast extended physical half-lives, these durations may not align with the FAPI ligands in tumors[265−269]. In contrast, radioisotopes with shorter half-lives, exemplified by ^{188}Re, ^{211}At, and ^{213}Bi, could deliver higher radiation doses to tumors for enhanced therapeutic efficacy[269−273]. Among them, ^{211}At stands out owing to its suitable half-life ($T_{1/2}$ = 7.21 h), high linear energy transfer, and limited radiation range, rendering it an optimal choice for FAPI ligands[274−280]. However, the scarcity of ^{211}At presents challenges for radiochemical investigations. Fortunately, iodine, which shares several properties with astatine, offers a viable alternative[281−284]. Radionuclides of iodine, specifically ^{125}I and ^{131}I, are readily accessible. Therefore, the use of iodine to conduct radiochemical studies based on FAPI derivatives is a favorable option. Ma et al.[73] synthesized FAPI precursors for ^{211}At and ^{131}I labeling, resulting in two radioactive tracers, [^{131}I]FAPI-02, and [^{131}I]FAPI-04 (**64** and **65**, Fig. 9). Both tracers exhibited radiochemical purities exceeding 99%, with [^{131}I]FAPI-02 displaying superior stability in serum and saline *in vitro*. Among the two tracers, [^{131}I]FAPI-04 outperformed [^{131}I]FAPI-02 in terms of FAP binding affinity, cellular internalization, and retention time. SPECT imaging analysis conducted in U87MG xenograft mice revealed that both tracers primarily underwent hepatobiliary and renal clearance. However, [^{131}I]FAPI-04 displayed heightened tumor accumulation and prolonged retention, yielding favorable tumor-to-organ ratios. This enhancement stemmed from the protracted circulation time and elevated affinity of [^{131}I]FAPI-04. In terms of antitumor effects, mice treated with this tracer exhibited suppressed tumor growth and prolonged median survival compared with those in the saline and Na^{131}I groups. Notably, no signs of metabolic toxicity were observed**.** Given the structural similarities between iodine and astatine, further exploration of their application in cancer therapy appears promising.

SPECT is used more frequently than PET, and ^{99m}Tc is the most commonly used SPECT detection radionuclide clinically. Nevertheless, the use of ^{99m}Tc is infrequent in radiolabeling FAPIs, and radiopharmaceuticals tailored explicitly for targeted imaging with boroPro derivatives are largely absent[285−288]. To address this gap, Trujilo-Benitez et al.[74] developed a novel FAPI radiopharmaceutical, [^{99m}Tc]iFAP (**66**, Fig. 9), for SPECT imaging in 2022. The radiopharmaceutical exhibited a radiochemical purity exceeding 98% when radiolabeled with ^{99m}Tc. *In vitro* experiments underscored its high stability and specificity for FAP. Subsequent SPECT/CT imaging in tumor-bearing mice revealed significantly elevated tumor uptake at 30 min post-injection, with continued tumor retention observed at 24 h. Notably, the radiopharmaceutical displayed no uptake in the left thigh, where inflammation had been induced, further highlighting its specificity. Interestingly, while the presence of the 4-position nitrogen atom in pyridine is recognized as critical for FAP specificity[36], the substitution of pyridine 4-carboxyl with 6-hydrazinylnicotinic acid

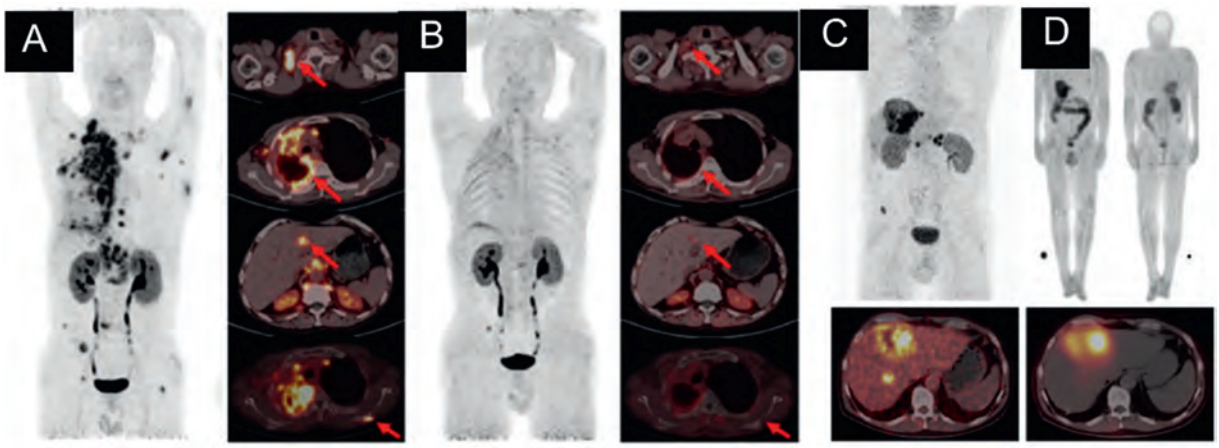

Figure 10 Therapeutic comparison of ^{177}Lu-FAP2286. (A) A patient with squamous cell carcinoma of the right lung. Maximum intensity projection (MIP) (left) and axial PET/CT images of [^{68}Ga]FAP-2286 PET/CT in a patient before treatment. Reprinted with the permission from Ref. 295. Copyright © 2022 Springer Nature. (B) MIP (left) and axial PET/CT images of [^{68}Ga]FAP-2286 PET/CT after nine weeks of treatment with [^{177}Lu]FAP-2286. Reprinted with the permission from Ref. 295. Copyright © 2022 Springer Nature. (C) PET images and a transverse PET/CT image captured with [^{68}Ga]FAP-2286 before treatment for the patients who participated in the study conducted by Professor Richard P. Baum. Reprinted with the permission from Ref. 296. Copyright © 2022 SNMMI. (D) Anterior and posterior views and transverse SPECT/CT images at 48 h after [^{177}Lu]FAP-2286 injection. Reprinted with the permission from Ref. 296. Copyright © 2022 SNMMI.

Table 5 Summary of the dosimetry evaluation of FAPIs in 26 organs of patients. Data are presented as the means followed by SDs for patients by OLINDA/EXM analysis, including [^{68}Ga]FAPI-02[76], [^{68}Ga]FAPI-04[76], [^{68}Ga]FAPI-46[48], [^{68}Ga]DOTA.SA.FAPi[48], [Al^{18}F]FAPI-74[54], [^{68}Ga]FAPI-74[54], [^{68}Ga]FAPI-RGD[70], [^{68}Ga]DOTA-2P(FAPI)$_2$[64], [^{177}Lu]DOTA.SA.FAPi[228], and [^{177}Lu]DOTAGA.(SA.FAPi)$_2$[229], which have been reported previously. This table highlights the uptake values of various radiolabeled FAPIs in different organs.

Mean absorbed dose	[^{68}Ga]FAPI-02 (mSv/MBq)	[^{68}Ga]FAPI-04 (mSv/MBq)	[^{68}Ga]FAPI-46 (mSv/MBq)	[^{68}Ga]DOTA.SA.FAPi (mSv/MBq)	[Al^{18}F]FAPI-74 mSv/100 MBq ± SD (n = 10)	[^{68}Ga]FAPI-74 mSv/100 MBq (n = 1)	[^{68}Ga]FAPI-RGD (mSv/MBq)	[^{68}Ga]DOTA-2P(FAPI)$_2$ (mSv/MBq)	[^{177}Lu]DOTA.SA.FAPi (Gy/GBq)	[^{177}Lu]DOTAGA.(SA.FAPi)$_2$ (Gy/GBq)
Adrenals	1.23E-02	1.12E-02	5.60E-03	7.77E-03	1.15 ± 0.09	1.29	1.04E-02	7.98E-05	7.79E-03	1.27E-02
Brain	9.54E-03	9.11E-03	4.59E-03	5.06E-03	0.78 ± 0.09	1.05	3.38E-03	3.16E-05	2.06E-05	1.17E-04
Breasts	9.58E-03	8.88E-03	4.55E-03	5.48E-03	0.78 ± 0.07	1.04	–	6.36E-05	4.39E-04	6.39E-04
Gallbladder wall	1.19E-02	1.13E-02	5.62E-03	8.37E-03	1.17 ± 0.10	1.33	8.35E-03	–	6.06E-03	7.95E-01
Lower large intestine wall	1.23E-02	1.17E-02	5.72E-03	6.41E-03	1.23 ± 0.16	1.31	–	–	–	–
Small intestine	1.19E-02	1.13E-02	5.48E-03	6.26E-03	1.16 ± 0.12	1.29	8.16E-03	5.18E-05	2.71E-03	9.24E-03
Stomach wall	1.13E-02	1.06E-02	5.32E-03	6.93E-03	1.06 ± 0.10	1.24	–	–	2.03E-03	6.62E-03
Upper large intestine wall	1.17E-02	1.11E-02	5.47E-03	6.65E-03	1.13 ± 0.11	1.27	–	–	–	–
Heart wall	4.73E-02	2.02E-02	1.11E-02	3.16E-02	2.29 ± 0.28	3.4	2.04E-02	–	1.40E-03	2.57E-03
Kidneys	4.45E-02	4.43E-02	1.60E-02	2.62E-02	2.94 ± 0.79	3.51	3.24E-02	1.01E-04	6.18E-01	3.74E-01
Liver	1.51E-02	1.46E-02	1.01E-02	3.84E-02	1.50 ± 0.36	1.33	1.45E-02	1.65E-03	1.15E-01	2.09E-01
Lungs	1.09E-02	9.89E-03	5.02E-03	6.62E-03	0.96 ± 0.07	1.16	2.33E-02	1.36E-03	6.10E-02	2.21E-03
Muscle	1.04E-02	9.91E-03	4.96E-03	5.79E-03	0.94 ± 0.10	1.14	–	4.19E-05	–	–
Ovaries	1.24E-02	1.19E-02	5.76E-03	6.48E-03	1.25 ± 0.16	1.33	–	5.94E-04	9.08E-04	2.23E-03
Pancreas	1.23E-02	1.13E-02	5.69E-03	5.46E-02	1.18 ± 0.10	1.32	3.06E-02	7.61E-04	3.69E-03	6.51E-01
Red marrow	3.28E-02	2.08E-02	7.08E-03	4.80E-03	1.12 ± 0.11	1.11	1.45E-02	1.12E-03	9.84E-04	1.73E-02
Osteogenic cells	2.94E-02	2.16E-02	9.38E-03	8.66E-03	1.53 ± 0.14	1.7	1.07E-02	6.47E-05	1.18E-03	8.57E-03
Skin	9.01E-03	8.63E-03	4.41E-03	4.96E-03	0.73 ± 0.08	1	–	–	–	–
Spleen	2.62E-02	1.05E-02	6.96E-03	2.68E-02	1.67 ± 0.44	1.19	2.25E-02	1.58E-04	3.99E-03	6.36E-03
Testes	1.04E-02	1.01E-02	4.88E-03	–	0.99 ± 0.13	1.16	7.13E-03	–	–	1.71E-04
Thymus	1.15E-02	1.01E-02	5.10E-03	6.56E-03	1.02 ± 0.09	1.21	7.41E-03	9.64E-06	1.22E-03	1.00E-03
Thyroid	1.03E-02	9.82E-03	4.84E-03	5.34E-03	0.91 ± 0.09	1.13	3.31E-02	3.11E-03	4.53E-04	3.98E-04
Urinary bladder wall	8.89E-02	9.91E-02	4.83E-02	5.21E-02	7.58 ± 2.84	9.86	2.26E-01	1.04E-03	4.05E-04	1.28E-03
Uterus	1.33E-02	1.30E-02	9.54E-03	6.98E-03	1.49 ± 0.25	1.46	–	1.27E-05	7.84E-04	2.18E-03
Total body	1.19E-02	1.09E-02	5.82E-03	7.05E-03	0.97 ± 0.09	1.29	8.92E-03	–	1.10E-02	2.33E-02
Effective dose (mSv/MBq)	1.80E-02	1.64E-02	7.80E-03	1.11E-02	1.41 ± 0.22	1.05	–	–	–	–

Table 6 Clinical trials of FAPI-based radiopharmaceuticals. This table highlights the clinical studies conducted on radiolabeled FAPIs. Our investigation shows that FAPI-04 and FAPI-46 are the most extensively researched radiopharmaceuticals targeting FAP. Names or registration numbers are retrieved from www.clinicaltrials.gov.

Radiopharmaceutical	Identifier	Phase	Tumor	Purpose	Status
[^{68}Ga]FAPI-04	NCT05003427	Early phase 1	Oral carcinoma	PET/CT	Recruiting
[^{68}Ga]FAPI-04	NCT04533828	Early phase 1	Liver fibrosis	PET/CT	Recruiting
[^{68}Ga]FAPI-04	NCT04831034	Early phase 1	Various fibrotic disease	PET/CT	Recruiting
[^{68}Ga]FAPI-04	NCT05275699	Phase 1	Keloid	PET/CT	Recruiting
[^{68}Ga]FAPI-04	NCT05121779	Phase 1	Pulmonary fibrosis	PET/CT	Not yet recruiting
[^{68}Ga]FAPI-04	NCT04504110	Phase 2	Epithelial ovarian cancer	PET/CT	Unknown
[^{68}Ga]FAPI-04	NCT04441606	Not applicable	Different types of cancer	PET/CT	Unknown
[^{68}Ga]FAPI-04	NCT05140746	Not applicable	Gastric cancer	PET/CT	Recruiting
[^{68}Ga]FAPI-04	NCT05275985	Not applicable	Pancreatic ductal carcinoma	PET/CT	Recruiting
[^{68}Ga]FAPI-04	NCT05264688	Not applicable	Hepatobiliary diseases	PET/CT	Recruiting
[^{68}Ga]FAPI-04	NCT05262647	Not applicable	Liver fibrosis	PET/CT	Recruiting
[^{68}Ga]FAPI-46	NCT05365802	Early phase 1	Lung fibrosis	PET/CT	Recruiting
[^{68}Ga]FAPI-46	NCT04147494	Early phase 1	Non-prostate cancers	PET/CT	Recruiting
[^{68}Ga]FAPI-46	NCT04457258	Early phase 1	Sarcoma	PET/CT	Recruiting
[^{68}Ga]FAPI-46	NCT04457232	Phase 1	Prostate cancer	PET/CT	Recruiting
[^{68}Ga]FAPI-46	NCT04459273	Phase 1	Various cancers	PET/CT	Recruiting
[^{68}Ga]FAPI-46	NCT05172310	Phase 1	Solid tumors	PET/CT	Recruiting
[^{68}Ga]FAPI-46	NCT05262855	Phase 2	Pancreatic ductal carcinoma	PET/CT	Recruiting
[^{68}Ga]FAPI-46	NCT05160051	Phase 2	Solid tumors	PET/CT	Recruiting
[^{68}Ga]FAPI-46	NCT05518903	Phase 2	Localized pancreatic ductal adenocarcinoma	PET/CT	Not yet recruiting
[^{68}Ga]FAPI-46	NCT05339113	Not applicable	Breast carcinoma	PET/CT	Recruiting
[^{68}Ga]FAPI-46	NCT05263700	Not applicable	Cancer of unknown primary site	PET/CT	Not yet recruiting
[^{18}F]FAPI-74	NCT05442151	Not applicable	Neoplasms	PET/CT	Recruiting
[^{18}F]FAPI-74	NCT05209750	Not applicable	Colorectal cancer	PET/CT	Recruiting
[^{68}Ga]DOTA-FAPI-04	NCT04499365	Early phase 1	Various types of cancer	PET/CT	Recruiting
[^{68}Ga]DOTA-FAPI-04	NCT04416165	Not applicable	Various types of cancer	PET/CT	Unknown
[^{68}Ga]NOTA-FAPI-04/[^{18}F]NOTA-FAPI-04	NCT04367948	Not applicable	Lymphoma	PET/CT	Not yet recruiting
[^{68}Ga]DOTA-FAPI-04	NCT04750772	Not applicable	Colorectal cancer	PET/CT	Recruiting
[^{68}Ga]DOTA-FAPI-46	NCT04941872	Not applicable	Various types of cancer	PET/CT	Recruiting
[^{68}Ga]DOTA-2P(FAPI)$_2$					
[^{18}F]AlF-NOTA-FAPI-04	NCT05574920	Not applicable	Breast cancer	PET/CT	Recruiting
[^{68}Ga]FAPI-RGD	NCT05543317	Not applicable	Various types of cancer	PET/CT	Recruiting
[^{68}Ga]FAP-CHX	NCT05506566	Phase 1 Phase 2	Various cancers	PET/CT	Recruiting
[^{68}Ga]FAPI-RGD	NCT05515783	Phase 1/2	Tumor	PET/CT	Recruiting
[^{68}Ga]NOTA-FAPI-04/[^{18}F]NOTA-FAPI-04	NCT05004961	Not applicable	Lymphoma	PET/CT	Recruiting
[^{177}Lu]EB-FAPI	NCT05400967	Early phase 1	Metastatic tumors	Treatment	Recruiting
[^{68}Ga]DOTA-FAPI/[^{177}Lu]DOTA-FAPI	NCT04849247	Phase 1	Locally advanced or metastatic cancer	Treatment	Recruiting
[^{177}Lu]DOTA-EB-FAPI	NCT05410821	Phase 2	Radioactive iodine refractory thyroid cancer	Treatment	Recruiting

showcased tumor selectivity in the case of [^{99m}Tc]iFAP. The hydrazine group within 6-hidrazinylnicotinic acid may influence the molecular orientation and offer additional van der Waals-type interactions and hydrogen bonding of iFAP when coupled with the FAP active center.

While ^{68}Ga, ^{64}Cu, and ^{18}F-labeled FAPIs have been successful in PET imaging of various tumors[54,78,80], harnessing ^{11}C, a commonly used radionuclide in the clinic, has remained unexplored. The short half-life of ^{11}C (20 min) could significantly reduce patients' waiting time for PET examinations[289–294]. Wang et al.[75] synthesized [^{11}C]RJ1101 and [^{11}C]RJ1102 (**67** and **68**, Fig. 9) by coupling two phenolic hydroxyl precursors (quinoline amide core and 2-cyanopyrrolide) with [^{11}C]CH_3I to broaden the spectrum of FAP-targeted tracers. PET imaging of U87MG tumor-bearing mice showed that the tracers exhibited specialized tumor uptake, akin to the tumor accumulation exhibited by [^{68}Ga]DOTA-FAPI-04. Notably, compared with [^{11}C]RJ1102, [^{11}C]RJ1101 featured a rapid metabolism rate from the hepatic, intestinal, and renal. Biodistribution studies revealed predominant tracer accumulation in tumors, kidneys, and liver, accompanied by favorable tumor-to-muscle ratios, surpassing those of [^{68}Ga]DOTA-FAPI-04. Difluoride atoms present in the proline derivative residues of compound **68** enhanced lipid solubility, leading to rapid organ accumulation and slow clearance, especially in tumors. This disparity prompted an evaluation of brain uptake of [^{11}C]RJ1102 and [^{68}Ga]DOTA-FAPI-04 in a U87MG orthotopic xenograft

glioma model. Notably, [^{11}C]RJ1102 exhibited greater tumor uptake at 60 min. The advantageous physical imaging properties of ^{11}C, coupled with its short half-life, positioned [^{11}C]RJ1101 and [^{11}C]RJ1102 as potential candidates for clinical translation.

This section presents different structures of FAPIs for labeling various radionuclides, including ^{11}C, ^{99m}Tc, and ^{131}I (Table 4). The introduction of [^{99m}Tc]iFAP expanded FAPI-based tumor diagnosis with SPECT, which has been widely used in clinical settings. FAP-2286 (**69**, Fig. 9), a cyclic peptide-based FAP-targeting radiopharmaceutical, has shown high binding affinity, *in vivo* stability, and effective anti-tumor properties in clinical studies[295,296] (Fig. 10). With its promising potential, FAP-2286 holds great promise for both tumor diagnosis and therapy.

4. Conclusions

Recent years have witnessed an upsurge in the progress of small molecule FAPIs, resulting in the initiation of clinical investigations of numerous inhibitors. A pivotal milestone was reached in 2014 when Jansen et al.[15] introduced the 4-quinolinoyl-Gly-2-cyanoPro scaffold (UAMC-1110), which has served as a foundation for diverse FAPIs. For FAPIs with different linkers conjugated with quinoline, FAPI-04 and FAPI-46, which maintain the active binding core structural motif (quinoline-Val-Pro) and a difluorine group, are successfully radiolabeled with imaging or therapeutic radionuclides. They are closely related in chemical structure, and are widely investigated in preclinical studies. Numerous studies have reported the uptake of different FAPIs in normal organs to investigate the safety of these radiopharmaceuticals[47]. The distribution of represented FAPIs in various organs and tissues are shown in Table 5[48,54,64,70,76,229]. To increase *in vivo* stability of Ga-68 labeled FAPIs, DATA^{5m}.SA.FAPi and AAZTA^{5}.SA.FAPi with novel chelators were synthesized. To improve tumor uptake, three strategies are mainly introduced, including albumin-binding, multimerization and heterodimerization. IPBA and EB are covalently coupled with the quinoline-Val-Pro motif through chemical reactions, and EB modified FAPIs have been proven effective in tumor therapy in the clinic. FAPI-multimers and heterodimers (FAPI/PSMA or FAPI/RGD) are effective methods for more accurate cancer diagnosis and reduced the rate of off-target effects. By modifying the structure of the core motif, FAP-based radiopharmaceuticals have been developed for many years and we collect clinical trials of various FAPIs in Table 6. Compared with [^{18}F]FDG, FAPIs demonstrate equivalent or superior selectivity in primary and/or metastatic tumors, especially in liver tumors, breast cancer, nasopharyngeal carcinoma, and gastrointestinal tumors. Moreover, FAPIs exhibit minimal uptake in normal brain tissues, rendering them invaluable for detecting brain pathologies. In addition, FAPIs also display notable uptake in other diseases, such as MI, RA, and atherosclerosis. Importantly, FAPIs exhibit promise in visualizing rare cancer types. The multimeric structure and albumin binding of FAPIs endow them with prolonged tumor retention and enhanced uptake, potentially positioning them as superior therapeutic agents compared with their monomeric counterparts.

Acknowledgments

This study was supported by the National Natural Science Foundation of China (No. 82372002), the Nonprofit Central Research Institute Fund of the Chinese Academy of Medical Sciences (No. 2022-RC350-04), the CAMS Innovation Fund for Medical Sciences (Nos. 2024-12M-ZH-009, 2023-I2M-2-006, 2023-I2M-QJ-010, 2021-I2M-1-026, and 2021-I2M-3-001, China), and the Beijing Nova Program and Beijing Nova Program Interdisciplinary Cooperation Project to K. H.. This work was also supported by the Beijing Natural Science Foundation (Nos. L234044, L248087, L246051 and 7252206, China), the Fundamental Research Funds for the Central Universities (Nos. 3332023044, 3332023151, China), the China Postdoctoral Science Foundation (No. 2025M773592), the China National Nuclear Corporation Young Talent Program, the special project of "Technological Innovation" project of CNNC Medical Industry Co. Ltd (ZHYLYB2021005), and Medical + X Innovation Team of the Discipline Construction Enhancement Project, the Second Affiliated Hospital of Soochow University (XKTJ-TD202410).

Author contributions

Yuxuan Wu: Formal analysis, Writing − original draft, Data curation, Writing − review & editing, Methodology. Xingkai Wang: Writing − review & editing, Investigation, Writing − original draft, Formal analysis, Methodology, Data curation. Xiaona Sun: Formal analysis, Writing − review & editing, Methodology, Writing − original draft, Data curation. Xin Gao: Data curation, Formal analysis, Writing − review & editing. Siqi Zhang: Supervision, Resources, Data curation. Jieting Shen: Validation, Data curation. Hao Tian: Data curation, Methodology. Xueyao Chen: Writing − review & editing, Methodology. Hongyi Huang: Visualization, Investigation. Shuo Jiang: Investigation. Boyang Zhang: Validation, Formal analysis. Yingzi Zhang: Validation, Software. Minzi Lu: Writing − review & editing. Hailong Zhang: Data curation. Zhicheng Sun: Resources. Ruping Liu: Funding acquisition, Writing − review & editing, Supervision. Hong Zhang: Writing − review & editing, Methodology, Supervision. Ming-Rong Zhang: Writing − review & editing, Conceptualization, Funding acquisition. Kuan Hu: Project administration, Funding acquisition, Conceptualization, Visualization, Resources, Investigation, Formal analysis, Validation, Methodology, Writing − original draft, Software, Data curation, Writing − review & editing, Supervision. Rui Wang: Writing − review & editing, Conceptualization, Supervision, Funding acquisition.

Conflicts of interest

The authors declare no conflicts of interest.

References

1. Nakakura EK. Progress in the march to precision cancer medicine: left, right, left. *JAMA Surg* 2018;**153**:67−8.
2. Anderson NM, Simon MC. The tumor microenvironment. *Curr Biol* 2020;**30**:R921−5.
3. Motofei IG. Biology of cancer; from cellular and molecular mechanisms to developmental processes and adaptation. *Semin Cancer Biol* 2022;**86**:600−15.
4. Poste G, Fidler IJ. The pathogenesis of cancer metastasis. *Nature* 1980;**283**:139−46.
5. Fidler IJ, Poste G. The "seed and soil" hypothesis revisited. *Lancet Oncol* 2008;**9**:808.
6. Hanahan D, Weinberg RA. Hallmarks of cancer: the next generation. *Cell* 2011;**144**:646−74.

7. Katheder NS, Rusten TE. Microenvironment and tumors—a nurturing relationship. *Autophagy* 2017;**13**:1241−3.
8. Mori Y, Dendl K, Cardinale J, Kratochwil C, Giesel FL, Haberkorn U. FAPI PET: fibroblast activation protein inhibitor use in oncologic and nononcologic disease. *Radiology* 2023;**306**:e220749.
9. Brennen WN, Isaacs JT, Denmeade SR. Rationale behind targeting fibroblast activation protein−expressing carcinoma-associated fibroblasts as a novel chemotherapeutic strategy. *Mol Cancer Therapeut* 2012;**11**:257−66.
10. Loktev A, Lindner T, Burger EM, Altmann A, Giesel F, Kratochwil C, et al. Development of fibroblast activation protein-targeted radiotracers with improved tumor retention. *J Nucl Med* 2019;**60**:1421−9.
11. Sun X, Wu Y, Wang X, Gao X, Zhang S, Sun Z, et al. Beyond small molecules: antibodies and peptides for fibroblast activation protein targeting radiopharmaceuticals. *Pharmaceutics* 2024;**16**:345.
12. Levy MT, McCaughan GW, Abbott CA, Park JE, Cunningham AM, Muller E, et al. Fibroblast activation protein: a cell surface dipeptidyl peptidase and gelatinase expressed by stellate cells at the tissue remodelling interface in human cirrhosis. *Hepatology* 1999;**29**:1768−78.
13. Park JE, Lenter MC, Zimmermann RN, Garin-Chesa P, Old LJ, Rettig WJ. Fibroblast activation protein, a dual specificity serine protease expressed in reactive human tumor stromal fibroblasts. *J Biol Chem* 1999;**274**:36505−12.
14. Scanlan MJ, Raj BK, Calvo B, Garin-Chesa P, Sanz-Moncasi MP, Healey JH, et al. Molecular cloning of fibroblast activation protein α, a member of the serine protease family selectively expressed in stromal fibroblasts of epithelial cancers. *Proc Natl Acad Sci U S A* 1994;**91**:5657−61.
15. Jansen K, Heirbaut L, Verkerk R, Cheng JD, Joossens J, Cos P, et al. Extended structure-activity relationship and pharmacokinetic investigation of (4-quinolinoyl)glycyl-2-cyanopyrrolidine inhibitors of fibroblast activation protein (FAP). *J Med Chem* 2014;**57**:3053−74.
16. Zhao L, Chen J, Pang Y, Fu K, Shang Q, Wu H, et al. Fibroblast activation protein-based theranostics in cancer research: a state-of-the-art review. *Theranostics* 2022;**12**:1557−69.
17. Li M, Younis MH, Zhang Y, Cai W, Lan X. Clinical summary of fibroblast activation protein inhibitor-based radiopharmaceuticals: cancer and beyond. *Eur J Nucl Med Mol Imag* 2022;**49**:2844−68.
18. Zhao L, Kang F, Pang Y, Fang J, Sun L, Wu H, et al. Fibroblast activation protein inhibitor tracers and their preclinical, translational, and clinical status in China. *J Nucl Med* 2024;**65**:4S−11S.
19. Cui X-Y, Li Z, Kong Z, Liu Y, Meng H, Wen Z, et al. Covalent targeted radioligands potentiate radionuclide therapy. *Nature* 2024; **630**:206−13.
20. Wu F, Yang J, Liu J, Wang Y, Mu J, Zeng Q, et al. Signaling pathways in cancer-associated fibroblasts and targeted therapy for cancer. *Signal Transduct Targeted Ther* 2021;**6**:218.
21. Coutts SJ, Kelly TA, Snow RJ, Kennedy CA, Barton RW, Adams J, et al. Structure−activity relationships of boronic acid inhibitors of dipeptidyl peptidase IV. 1. Variation of the P2 position of Xaa-boroPro dipeptides. *J Med Chem* 1996;**39**:2087−94.
22. Narra K, Mullins SR, Lee H-O, Strzemkowski-Brun B, Magalong K, Christiansen VJ, et al. Phase II trial of single agent Val-boroPro (talabostat) inhibiting fibroblast activation protein in patients with metastatic colorectal cancer. *Cancer Biol Ther* 2007;**6**:1691−9.
23. Okondo MC, Johnson DC, Sridharan R, Bin Go E, Chui AJ, Wang MS, et al. DPP8 and DPP9 inhibition induces pro-caspase-1-dependent monocyte and macrophage pyroptosis. *Nat Chem Biol* 2017;**13**:46−53.
24. Metcalf D. Hematopoietic cytokines. *Blood* 2008;**111**:485−91.
25. Di Rosa F. T-lymphocyte interaction with stromal, bone and hematopoietic cells in the bone marrow. *Immunol Cell Biol* 2009;**87**: 20−9.
26. Rashid A, Dzneladze I, He R, Woolley JF, Jain MD, Minden MD. CSF1R is associated with poor overall survival in AML and mediates supportive interactions between AML and stromal cells in the AML microenvironment. *Blood* 2016;**128**:2666.
27. Adams S, Miller GT, Jesson MI, Watanabe T, Jones B, Wallner BP. PT-100, a small molecule dipeptidyl peptidase inhibitor, has potent antitumor effects and augments antibody-mediated cytotoxicity *via* a novel immune mechanism. *Cancer Res* 2004;**64**:5471−80.
28. Tran T, Quan C, Edosada CY, Mayeda M, Wiesmann C, Sutherlin D, et al. Synthesis and structure−activity relationship of *N*-acyl-Gly-, *N*-acyl-Sar- and *N*-blocked-boroPro inhibitors of FAP, DPP4, and POP. *Bioorg Med Chem Lett* 2007;**17**:1438−42.
29. Tsai TY, Yeh TK, Chen X, Hsu T, Jao YC, Huang CH, et al. Substituted 4-carboxymethylpyroglutamic acid diamides as potent and selective inhibitors of fibroblast activation protein. *J Med Chem* 2010;**53**:6572−83.
30. Ryabtsova O, Jansen K, Van Goethem S, Joossens J, Cheng JD, Lambeir AM, et al. Acylated Gly-(2-cyano)pyrrolidines as inhibitors of fibroblast activation protein (FAP) and the issue of FAP/prolyl oligopeptidase (PREP)-selectivity. *Bioorg Med Chem Lett* 2012;**22**:3412−7.
31. Van der Veken P, Haemers A, Augustyns K. Prolyl peptidases related to dipeptidyl peptidase IV: potential of specific inhibitors in drug discovery. *Curr Top Med Chem* 2007;**7**:621−35.
32. Juillerat-Jeanneret L, Tafelmeyer P, Golshayan D. Fibroblast activation protein-α in fibrogenic disorders and cancer: more than a prolyl-specific peptidase?. *Expert Opin Ther Targets* 2017;**21**:977−91.
33. Poplawski SE, Lai JH, Li Y, Jin Z, Liu Y, Wu W, et al. Identification of Selective and potent inhibitors of fibroblast activation protein and prolyl oligopeptidase. *J Med Chem* 2013;**56**:3467−77.
34. Matthias E, Elke L, Michael M, Moh T, Leo T, Herbert N, et al. 8-(3-(*R*)-Aminopiperidin-1-yl)-7-but-2-ynyl-3-methyl-1-(4-methyl-quinazolin-2-ylmethyl)-3,7-dihydropurine-2,6-dione (BI 1356), a highly potent, selective, long-acting, and orally bioavailable DPP-4 inhibitor for the treatment of type 2 diabetes. *J Med Chem* 2007;**50**:6450−3.
35. Jansen K, Heirbaut L, Cheng JD, Joossens J, Ryabtsova O, Cos P, et al. Selective inhibitors of fibroblast activation protein (FAP) with a (4-quinolinoyl)-glycyl-2-cyanopyrrolidine Scaffold. *ACS Med Chem Lett* 2013;**4**:491−6.
36. Poplawski SE, Lai JH, Li Y, Jin Z, Liu Y, Wu W, et al. Identification of selective and potent inhibitors of fibroblast activation protein and prolyl oligopeptidase. *J Med Chem* 2013;**56**:3467−77.
37. Ma J, Zhang S, Yang N, Shang J, Gao X, Chen J, et al. Discovery of a highly specific radiolabeled antibody targeting B-cell maturation antigen: applications in PET imaging of multiple myeloma. *Eur J Nucl Med Mol Imag* 2025;**52**:599−610.
38. Sgouros G, Bodei L, McDevitt MR, Nedrow JR. Radiopharmaceutical therapy in cancer: clinical advances and challenges. *Nat Rev Drug Discov* 2020;**19**:589−608.
39. Zhang J, Zhao T, Jakobsson V, Chen X. Clinical tra Radiopharmaceutical therapy in cancer: clinical advances and challenges. *Nat Rev Drug Discov* 2020;**19**:589-608nslation of radiotheranostics for precision oncology. *Nat Rev Bioeng* 2023;**1**:612−4.
40. Bodei L, Herrmann K, Schoder H, Scott AM, Lewis JS. Radiotheranostics in oncology: current challenges and emerging opportunities. *Nat Rev Clin Oncol* 2022;**19**:534−50.
41. Zhang L, Zhang S, Wu J, Wang Y, Wu Y, Sun X, et al. Linear peptide-based PET tracers for imaging PD-L1 in tumors. *Mol Pharm* 2023;**20**:4256−67.
42. Zhang L, Zhang S, Wu W, Wang X, Shen J, Wang D, et al. Development of a ^{68}Gallium-labeled D-Peptide PET Tracer for imaging programmed death-ligand 1 expression. *J Vis Exp* 2023;**192**:e65047.
43. Sun X, Zhang S, Jiang S, Shen J, Wu Y, Zhang H, et al. Combined positron emission tomography-guided modified black phosphorus nanosheet-based photothermal therapy and anti programmed cell death protein ligand 1 therapy. *iRADIOLOGY* 2024;**2**:103−12.
44. Zhang S, Ma X, Wu J, Shen J, Shi Y, Wang X, et al. Enhanced radiotheranostic targeting of integrin $\alpha_v\beta_1$ with PEGylation-enabled peptide multidisplay platform (PEGibody): a strategy for prolon ged tumor retention with fast blood clearance. *Acta Pharm Sin B* 2025;**15**:692−706.
45. Loktev A, Lindner T, Mier W, Debus J, Altmann A, Jager D, et al. A Tumor-imaging method targeting cancer-associated fibroblasts. *J Nucl Med* 2018;**59**:1423−9.

46. Lindner T, Loktev A, Altmann A, Giesel F, Kratochwil C, Debus J, et al. Development of quinoline-based theranostic ligands for the targeting of fibroblast activation protein. *J Nucl Med* 2018;**59**: 1415−22.
47. Liu Y, Watabe T, Kaneda-Nakashima K, Shirakami Y, Naka S, Ooe K, et al. Fibroblast activation protein targeted therapy using [^{177}Lu]FAPI-46 compared with [^{225}Ac]FAPI-46 in a pancreatic cancer model. *Eur J Nucl Med Mol Imag* 2022;**49**:871−80.
48. Ballal S, Yadav MP, Moon ES, Kramer VS, Roesch F, Kumari S, et al. Biodistribution, pharmacokinetics, dosimetry of [^{68}Ga]Ga-DOTA.SA.FAPi, and the head-to-head comparison with [^{18}F]FDG PET/CT in patients with various cancers. *Eur J Nucl Med Mol Imag* 2021;**48**:1915−31.
49. Backhaus P, Gierse F, Burg MC, Buether F, Asmus I, Dorten P, et al. Translational imaging of the fibroblast activation protein (FAP) using the new ligand [^{68}Ga]Ga-OncoFAP-DOTAGA. *Eur J Nucl Med Mol Imag* 2022;**49**:1822−32.
50. Slania SL, Das D, Lisok A, Du Y, Jiang Z, Mease RC, et al. Imaging of fibroblast activation protein in cancer xenografts using novel (4-quinolinoyl)-glycyl-2-cyanopyrrolidine-based small molecules. *J Med Chem* 2021;**64**:4059−70.
51. Lin JJ, Chuang CP, Lin JY, Huang FT, Huang CW. Rational design, pharmacomodulation, and synthesis of [^{68}Ga]Ga-Alb-FAPtp-01, a selective tumor-associated fibroblast activation protein tracer for PET imaging of Glioma. *ACS Sens* 2021;**6**:3424−35.
52. Hu K, Li J, Wang L, Huang Y, Li L, Ye S, et al. Preclinical evaluation and pilot clinical study of [^{18}F]AlF-labeled FAPI-tracer for PET imaging of cancer associated fibroblasts. *Acta Pharm Sin B* 2022;**12**: 867−75.
53. Potemkin R, Strauch B, Kuwert T, Prante O, Maschauer S. Development of ^{18}F-fluoroglycosylated PSMA-ligands with improved renal clearance behavior. *Mol Pharm* 2020;**17**:933−43.
54. Giesel FL, Adeberg S, Syed M, Lindner T, Jimenez-Franco LD, Mavriopoulou E, et al. FAPI-74 PET/CT using either ^{18}F-AlF or cold-kit ^{68}Ga labeling: biodistribution, radiation dosimetry, and tumor delineation in lung cancer patients. *J Nucl Med* 2021;**62**:201−7.
55. Wang S, Zhou X, Xu X, Ding J, Liu S, Hou X, et al. Clinical translational evaluation of Al^{18}F-NOTA-FAPI for fibroblast activation protein-targeted tumour imaging. *Eur J Nucl Med Mol Imag* 2021;**48**:4259−71.
56. Wei Y, Zheng J, Ma L, Liu X, Xu S, Wang S, et al. [^{18}F]AlF-NOTA-FAPI-04: FAP-targeting specificity, biodistribution, and PET/CT imaging of various cancers. *Eur J Nucl Med Mol Imag* 2022;**49**:2761−73.
57. Yu Z, Jiang Z, Cheng X, Yuan L, Chen H, Ai L, et al. Development of fibroblast activation protein-α radiopharmaceuticals: recent advances and perspectives. *Eur J Med Chem* 2024;**277**:116787.
58. Kelly JM, Jeitner TM, Ponnala S, Williams C, Nikolopoulou A, DiMagno S, et al. A trifunctional theranostic ligand targeting fibroblast activation protein-α (FAPα). *Mol Imag Biol* 2021;**23**:686−96.
59. Xu M, Zhang P, Ding J, Chen J, Huo L, Liu Z. Albumin binder-conjugated fibroblast activation protein inhibitor radiopharmaceuticals for cancer therapy. *J Nucl Med* 2022;**63**:952−8.
60. Wen X, Xu P, Shi M, Liu J, Zeng X, Zhang Y, et al. Evans blue-modified radiolabeled fibroblast activation protein inhibitor as long-acting cancer therapeutics. *Theranostics* 2022;**12**:422−33.
61. Meng L, Fang J, Zhao L, Wang T, Yuan P, Zhao Z, et al. Rational design and pharmacomodulation of protein-binding theranostic radioligands for targeting the fibroblast activation protein. *J Med Chem* 2022;**65**:8245−57.
62. Ding J, Xu M, Chen J, Zhang P, Huo L, Kong Z, et al. ^{86}Y-labeled albumin-binding fibroblast activation protein inhibitor for late-time-point cancer diagnosis. *Mol Pharm* 2022;**19**:3429−38.
63. Zhang P, Xu M, Ding J, Chen J, Zhang T, Huo L, et al. Fatty acid-conjugated radiopharmaceuticals for fibroblast activation protein-targeted radiotherapy. *Eur J Nucl Med Mol Imag* 2022;**49**:1985−96.
64. Zhao L, Niu B, Fang J, Pang Y, Li S, Xie C, et al. Synthesis, preclinical evaluation, and a pilot clinical PET imaging study of ^{68}Ga-labeled FAPI dimer. *J Nucl Med* 2022;**63**:862−8.
65. Ruan Q, Feng J, Jiang Y, Zhang X, Duan X, Wang Q, et al. Preparation and bioevaluation of ^{99m}Tc-labeled FAP inhibitors as tumor radiotracers to target the fibroblast activation protein. *Mol Pharm* 2022;**19**:160−71.
66. Li H, Ye S, Li L, Zhong J, Yan Q, Zhong Y, et al. ^{18}F- or ^{177}Lu-labeled bivalent ligand of fibroblast activation protein with high tumor uptake and retention. *Eur J Nucl Med Mol Imaging* 2022;**49**:2705−15.
67. Spatz S, Tolkach Y, Jung K, Stephan C, Busch J, Ralla B, et al. Comprehensive evaluation of prostate specific membrane antigen expression in the vasculature of renal tumors: implications for imaging studies and prognostic role. *J Urol* 2018;**199**:370−7.
68. Hu K, Li L, Huang Y, Ye S, Zhong J, Yan Q, et al. Radiosynthesis and preclinical evaluation of bispecific PSMA/FAP heterodimers for tumor imaging. *Pharmaceuticals* 2022;**15**:383.
69. Boinapally S, Lisok A, Lofland G, Minn I, Yan Y, Jiang Z, et al. Hetero-bivalent agents targeting FAP and PSMA. *Eur J Nucl Med Mol Imag* 2022;**49**:4369−81.
70. Zang J, Wen X, Lin R, Zeng X, Wang C, Shi M, et al. Synthesis, preclinical evaluation and radiation dosimetry of a dual targeting PET tracer [^{68}Ga]Ga-FAPI-RGD. *Theranostics* 2022;**12**:7180−90.
71. Roy J, Hettiarachchi SU, Kaake M, Mukkamala R, Low PS. Design and validation of fibroblast activation protein alpha targeted imaging and therapeutic agents. *Theranostics* 2020;**10**:5778−89.
72. Langer LBN, Hess A, Korkmaz Z, Tillmanns J, Reffert LM, Bankstahl JP, et al. Molecular imaging of fibroblast activation protein after myocardial infarction using the novel radiotracer [^{68}Ga] MHLL1. *Theranostics* 2021;**11**:7755−66.
73. Ma H, Li F, Shen G, Cai H, Liu W, Lan T, et al. Synthesis and preliminary evaluation of I-131-labeled FAPI tracers for cancer theranostics. *Mol Pharm* 2021;**18**:4179−87.
74. Trujillo-Benitez D, Luna-Gutierrez M, Ferro-Flores G, Ocampo-Garcia B, Santos-Cuevas C, Bravo-Villegas G, et al. Design, synthesis and preclinical assessment of Tc-99m-iFAP for *in vivo* fibroblast activation protein (FAP) imaging. *Molecules* 2022;**27**: 264.
75. Wang C, Hu Z, Ding F, Zhao H, Du F, Lv C, et al. Radiosynthesis and First Preclinical Evaluation of the novel ^{11}C-labeled FAP inhibitor ^{11}C-FAPI: a comparative study of ^{11}C-FAPIs and (^{68}Ga) Ga-DOTA-FAPI-04 in a high-FAP-expression mouse model. *Front Chem* 2022; **10**:939160.
76. Giesel FL, Kratochwil C, Lindner T, Marschalek MM, Loktev A, Lehnert W, et al. ^{68}Ga-FAPI PET/CT: biodistribution and preliminary dosimetry estimate of 2 DOTA-containing FAP-targeting agents in patients with various cancers. *J Nucl Med* 2019;**60**:386−92.
77. Kratochwil C, Flechsig P, Lindner T, Abderrahim L, Altmann A, Mier W, et al. ^{68}Ga-FAPI PET/CT: tracer uptake in 28 different kinds of cancer. *J Nucl Med* 2019;**60**:801−5.
78. Chen H, Pang Y, Wu J, Zhao L, Hao B, Wu J, et al. Comparison of [^{68}Ga]Ga-DOTA-FAPI-04 and [^{18}F]FDG PET/CT for the diagnosis of primary and metastatic lesions in patients with various types of cancer. *Eur J Nucl Med Mol Imag* 2020;**47**:1820−32.
79. Ding F, Huang C, Liang C, Wang C, Liu J, Tang D. ^{68}Ga-FAPI-04 vs. [^{18}F]-FDG in a longitudinal preclinical PET imaging of metastatic breast cancer. *Eur J Nucl Med Mol Imag* 2021;**49**:290−300.
80. Watabe T, Liu Y, Kaneda-Nakashima K, Shirakami Y, Lindner T, Ooe K, et al. Theranostics targeting fibroblast activation protein in the tumor stroma: ^{64}Cu- and ^{225}Ac-labeled FAPI-04 in pancreatic cancer xenograft mouse models. *J Nucl Med* 2020;**61**:563−9.
81. Zhang H, An J, Wu P, Zhang C, Zhao Y, Tan D, et al. The application of [^{68}Ga]-Labeled FAPI-04 PET/CT for targeting and early detection of pancreatic carcinoma in patient-derived orthotopic xenograft models. *Contrast Media Mol Imaging* 2022;**2022**:6596702.
82. Varasteh Z, Mohanta S, Robu S, Braeuer M, Li YF, Omidvari N, et al. Molecular imaging of fibroblast activity after myocardial infarction using a ^{68}Ga-labeled fibroblast activation protein inhibitor, FAPI-04. *J Nucl Med* 2019;**60**:1743−9.
83. Ferdinandus J, Kessler L, Hirmas N, Trajkovic-Arsic M, Hamacher R, Umutlu L, et al. Equivalent tumor detection for early

and late FAPI-46 PET acquisition. *Eur J Nucl Med Mol Imag* 2021; **48**:3221−7.
84. Moon ES, Elvas F, Vliegen G, De Lombaerde S, Vangestel C, De Bruycker S, et al. Targeting fibroblast activation protein (FAP): next generation PET radiotracers using squaramide coupled bifunctional DOTA and DATA(5m) chelators. *EJNMMI Radiopharm Chem* 2020; **5**:1−20.
85. Storer RI, Aciro C, Jones LH. Squaramides: physical properties, synthesis and applications. *Chem Soc Rev* 2011;**40**:2330−46.
86. Wurm FR, Klok HA. Be squared: expanding the horizon of squaric acid-mediated conjugations. *Chem Soc Rev* 2013;**42**:8220−36.
87. Wurm F, Steinbach T, Klok HA. One-pot squaric acid diester mediated aqueous protein conjugation. *Chem Commun* 2013;**49**: 7815−7.
88. Ximenis M, Bustelo E, Algarra AG, Vega M, Rotger C, Basallote MG, et al. Kinetic analysis and mechanism of the hydrolytic degradation of squaramides and squaramic acids. *J Org Chem* 2017;**82**:2160−70.
89. Ding N, Zhou T, Weng W, Lin Z, Liu S, Maitarad P, et al. Multivariate synthetic strategy for improving crystallinity of zwitterionic squaraine-linked covalent organic frameworks with enhanced photothermal performance. *Small* 2022;**18**:2201275.
90. Klasen B, Moon ES, Rosch F. AAZTA(5)-squaramide ester competing with DOTA-, DTPA- and CHX-A''-DTPA-analogues: promising tool for ^{177}Lu-labeling of monoclonal antibodies under mild conditions. *Nucl Med Biol* 2021;**96**−**97**:80−93.
91. Klasen B, Lemcke D, Mindt TL, Gasser G, Rosch F. Development and *in vitro* evaluation of new bifunctional ^{89}Zr-chelators based on the 6-amino-1,4-diazepane scaffold for immuno-PET applications. *Nucl Med Biol* 2021;**102**−**103**:12−23.
92. Grus T, Lahnif H, Klasen B, Moon E-S, Greifenstein L, Roesch F. Squaric acid-based radiopharmaceuticals for tumor imaging and therapy. *Bioconjug Chem* 2021;**32**:1223−31.
93. Tietze LF, Arlt M, Beller M, Glüsenkamp KH, Jähde E, Rajewsky MF. Squaric acid diethyl ester: a new coupling reagent for the formation of drug biopolymer conjugates. synthesis of squaric acid ester amides and diamides. *Chem Ber* 1991;**124**:1215−21.
94. Greifenstein L, Engelbogen N, Lahnif H, Sinnes JP, Bergmann R, Bachmann M, et al. Synthesis, labeling and preclinical evaluation of a squaric acid containing PSMA inhibitor labeled with ^{68}Ga: a comparison with PSMA-11 and PSMA-617. *ChemMedChem* 2020; **15**:695−704.
95. Greifenstein L, Grus T, Nagel J, Sinnes JP, Rosch F. Synthesis and labeling of a squaric acid containing PSMA-inhibitor coupled to AAZTA^5 for versatile labeling with ^{44}Sc, ^{64}Cu, ^{68}Ga and ^{177}Lu. *Appl Radiat Isot* 2020;**156**:108867.
96. Millul J, Bassi G, Mock J, Elsayed A, Pellegrino C, Zana A, et al. An ultra-high-affinity small organic ligand of fibroblast activation protein for tumor-targeting applications. *Proc Natl Acad Sci U S A* 2021; **118**:e2101852118.
97. Jönsson L, Stenvall A, Mattsson E, Larsson E, Sundlöv A, Ohlsson T, et al. Quantitative analysis of phantom studies of ^{111}In and ^{68}Ga imaging of neuroendocrine tumours. *EJNMMI Physics* 2018;**5**:1−13.
98. Furukawa T, Kimura H, Sasaki M, Yamada T, Iwasawa T, Yagi Y, et al. Novel [^{111}In]In-BnDTPA-EphA2-230-1 antibody for single-photon emission computed tomography imaging tracer targeting of EphA2. *ACS Omega* 2023;**8**:7030−5.
99. Lezaic L, Erba PA, Decristoforo C, Zaletel K, Mikolajczak R, Maecke H, et al. [^{111}In]In-CP04 as a novel cholecystokinin-2 receptor ligand with theranostic potential in patients with progressive or metastatic medullary thyroid cancer: final results of a GRAN-T-MTC phase I clinical trial. *Eur J Nucl Med Mol Imag* 2023;**50**: 892−907.
100. Westerlund K, Honarvar H, Norrstrom E, Strand J, Mitran B, Orlova A, et al. Increasing the net negative charge by replacement of dota chelator with dotaga improves the biodistribution of radiolabeled second-generation synthetic affibody molecules. *Mol Pharm* 2016;**13**:1668−78.
101. Xavier ME, Liu S, Leppla SH, Cornelissen B. pre-labelling versus direct labelling of anthrax proteins for imaging of matrix metalloproteinases activity using DOTA-GA. *Nucl Med Biol* 2019;**72**−**73**: 49−54.
102. Moreau M, Raguin O, Vrigneaud JM, Collin B, Bernhard C, Tizon X, et al. DOTAGA-trastuzumab. A new antibody conjugate targeting HER2/Neu antigen for diagnostic purposes. *Bioconjug Chem* 2012; **23**:1181−8.
103. Yang X, Nimmagadda S, Steven R, Slania S, Pomper M. Imaging and radiotherapeutics agents targeting fibroblast-activating-protein-alpha (FAP-alpha). *United States patent US 2020330624A1* ·2020 Oct 22.
104. Guichard MJ, Leal T, Vanbever R. PEGylation, an approach for improving the pulmonary delivery of biopharmaceuticals. *Curr Opin Colloid Interface Sci* 2017;**31**:43−50.
105. Wu Z, Li ZB, Cai W, He L, Chin FT, Li F, et al. ^{18}F-labeled mini-PEG spacered RGD dimer (^{18}F-FPRGD2): synthesis and microPET imaging of $\alpha_v\beta_3$ integrin expression. *Eur J Nucl Med Mol Imag* 2007; **34**:1823−31.
106. Fang Y, Xue J, Gao S, Lu A, Yang D, Jiang H, et al. Cleavable PEGylation: a strategy for overcoming the “"PEG dilemma"” in efficient drug delivery. *Drug Deliv* 2017;**24**:22−32.
107. Fresacher K, Helbok A, Reiser M, Blass S, Rangger C, Mair C, et al. Comparison of PEGylated and non-PEGylated proticles: an *in vitro* and *in vivo* study. *Eur J Pharmaceut Sci* 2019;**139**:105063.
108. Yadav D, Dewangan HK. PEGYLATION: an important approach for novel drug delivery system. *J Biomater Sci Polym Ed* 2021;**32**: 266−80.
109. Turecek PL, Bossard MJ, Graninger M, Gritsch H, Höllriegl W, Kaliwoda M, et al. BAX 855, a PEGylated rFVIII product with prolonged half-life. *Hämostaseologie* 2012;**32**:29−38.
110. Veronese FM, Pasut G. PEGylation, successful approach to drug delivery. *Drug Discov Today* 2005;**10**:1451−8.
111. Li S, Chen H, Liu H, Liu L, Yuan Y, Mao C, et al. *In vivo* real-time pharmaceutical evaluations of near-infrared ii fluorescent nanomedicine bound polyethylene glycol ligands for tumor photothermal ablation. *ACS Nano* 2020;**14**:13681−90.
112. Xu M, Bi J, Liang B, Wang X, Mo R, Feng N, et al. PEGylation prolongs the half-life of equine anti-SARS-CoV-2 specific F(ab′)$_2$. *Int J Mol Sci* 2023;**24**:3387.
113. Wen X, Shi C, Yang L, Zeng X, Lin X, Huang J, et al. A radioiodinated FR-beta-targeted tracer with improved pharmacokinetics through modification with an albumin binder for imaging of macrophages in AS and NAFL. *Eur J Nucl Med Mol Imag* 2022;**49**:503−16.
114. Kuan H, Masayuki H, Xie L, Zhang Y, Kotaro N, Hisashi S, et al. Developing native peptide-based radiotracers for PD-L1 PET imaging and improving imaging contrast by pegylation. *Chem Commun* 2019;**55**:4162−5.
115. Huang S, Wu H, Li B, Fu L, Sun P, Wang M, et al. Automated radiosynthesis and preclinical evaluation of Al[^{18}F]F-NOTA-P-GnRH for PET imaging of GnRH receptor-positive tumors. *Nucl Med Biol* 2020;**82**−**83**:64−71.
116. Ahenkorah S, Murce E, Cawthorne C, Ketchemen JP, Deroose CM, Cardinaels T, et al. 3p-C-NETA: a versatile and effective chelator for development of Al^{18}F-labeled and therapeutic radiopharmaceuticals. *Theranostics* 2022;**12**:5971−85.
117. Huynh PT, Soni N, Pal R, Sarkar S, Jung JM, Lee W, et al. Direct radiofluorination of a heat-sensitive antibody by Al-^{18}F complexation. *New J Chem* 2019;**43**:15389−95.
118. Cleeren F, Lecina J, Billaud EM, Ahamed M, Verbruggen A, Bormans GM. New chelators for low temperature Al^{18}F-labeling of biomolecules. *Bioconjug Chem* 2016;**27**:790−8.
119. Liu S, Liu H, Jiang H, Xu Y, Zhang H, Cheng Z. One-step radiosynthesis of ^{18}F-AlF-NOTA-RGD$_2$ for tumor angiogenesis PET imaging. *Eur J Nucl Med Mol Imag* 2011;**38**:1732−41.

120. Penchala SC, Miller MR, Pal A, Dong J, Madadi NR, Xie J, et al. A biomimetic approach for enhancing the *in vivo* half-life of peptides. *Nat Chem Biol* 2015;**11**:793−8.
121. Huang J, Fu L, Hu K, Huang S, Han Y, Lin R, et al. Automatic production and preliminary PET imaging of a new imaging agent [^{18}F]AlF-FAPT. *Front Oncol* 2021;**11**:802676.
122. Boschi A, Martini P, Uccelli L. ^{188}Re(V) Nitrido radiopharmaceuticals for radionuclide therapy. *Pharmaceuticals* 2017;**10**:12.
123. Guo R, Xi Y, Zhang M, Miao Y, Zhang M, Li B. Human sodium iodide transporter gene-mediated imaging and therapy of mouse glioma, comparison between ^{188}Re and ^{131}I. *Oncol Lett* 2018;**15**: 3911−7.
124. Lindner T, Altmann A, Kramer S, Kleist C, Loktev A, Kratochwil C, et al. Design and development of ^{99m}Tc-labeled FAPI tracers for SPECT imaging and ^{188}Re therapy. *J Nucl Med* 2020;**61**:1507−13.
125. Toms J, Kogler J, Maschauer S, Daniel C, Schmidkonz C, Kuwert T, et al. Targeting fibroblast activation protein: radiosynthesis and preclinical evaluation of an ^{18}F-labeled FAP inhibitor. *J Nucl Med* 2020; **61**:1806−13.
126. Maschauer S, Einsiedel J, Haubner R, Hocke C, Ocker M, Hubner H, et al. Labeling and glycosylation of peptides using click chemistry: a general approach to ^{18}F-glycopeptides as effective imaging probes for positron emission tomography. *Angew Chem Int Ed* 2010;**49**:976−9.
127. Davis BG, Robinson MA. Drug delivery systems based on sugar-macromolecule conjugates. *Curr Opin Drug Discov Dev* 2002;**5**: 279−88.
128. Seemann J, Waldron B, Parker D, Roesch F. DATATOC: a novel conjugate for kit-type ^{68}Ga labelling of TOC at ambient temperature. *EJNMMI Radiopharm Chem* 2017;**1**:4.
129. Sinnes JP, Nagel J, Waldron BP, Maina T, Nock BA, Bergmann RK, et al. Instant kit preparation of ^{68}Ga-radiopharmaceuticals *via* the hybrid chelator DATA: clinical translation of [^{68}Ga]Ga-DATA-TOC. *EJNMMI Res* 2019;**9**:48.
130. Escudero-Castellanos A, Kurth J, Imlimthan S, Menendez E, Pilatis E, Moon ES, et al. Translational assessment of a DATA-functionalized FAP inhibitor with facile ^{68}Ga-labeling at room temperature. *Eur J Nucl Med Mol Imag* 2023;**50**:3202−13.
131. Kanellopoulos P, Nock BA, Greifenstein L, Baum RP, Roesch F, Maina T. [^{68}Ga]Ga-DATA^{5m}-LM$_4$, a PET radiotracer in the diagnosis of SST$_2$R-positive tumors: preclinical and first clinical results. *Int J Mol Sci* 2022;**23**:14590.
132. Spang P, Herrmann C, Roesch F. Bifunctional Gallium-68 chelators: past, present, and future. *Semin Nucl Med* 2016;**46**:373−94.
133. Yadav D, Ballal S, Yadav MP, Tripathi M, Roesch F, Bal C. Evaluation of [^{68}Ga]Ga-DATA-TOC for imaging of neuroendocrine tumours: comparison with [^{68}Ga]Ga-DOTA-NOC PET/CT. *Eur J Nucl Med Mol Imag* 2020;**47**:860−9.
134. Kreppel B, Gärtner F C. [^{68}Ga]Ga-DATA^{5m}.SA .FAPi PET/CT: specific tracer-uptake in focal nodular hyperplasia and potential role in liver tumor imaging. *Nuklearmedizin* 2020;**59**:387−9.
135. Kreppel B, Gonzalez-Carmona MA, Feldmann G, Küppers J, Moon ES, Marinova M, et al. Fibroblast activation protein inhibitor (FAPi) positive tumour fraction on PET/CT correlates with Ki-67 in liver metastases of neuroendocrine tumours. *Nuklearmedizin* 2021; **60**:344−54.
136. Rebelos E, Mari A, Oikonen V, Iida H, Nuutila P, Ferrannini E. Evaluation of renal glucose uptake with [^{18}F]FDG-PET: methodological advancements and metabolic outcomes. *Metabolism* 2023; **141**:155382.
137. Meijer TWH, de Geus-Oei LF, Visser EP, Oyen WJG, Looijen-Salamon MG, Visvikis D, et al. Tumor delineation and quantitative assessment of glucose metabolic rate within histologic subtypes of non-small cell lung cancer by using dynamic ^{18}F fluorodeoxyglucose PET. *Radiology* 2017;**283**:547−59.
138. Seban RD, Champion L, Schwartz LH, Dercle L. Spleen glucose metabolism on [^{18}F]-FDG PET/CT: a dynamic double-edged biomarker predicting outcome in cancer patients. *Eur J Nucl Med Mol Imag* 2021;**48**:2309−11.
139. Deichen JT, Prante O, Gack M, Schmiedehausen K, Kuwert T. Uptake of [^{18}F]fluorodeoxyglucose in human monocyte-macrophages *in vitro*. *Eur J Nucl med Mol imaging* 2003;**30**:267−73.
140. Greifenstein L, Kramer CS, Moon ES, Rosch F, Klega A, Landvogt C, et al. From automated synthesis to *in vivo* application in multiple types of cancer-clinical results with [^{68}Ga]Ga-DATA^{5m}.SA. FAPi. *Pharmaceuticals* 2022;**15**:1000.
141. Moon ES, Van Rymenant Y, Battan S, De Loose J, Bracke A, Van der Veken P, et al. *In vitro* evaluation of the squaramide-conjugated fibroblast activation protein inhibitor-based agents AAZTA^5.SA. FAPi and DOTA.SA.FAPi. *Molecules* 2021;**26**:3482.
142. Nagy G, Szikra D, Trencsenyi G, Fekete A, Garai I, Giani AM, et al. AAZTA: an ideal chelating agent for the development of ^{44}Sc PET imaging agents. *Angew Chem Int Ed* 2017;**56**:2118−22.
143. Waldron BP, Parker D, Burchardt C, Yufit DS, Zimny M, Roesch F. Structure and stability of hexadentate complexes of ligands based on AAZTA for efficient PET labelling with Gallium-68. *Chem Commun* 2013;**49**:579−81.
144. Sinnes JP, Nagel J, Rosch F. AAZTA^5/AAZTA^5-TOC: synthesis and radiochemical evaluation with ^{68}Ga, ^{44}Sc and ^{177}Lu. *EJNMMI Radiopharm Chem* 2019;**4**:18.
145. Nock BA, Kanellopoulos P, Moon ES, Rouchota M, Loudos G, Ballal S, et al. [^{111}In]In/[^{177}Lu]Lu-AAZTA^5-LM4 SST$_2$R-antagonists in cancer theranostics: from preclinical testing to first patient results. *Pharmaceutics* 2023;**15**:776.
146. Kumar K. The current status of the production and supply of Gallium-68. *Cancer Biother Radiopharm* 2020;**35**:163−6.
147. Olde Heuvel J, de Wit-van der Veen BJ, Vyas KN, Tuch DS, Grootendorst MR, Stokkel MPM, et al. Performance evaluation of Cerenkov luminescence imaging: a comparison of ^{68}Ga with ^{18}F. *EJNMMI Phys* 2019;**6**:17.
148. Kommidi H, Guo H, Chen N, Kim D, He B, Wu AP, et al. An [^{18}F]-positron-emitting, fluorescent, cerebrospinal fluid probe for imaging damage to the brain and spine. *Theranostics* 2017;**7**:2377−91.
149. Kobayashi R, Chen X, Werner RA, Lapa C, Javadi MS, Higuchi T. New horizons in cardiac innervation imaging: introduction of novel ^{18}F-labeled PET tracers. *Eur J Nucl Med Mol Imag* 2017;**44**: 2302−9.
150. Carter LM, Kesner AL, Pratt EC, Sanders VA, Massicano AVF, Cutler CS, et al. The impact of positron range on PET resolution, evaluated with phantoms and PHITS Monte Carlo Simulations for conventional and non-conventional radionuclides. *Mol Imag Biol* 2020;**22**:73−84.
151. Ahmed H, Haider A, Gisler L, Schibli R, Gebhard C, Ametamey SM. [^{18}F]Flurpiridaz: facile and improved precursor synthesis for this next-generation cardiac positron emission tomography imaging agent. *ChemMedChem* 2020;**15**:1040−3.
152. Hatazawa J. The clinical value of breast specific gamma imaging and positron imaging: an update. *Semin Nucl Med* 2022;**52**:619−27.
153. Chen Z, Mori W, Fu H, Schafroth MA, Hatori A, Shao T, et al. Design, synthesis, and evaluation of ^{18}F-Labeled monoacylglycerol lipase inhibitors as novel positron emission tomography probes. *J Med Chem* 2019;**62**:8866−72.
154. Chen Z, Mori W, Rong J, Schafroth MA, Shao T, Van RS, et al. Development of a highly-specific ^{18}F-labeled irreversible positron emission tomography tracer for monoacylglycerol lipase mapping. *Acta Pharm Sin B* 2021;**11**:1686−95.
155. Sahnoun S, Conen P, Mottaghy FM. The battle on time, money and precision: Da[^{18}F]id *vs*. [^{68}Ga]liath. *Eur J Nucl Med Mol Imag* 2020; **47**:2944−6.
156. Hu K, Wang L, Wu H, Huang S, Tian Y, Wang Q, et al. [^{18}F]FAPI-42 PET imaging in cancer patients: optimal acquisition time, biodistribution, and comparison with [^{68}Ga]Ga-FAPI-04. *Eur J Nucl Med Mol Imag* 2022;**49**:2833−43.
157. Banerjee SR, Pomper MG. Clinical applications of Gallium-68. *Appl Radiat Isot* 2013;**76**:2−13.
158. Hou J, Long T, He Z, Zhou M, Yang N, Chen D, et al. Evaluation of ^{18}F-AlF-NOTA-octreotide for imaging neuroendocrine neoplasms:

comparison with ^{68}Ga-DOTATATE PET/CT. *EJNMMI Res* 2021;**11**: 55.
159. Lindner T, Altmann A, Giesel F, Kratochwil C, Kleist C, Kramer S, et al. ^{18}F-labeled tracers targeting fibroblast activation protein. *EJNMMI Radiopharm Chem* 2021;**6**:26.
160. Giesel FL, Kratochwil C, Schlittenhardt J, Dendl K, Eiber M, Staudinger F, et al. Head-to-head intra-individual comparison of biodistribution and tumor uptake of ^{68}Ga-FAPI and ^{18}F-FDG PET/CT in cancer patients. *Eur J Nucl Med Mol Imag* 2021;**48**: 4377−85.
161. Dendl K, Finck R, Giesel FL, Kratochwil C, Lindner T, Mier W, et al. FAP imaging in rare cancer entities-first clinical experience in a broad spectrum of malignancies. *Eur J Nucl Med Mol Imag* 2022;**49**: 721−31.
162. Wei Y, Cheng K, Fu Z, Zheng J, Mu Z, Zhao C, et al. [^{18}F]AlF-NOTA-FAPI-04 PET/CT uptake in metastatic lesions on PET/CT imaging might distinguish different pathological types of lung cancer. *Eur J Nucl Med Mol Imag* 2022;**49**:1671−81.
163. Fan A, Wu G, Wang J, Lu L, Wang J, Wei H, et al. Inhibition of fibroblast activation protein ameliorates cartilage matrix degradation and osteoarthritis progression. *Bone Res* 2023;**11**:3−15.
164. Bauer S, Jendro MC, Wadle A, Kleber S, Stenner F, Dinser R, et al. Fibroblast activation protein is expressed by rheumatoid myofibroblast-like synoviocytes. *Arthritis Res Ther* 2006;**8**: R171−82.
165. Croft AP, Campos J, Jansen K, Turner JD, Marshall J, Attar M, et al. Distinct fibroblast subsets drive inflammation and damage in arthritis. *Nature* 2019;**570**:246−51.
166. Ge L, Fu Z, Wei Y, Shi D, Geng Y, Fan H, et al. Preclinical evaluation and pilot clinical study of [^{18}F]AlF-NOTA-FAPI-04 for PET imaging of rheumatoid arthritis. *Eur J Nucl Med Mol Imag* 2022;**49**:4025−36.
167. Kim D, Park JH, Kim TY, Kim DG, Byun JH, Kim HS. Enhanced half-life and antitumor activity of interleukin-15 through genetic fusion of a serum albumin-specific protein binder. *Int J Pharm* 2022; **625**:122059.
168. Deng S, Zeng D, Luo Y, Zhao J, Li X, Zhao Z, et al. Enhancement of cell uptake and antitumor activity of selenadiazole derivatives through interaction and delivery by serum albumin. *RSC Adv* 2017;**7**: 16721−9.
169. Brandt F, Ullrich M, Laube M, Kopka K, Bachmann M, Loser R, et al. "Clickable" albumin binders for modulating the tumor uptake of targeted radiopharmaceuticals. *J Med Chem* 2022;**65**:710−33.
170. Feng L, Fang J, Zeng X, Liu H, Zhang J, Huang L, et al. ^{68}Ga-labeled maleimide for blood pool and lymph pet imaging through covalent bonding to serum albumin *in vivo*. *ACS Omega* 2022;**7**:28597−604.
171. Kuo HT, Lin KS, Zhang Z, Uribe CF, Merkens H, Zhang C, et al. ^{177}Lu-labeled albumin-binder-conjugated PSMA-targeting agents with extremely high tumor uptake and enhanced tumor-to-kidney absorbed dose ratio. *J Nucl Med* 2021;**62**:521−7.
172. Desai N, Trieu V, Yao Z, Louie L, Ci S, Yang A, et al. Increased antitumor activity, intratumor paclitaxel concentrations, and endothelial cell transport of cremophor-free, albumin-bound paclitaxel, ABI-007, compared with cremophor-based paclitaxel. *Clin Cancer Res* 2006;**12**:1317−24.
173. Pei Q, Hu X, Zheng X, Xia R, Liu S, Xie Z, et al. Albumin-bound paclitaxel dimeric prodrug nanoparticles with tumor redox heterogeneity-triggered drug release for synergistic photothermal/chemotherapy. *Nano Res* 2019;**12**:877−87.
174. Pascual-Pasto G, Castillo-Ecija H, Unceta N, Aschero R, Resa-Pares C, Gomez-Caballero A, et al. SPARC-mediated long-term retention of nab-paclitaxel in pediatric sarcomas. *J Control Release* 2022;**342**:81−92.
175. Chen Y, Han L, Qiu X, Wang M, Chen Z, Cai Y, et al. Reassembling of albumin-bound paclitaxel mitigates myelosuppression and improves its antitumoral efficacy *via* neutrophil-mediated targeting drug delivery. *Drug Deliv* 2022;**29**:728−42.
176. Rosenberg A, Agrawal N, Gooi Z, Blair EA, Pearson AT, Juloori A, et al. 867P A phase I trial of nab-paclitaxel-based induction followed by nab-paclitaxel-based concurrent chemotherapy and re-irradiation in previously treated head and neck squamous cell carcinoma. *Ann Oncol* 2021;**32**:S790.
177. Muller C, Struthers H, Winiger C, Zhernosekov K, Schibli R. DOTA conjugate with an albumin-binding entity enables the first folic acid-targeted ^{177}Lu-radionuclide tumor therapy in mice. *J Nucl Med* 2013; **54**:124−31.
178. Farkas R, Siwowska K, Ametamey SM, Schibli R, van der Meulen NP, Muller C. ^{64}Cu- and ^{68}Ga-based PET imaging of folate receptor-positive tumors: development and evaluation of an albumin-binding NODAGA-folate. *Mol Pharm* 2016;**13**:1979−87.
179. Kelly JM, Amor-Coarasa A, Nikolopoulou A, Wustemann T, Barelli P, Kim D, et al. Dual-target binding ligands with modulated pharmacokinetics for endoradiotherapy of prostate cancer. *J Nucl Med* 2017;**58**:1442−9.
180. Benesova M, Umbricht CA, Schibli R, Muller C. Albumin-binding PSMA ligands: optimization of the tissue distribution profile. *Mol Pharm* 2018;**15**:934−46.
181. Kuo HT, Merkens H, Zhang Z, Uribe CF, Lau J, Zhang C, et al. Enhancing treatment efficacy of ^{177}Lu-PSMA-617 with the conjugation of an albumin-binding motif: preclinical dosimetry and endoradiotherapy studies. *Mol Pharm* 2018;**15**:5183−91.
182. Umbricht CA, Benesova M, Schibli R, Muller C. Preclinical development of novel PSMA-targeting radioligands: modulation of albumin-binding properties to improve prostate cancer therapy. *Mol Pharm* 2018;**15**:2297−306.
183. Liu T, Liu C, Ren Y, Guo X, Jiang J, Xie Q, et al. Development of an albumin-based PSMA probe with prolonged half-life. *Front Mol Biosci* 2020;**7**:585024.
184. Ren Y, Liu T, Liu C, Guo X, Wang F, Zhu H, et al. An albumin-binding PSMA ligand with higher tumor accumulation for PET imaging of prostate cancer. *Pharmaceuticals* 2022;**15**:513.
185. Kelly JM, Jeitner TM, Ponnala S, Williams C Jr, Nikolopoulou A, DiMagno SG, et al. A trifunctional theranostic ligand targeting fibroblast activation protein-α(FAPα). *Mol Imag Biol* 2021;**23**:686−96.
186. Wen X, Shi C, Xu D, Zhang P, Li Z, Li J, et al. Radioiodinated portable albumin binder as a versatile agent for *in vivo* imaging with single-photon emission computed tomography. *Mol Pharm* 2019;**16**: 816−24.
187. Davis RA, Hausner SH, Harris R, Sutcliffe JL. A comparison of evans blue and 4-(p-Iodophenyl)butyryl albumin binding moieties on an integrin $\alpha_v\beta_6$ binding peptide. *Pharmaceutics* 2022;**14**:745.
188. Yao L, Xue X, Yu P, Ni Y, Chen F. Evans blue dye: a revisit of its applications in biomedicine. *Contrast Media Mol Imaging* 2018; **2018**:7628037.
189. Wang Y, Lang L, Huang P, Wang Z, Jacobson O, Kiesewetter DO, et al. *In vivo* albumin labeling and lymphatic imaging. *Proc Natl Acad Sci U S A* 2015;**112**:208−13.
190. Shan L, Zhuo X, Zhang F, Dai Y, Zhu G, Yung BC, et al. A paclitaxel prodrug with bifunctional folate and albumin binding moieties for both passive and active targeted cancer therapy. *Theranostics* 2018;**8**: 2018−30.
191. Chen H, Tong X, Lang L, Jacobson O, Yung BC, Yang X, et al. Quantification of tumor vascular permeability and blood volume by positron emission tomography. *Theranostics* 2017;**7**:2363−76.
192. Wen X, Xu P, Zeng X, Liu J, Du C, Zeng X, et al. Development of [^{177}Lu]Lu-LNC1003 for radioligand therapy of prostate cancer with a moderate level of PSMA expression. *Eur J Nucl Med Mol Imag* 2023;**50**:2846−60.
193. Xu D, Lin X, Zeng X, Wen X, Li J, Li Y, et al. Radioiodinated 4-(*p*-Iodophenyl) butanoic acid-modified estradiol derivative for ER targeting SPECT imaging. *Anal Chem* 2021;**93**:13998−4006.
194. Chen H, Jacobson O, Niu G, Weiss ID, Kiesewetter DO, Liu Y, et al. Novel "Add-On" molecule based on evans blue confers superior pharmacokinetics and transforms drugs to theranostic agents. *J Nucl Med* 2017;**58**:590−7.
195. Muller C, Farkas R, Borgna F, Schmid RM, Benesova M, Schibli R. Synthesis, radiolabeling, and characterization of plasma protein-

binding ligands: potential tools for modulation of the pharmacokinetic properties of (radio)pharmaceuticals. *Bioconjug Chem* 2017;**28**: 2372−83.
196. Lau J, Jacobson O, Niu G, Lin KS, Benard F, Chen X. Bench to bedside: albumin binders for improved cancer radioligand therapies. *Bioconjug Chem* 2019;**30**:487−502.
197. Jacobson O, Kiesewetter DO, Chen X. Albumin-binding evans blue derivatives for diagnostic imaging and production of long-acting therapeutics. *Bioconjug Chem* 2016;**27**:2239−47.
198. Liu Z, Chen X. Simple Bioconjugate chemistry serves great clinical advances: albumin as a versatile platform for diagnosis and precision therapy. *Chem Soc Rev* 2016;**45**:1432−56.
199. Bandara N, Jacobson O, Mpoy C, Chen X, Rogers BE. Novel structural modification based on evans blue dye to improve pharmacokinetics of a somastostatin-receptor-based theranostic Agent. *Bioconjug Chem* 2018;**29**:2448−54.
200. Chen H, Wang G, Lang L, Jacobson O, Kiesewetter DO, Liu Y, et al. Chemical conjugation of evans blue derivative: a strategy to develop long-acting therapeutics through albumin binding. *Theranostics* 2016;**6**:243−53.
201. Suk JS, Xu Q, Kim N, Hanes J, Ensign LM. PEGylation as a strategy for improving nanoparticle-based drug and gene delivery. *Adv Drug Deliv Rev* 2016;**99**:28−51.
202. Kusznir EA, Hau JC, Portmann M, Reinhart AG, Falivene F, Bastien J, et al. Propensities of fatty acid-modified ASOs: Self-assembly *vs*. albumin binding. *Bioconjug Chem* 2023;**34**:866−79.
203. Zhu TT, Zhang Y, Luo XA, Wang SZ, Jia MQ, Chen ZX. Difference in binding of long- and medium-chain fatty acids with serum albumin: the role of macromolecular crowding effect. *J Agric Food Chem* 2018;**66**:1242−50.
204. Haeri HH, Schunk B, Tomaszewski J, Schimm H, Gelos MJ, Hinderberger D. Fatty acid binding to human serum albumin in blood serum characterized by EPR spectroscopy. *Chemistry Open* 2019;**8**: 650−6.
205. Cho J, Lim SI, Yang BS, Hahn YS, Kwon I. Generation of therapeutic protein variants with the human serum albumin binding capacity *via* site-specific fatty acid conjugation. *Sci Rep* 2017;**7**:18041.
206. Madsen K, Knudsen LB, Agersoe H, Nielsen PF, Thøgersen H, Wilken M, et al. Structure−activity and protraction relationship of long-acting glucagon-like peptide-1 derivatives: importance of fatty acid length, polarity, and bulkiness. *J Med Chem* 2007;**50**:6126−32.
207. Burchardt C, Riss PJ, Zoller F, Maschauer S, Prante O, Kuwert T, et al. [^{68}Ga]Ga-DO$_2$A-(OBu-l-tyr)$_2$: synthesis, ^{68}Ga-radiolabeling and *in vitro* studies of a novel ^{68}Ga-DO$_2$A-tyrosine conjugate as potential tumor tracer for PET. *Bioorg Med Chem Lett* 2009;**19**: 3498−501.
208. Riss PJ, Burchardt C, Roesch F. A methodical ^{68}Ga-labelling study of DO2A-(butyl-L-tyrosine)$_2$ with cation-exchanger post-processed ^{68}Ga: practical aspects of radiolabelling. *Contrast Media Mol Imaging* 2011;**6**:492−8.
209. Chauhan K, Tiwari AK, Chadha N, Kaul A, Singh AK, Datta A. Chalcone based homodimeric PET agent, ^{11}C-(Chal)2DEA-Me, for beta amyloid imaging: synthesis and bioevaluation. *Mol Pharm* 2018; **15**:1515−25.
210. Zia NA, Cullinane C, Van Zuylekom JK, Waldeck K, McInnes LE, Buncic G, et al. A bivalent inhibitor of prostate specific membrane antigen radiolabeled with Copper-64 with high tumor uptake and retention. *Angew Chem Int Ed Engl* 2019;**58**:14991−4.
211. Liu S. Radiolabeled Cyclic RGD peptides as integrin $\alpha_v\beta_3$-targeted radiotracers: maximizing binding affinity *via* bivalency. *Bioconjug Chem* 2009;**20**:2199−213.
212. Janssen M, Oyen WJ, Massuger LF, Frielink C, Dijkgraaf I, Edwards DS, et al. Comparison of a monomeric and dimeric radiolabeled RGD-peptide for tumor targeting. *Cancer Biother Radiopharm* 2004;**17**:641−6.
213. Durkan K, Jiang Z, Rold TL, Sieckman GL, Hoffman TJ, Bandari RP, et al. A heterodimeric [RGD-Glu-[^{64}Cu-NO2A]-6-Ahx-RM2] $\alpha_v\beta_3$/GRPr-targeting antagonist radiotracer for PET imaging of prostate tumors. *Nucl Med Biol* 2014;**41**:133−9.
214. Echigo H, Mishiro K, Fuchigami T, Shiba K, Kinuya S, Ogawa K. Synthesis and evaluation of a dimeric RGD peptide as a preliminary study for radiotheranostics with radiohalogens. *Molecules* 2021;**26**: 6107.
215. Liolios C, Buchmuller B, Bauder-Wust U, Schafer M, Leotta K, Haberkorn U, et al. Monomeric and Dimeric ^{68}Ga-labeled bombesin analogues for positron emission tomography (PET) imaging of tumors expressing gastrin-releasing peptide receptors (GRPrs). *J Med Chem* 2018;**61**:2062−74.
216. Abouzayed A, Yim CB, Mitran B, Rinne SS, Tolmachev V, Larhed M, et al. Synthesis and preclinical evaluation of radioiodinated GRPR/PSMA bispecific heterodimers for the theranostics application in prostate cancer. *Pharmaceutics* 2019;**11**:358.
217. Lundmark F, Abouzayed A, Mitran B, Rinne SS, Varasteh Z, Larhed M, et al. Heterodimeric radiotracer targeting PSMA and GRPR for imaging of prostate cancer-optimization of the affinity towards PSMA by linker modification in murine model. *Pharmaceutics* 2020;**12**:614.
218. Israel I, Elflein K, Schirbel A, Chen K, Samnick S. A comparison of the monomeric [^{68}Ga]NODAGA-NGR and dimeric [^{68}Ga]NOTA-(NGR)$_2$ as aminopeptidase N ligand for positron emission tomography imaging in tumor-bearing mice. *Eur J Pharmaceut Sci* 2021; **166**:105964.
219. Wu Z, Li ZB, Chen K, Cai W, He L, Chin FT, et al. microPET of tumor integrin $\alpha_v\beta_3$ expression using ^{18}F-labeled PEGylated tetrameric RGD peptide (^{18}F-FPRGD4). *J Nucl Med* 2007;**48**:1536−44.
220. Lang L, Li W, Guo N, Ma Y, Zhu L, Kiesewetter DO, et al. Comparison study of [^{18}F]FAl-NOTA-PRGD2, [^{18}F]FPPRGD2, and [^{68}Ga]Ga-NOTA-PRGD2 for PET imaging of U87MG tumors in mice. *Bioconjug Chem* 2011;**22**:2415−22.
221. Chen M, Feng X, Xu W, Wang Y, Yang Y, Jiang Z, et al. PEGylated polyurea bearing hindered urea bond for drug delivery. *Molecules* 2019;**24**:1538.
222. Li Y, Liu Q, Li W, Zhang T, Li H, Li R, et al. Design and validation of PEG-derivatized vitamin E copolymer for drug delivery into breast cancer. *Bioconjug Chem* 2016;**27**:1889−99.
223. Wieczorek S, Dallmann A, Kochovski Z, Borner HG. Advancing drug formulation additives toward precision additives with release mediating peptide interlayer. *J Am Chem Soc* 2016;**138**:9349−52.
224. Wang MQ, Zou H, Liu WB, Liu N, Wu ZQ. Bottlebrush polymers based on RAFT and the "C1" polymerization method: controlled synthesis and application in anticancer drug delivery. *ACS Macro Lett* 2022;**11**:179−85.
225. Li ZB, Cai W, Cao Q, Chen K, Wu Z, He L, et al. ^{64}Cu-labeled tetrameric and octameric RGD peptides for small-animal PET of tumor $\alpha_v\beta_3$ integrin expression. *J Nucl Med* 2007;**48**:1162−71.
226. Liu Y, Wu W, Cai C, Zhang H, Shen H, Han Y. Patient-derived xenograft models in cancer therapy: technologies and applications. *Signal Transduct Targeted Ther* 2023;**8**:160−83.
227. Zhao L, Chen J, Pang Y, Fang J, Fu K, Meng L, et al. Development of fibroblast activation protein inhibitor-based dimeric radiotracers with improved tumor retention and antitumor efficacy. *Mol Pharm* 2022; **19**:3640−51.
228. Ballal S, Yadav MP, Moon ES, Kramer VS, Roesch F, Kumari S, et al. First-in-human results on the biodistribution, pharmacokinetics, and dosimetry of [^{177}Lu]Lu-DOTA.SA.FAPi and [^{177}Lu]Lu-DOTAGA.(SA.FAPi)$_2$. *Pharmaceuticals* 2021;**14**:1212.
229. Huang Y, Li H, Ye S, Tang G, Liang Y, Hu K. Synthesis and preclinical evaluation of an Al^{18}F radiofluorinated bivalent PSMA ligand. *Eur J Med Chem* 2021;**221**:113502.
230. Kumar K. ^{18}F-AlF-Labeled biomolecule conjugates as imaging pharmaceuticals. *J Nucl Med* 2018;**59**:1208−9.
231. McBride WJ, Sharkey RM, Karacay H, D'Souza CA, Rossi EA, Laverman P, et al. A novel method of ^{18}F radiolabeling for PET. *J Nucl Med* 2009;**50**:991−8.

232. Laverman P, D'Souza CA, Eek A, McBride WJ, Sharkey RM, Oyen WJ, et al. Optimized labeling of NOTA-conjugated octreotide with F-18. *Tumour Biol* 2012;**33**:427−34.
233. Behnammanesh H, Jokar S, Erfani M, Geramifar P, Sabzevari O, Amini M, et al. Design, preparation and biological evaluation of a ^{177}Lu-labeled somatostatin receptor antagonist for targeted therapy of neuroendocrine tumors. *Bioorg Chem* 2020;**94**:103381−9.
234. Pfannkuchen N, Meckel M, Bergmann R, Bachmann M, Bal C, Sathekge M, et al. Novel radiolabeled bisphosphonates for PET diagnosis and endoradiotherapy of bone metastases. *Pharmaceuticals* 2017;**10**:45−56.
235. Banerjee SR, Kumar V, Lisok A, Chen J, Minn I, Brummet M, et al. ^{177}Lu-labeled low-molecular-weight agents for PSMA-targeted radiopharmaceutical therapy. *Eur J Nucl Med Mol Imag* 2019;**46**: 2545−57.
236. Chen J, Zhou J, Gao Z, Li X, Wang F, Duan X, et al. Multiplexed targeting of Barrett's Neoplasia with a heterobivalent ligand: imaging study on mouse xenograft *in vivo* and human specimens *ex vivo. J Med Chem* 2018;**61**:5323−31.
237. Budzinski J, Maschauer S, Kobayashi H, Couvineau P, Vogt H, Gmeiner P, et al. Bivalent ligands promote endosomal trafficking of the dopamine D3 receptor-neurotensin receptor 1 heterodimer. *Commun Biol* 2021;**4**:1062.
238. Judmann B, Braun D, Wangler B, Schirrmacher R, Fricker G, Wangler C. Current state of radiolabeled heterobivalent peptidic ligands in tumor imaging and therapy. *Pharmaceuticals* 2020;**13**:173.
239. Zhang J, Mao F, Niu G, Peng L, Lang L, Li F, et al. ^{68}Ga-BBN-RGD PET/CT for GRPR and integrin $\alpha_v\beta_3$ imaging in patients with breast cancer. *Theranostics* 2018;**8**:1121−30.
240. Rivera-Bravo B, Ramirez-Nava G, Mendoza-Figueroa MJ, Ocampo-Garcia B, Ferro-Flores G, Avila-Rodriguez MA, et al. [^{68}Ga]Ga-iPSMA-Lys^3-bombesin: biokinetics, dosimetry and first patient PET/CT imaging. *Nucl Med Biol* 2021;**96**−**97**:54−60.
241. Luo H, England CG, Goel S, Graves SA, Ai F, Liu B, et al. ImmunoPET and near-infrared fluorescence imaging of pancreatic cancer with a dual-labeled bispecific antibody fragment. *Mol Pharm* 2017; **14**:1646−55.
242. Li ZB, Wu Z, Chen K, Ryu EK, Chen X. ^{18}F-labeled BBN-RGD heterodimer for prostate cancer imaging. *J Nucl Med* 2008;**49**: 453−61.
243. Zhang J, Niu G, Lang L, Li F, Fan X, Yan X, et al. Clinical translation of a dual integrin $\alpha_v\beta_3$- and gastrin-releasing peptide receptor-targeting PET Radiotracer, ^{68}Ga-BBN-RGD. *J Nucl Med* 2017;**58**:228−34.
244. Silver DA, Pellicer I, Fair WR, Heston WD, Cordon-Cardo C. Prostate-specific membrane antigen expression in normal and malignant human tissues. *Clin Cancer Res* 1997;**3**:81−5.
245. Chang SS, Reuter VE, Heston WD, Bander NH, Grauer LS, Gaudin PB. Five different anti-prostate-specific membrane antigen (PSMA) antibodies confirm PSMA expression in tumor-associated neovasculature. *Cancer Res* 1999;**59**:3192−8.
246. Hofstetter G, Grech C, Pils D, Pammer J, Neudert B, Potsch N, et al. Prostate-specific membrane antigen (PSMA) expression in tumor-associated neovasculature is an independent prognostic marker in patients with ovarian cancer. *J Personalized Med* 2022;**12**:551.
247. Stock K, Steinestel K, Wiesch R, Mikesch JH, Hansmeier A, Trautmann M, et al. Neovascular prostate-specific membrane antigen expression is associated with improved overall survival under palliative chemotherapy in patients with pancreatic ductal adenocarcinoma. *BioMed Res Int* 2017;**2017**:2847303.
248. Abdel Maguid MS, Saad El Dine MG, Gabal SM, Abou Fandoud SM. Prostate-specific membrane antigen (PSMA) expression in the neovasculature of high grade gliomas (histopathological and immunohistochemical study). *Asian Pac J Cancer Prev APJCP* 2023;**24**:1797−808.
249. Zubal M, Vymolova B, Matrasova I, Vymola P, Veprkova J, Syrucek M, et al. Fibroblast activation protein as a potential theranostic target in brain metastases of diverse solid tumours. *Pathology* 2023;**55**:806−17.
250. Liu F, Qi L, Liu B, Liu J, Zhang H, Che D, et al. Fibroblast activation protein overexpression and clinical implications in solid tumors: a meta-analysis. *PLoS One* 2015;**10**:e0116683.
251. de Galiza Barbosa F, Queiroz MA, Nunes RF, Costa LB, Zaniboni EC, Marin JFG, et al. Nonprostatic diseases on PSMA PET imaging: a spectrum of benign and malignant findings. *Cancer Imaging* 2020;**20**:23.
252. Cai J, Yang D, Sun H, Xiao L, Han F, Zhang M, et al. A multifactorial analysis of FAP to regulate gastrointestinal cancers progression. *Front Immunol* 2023;**14**:1183440.
253. Fu H, Wu J, Huang J, Sun L, Wu H, Guo W, et al. ^{68}Ga Fibroblast Activation protein inhibitor PET/CT in the detection of metastatic thyroid cancer: comparison with ^{18}F-FDG PET/CT. *Radiology* 2022; **304**:397−405.
254. Endo H, Tagai K, Ono M, Ikoma Y, Oyama A, Matsuoka K, et al. A Machine learning−based approach to discrimination of tauopathies using [^{18}F]PM-PBB3 PET images. *Mov Disord* 2022;**37**:2236−46.
255. Kalaei Z, Manafi-Farid R, Rashidi B, Kiani FK, Zarei A, Fathi M, et al. The prognostic and therapeutic value and clinical implications of fibroblast activation protein-alpha as a novel biomarker in colorectal cancer. *Cell Commun Signal* 2023;**21**:139.
256. Hangaard L, Jochumsen MR, Vendelbo MH, Bouchelouche K. Metastases from colorectal cancer avid on ^{68}Ga-PSMA PET/CT. *Clin Nucl Med* 2017;**42**:532−3.
257. Verma P, Malhotra G, Agrawal R, Sonavane S, Meshram V, Asopa RV. Evidence of prostate-specific membrane antigen expression in metastatic differentiated thyroid cancer using ^{68}Ga-PSMA-HBED-CC PET/CT. *Clin Nucl Med* 2018;**43**:e265−8.
258. Haffner MC, Kronberger IE, Ross JS, Sheehan CE, Zitt M, Muhlmann G, et al. Prostate-specific membrane antigen expression in the neovasculature of gastric and colorectal cancers. *Hum Pathol* 2009;**40**:1754−61.
259. Liu Z, Wang F, Chen X. Integrin $\alpha_v\beta_3$-targeted cancer therapy. *Drug Dev Res* 2008;**69**:329−39.
260. Meletta R, Herde AM, Chiotellis A, Isa M, Rancic Z, Borel N, et al. Evaluation of the radiolabeled boronic acid-based FAP inhibitor MIP-1232 for atherosclerotic plaque imaging. *Molecules* 2015;**20**: 2081−99.
261. Tillmanns J, Hoffmann D, Habbaba Y, Schmitto JD, Sedding D, Fraccarollo D, et al. Fibroblast activation protein alpha expression identifies activated fibroblasts after myocardial infarction. *J Mol Cell Cardiol* 2015;**87**:194−203.
262. Diekmann J, Koenig T, Thackeray JT, Derlin T, Czerner C, Neuser J, et al. Cardiac Fibroblast activation in patients early after acute myocardial infarction: integration with MR tissue characterization and subsequent functional outcome. *J Nucl Med* 2022;**63**:1415−23.
263. Hoffmann DB, Fraccarollo D, Galuppo P, Frantz S, Bauersachs J, Tillmanns J. Genetic ablation of fibroblast activation protein alpha attenuates left ventricular dilation after myocardial infarction. *PLoS One* 2021;**16**:e0248196.
264. Diekmann J, Koenig T, Zwadlo C, Derlin T, Neuser J, Thackeray JT, et al. Molecular imaging identifies fibroblast activation beyond the infarct region after acute myocardial infarction. *J Am Coll Cardiol* 2021;**77**:1835−7.
265. Collamati F, Bellini F, Bocci V, De Lucia E, Ferri V, Fioroni F, et al. Time evolution of DOTATOC uptake in neuroendocrine tumors in view of a possible application of radioguided surgery with β-decay. *J Nucl Med* 2015;**56**:1501−6.
266. Ehlerding EB, Lacognata S, Jiang D, Ferreira CA, Goel S, Hernandez R, et al. Targeting angiogenesis for radioimmunotherapy with a ^{177}Lu-labeled antibody. *Eur J Nucl Med Mol Imag* 2018;**45**:123−31.
267. Scheinberg DA, McDevitt MR. Actinium-225 in targeted alpha-particle therapeutic applications. *Curr Rad* 2011;**4**:306−20.
268. Miederer M, Henriksen G, Alke A, Mossbrugger I, Quintanilla-Martinez L, Senekowitsch-Schmidtke R, et al. Preclinical evaluation of the α-particle generator nuclide ^{225}Ac for somatostatin receptor radiotherapy of neuroendocrine tumors. *Clin Cancer Res* 2008;**14**: 3555−61.

269. Muller C, van der Meulen NP, Benesova M, Schibli R. Therapeutic radiometals beyond ^{177}Lu and ^{90}Y: production and application of promising α-particle, β^--particle, and auger electron emitters. *J Nucl Med* 2017;**58**:91-6S.
270. Knapp FF Jr. Rhenium-188 - a generator-derived radioisotope for cancer therapy. *Cancer Biother Radiopharm* 1998;**13**:337−49.
271. Morgenstern A, Apostolidis C, Bruchertseifer F. Supply and clinical application of Actinium-225 and bismuth-213. *Semin Nucl Med* 2020;**50**:119−23.
272. Kato H, Huang X, Kadonaga Y, Katayama D, Ooe K, Shimoyama A, et al. Intratumoral administration of astatine-211-labeled gold nanoparticle for alpha therapy. *J Nanobiotechnol* 2021;**19**:223.
273. Huang X, Kaneda-Nakashima K, Kadonaga Y, Kabayama K, Shimoyama A, Ooe K, et al. Astatine-211-labeled gold nanoparticles for targeted alpha-particle therapy *via* intravenous injection. *Pharmaceutics* 2022;**14**:2705.
274. Guerard F, Gestin JF, Brechbiel MW. Production of [^{211}At]-astatinated radiopharmaceuticals and applications in targeted alpha-particle therapy. *Cancer Biother Radiopharm* 2013;**28**:1−20.
275. O'Hara MJ, Krzysko AJ, Hamlin DK, Li Y, Dorman EF, Wilbur DS. Development of an autonomous solvent extraction system to isolate astatine-211 from dissolved cyclotron bombarded bismuth targets. *Sci Rep* 2019;**9**:20318−32.
276. Qiu H, Santos EB, Storb RF, Hamlin DK, Wilbur DS, Sandmaier BM. Addition of astatine-211-labeled anti-CD45 antibody to total body irradiation (tbi) as conditioning for DLA-identical marrow transplantation: a novel strategy to overcome graft rejection in a canine presensitization model. *Blood* 2016;**128**:2152.
277. Batra V, Samanta M, Makvandi M, Groff D, Martorano P, Elias J, et al. Preclinical development of [^{211}At]meta- astatobenzylguanidine ([^{211}At]MABG) as an alpha particle radiopharmaceutical therapy for neuroblastoma. *Clin Cancer Res* 2022;**28**:4146−57.
278. Li F, Yang Y, Liao J, Liu N. Recent progress of astatine-211 in endoradiotherapy: great advances from fundamental properties to targeted radiopharmaceuticals. *Chin Chem Lett* 2022;**33**:3325−38.
279. Xie L, Zhang L, Hu K, Hanyu M, Zhang Y, Fujinaga M, et al. A ^{211}At-labelled mGluR1 inhibitor induces cancer senescence to elicit long-lasting anti-tumor efficacy. *Cell Rep Med* 2023;**4**:100960−75.
280. Shi X, Li Q, Zhang L, Hanyu M, Xie L, Hu K, et al. ^{211}At-labeled polymer nanoparticles for targeted radionuclide therapy of glucose-dependent insulinotropic polypeptide receptor (GIPR)-overexpressed cancer. *Bioconjug Chem* 2021;**32**:1763−72.
281. Ogawa K, Takeda T, Mishiro K, Toyoshima A, Shiba K, Yoshimura T, et al. Radiotheranostics coupled between an At-211-Labeled RGD peptide and the corresponding radioiodine-labeled RGD peptide. *ACS Omega* 2019;**4**:4584−91.
282. Watabe T, Kaneda-Nakashima K, Liu Y, Shirakami Y, Ooe K, Toyoshima A, et al. Enhancement of ^{211}At uptake *via* the sodium iodide symporter by the addition of ascorbic acid in targeted alpha-therapy of thyroid cancer. *J Nucl Med* 2019;**60**:1301−7.
283. Wilbur DS. Enigmatic astatine. *Nat Chem* 2013;**5**:246.
284. Andersson H, Palm S, Lindegren S, Bäck T, Jacobsson L, Leser G, et al. Comparison of the therapeutic efficacy of ^{211}At- and ^{131}I-labelled monoclonal antibody MOv18 in nude mice with intraperitoneal growth of human ovarian cancer. *Anticancer Res* 2001;**21**:409−12.
285. Gumiela M. Cyclotron production of ^{99m}Tc: comparison of known separation technologies for isolation of ^{99m}Tc from molybdenum targets. *Nucl Med Biol* 2018;**58**:33−41.
286. Duatti A. Review on ^{99m}Tc radiopharmaceuticals with emphasis on new advancements. *Nucl Med Biol* 2021;**92**:202−16.
287. Hou X, Tanguay J, Vuckovic M, Buckley K, Schaffer P, Benard F, et al. Imaging study of using radiopharmaceuticals labeled with cyclotron-produced ^{99m}Tc. *Phys Med Biol* 2016;**61**:8199−213.
288. Pillai MR, Knapp FF Jr. Overcoming the ^{99m}Tc shortage: are options being overlooked?. *J Nucl Med* 2011;**52**:15-28N.
289. Boscutti G, Huiban M, Passchier J. Use of carbon-11 labelled tool compounds in support of drug development. *Drug Discov Today Technol* 2017;**25**:3−10.
290. Allard M, Fouquet E, James D, Szlosek-Pinaud M. State of art in ^{11}C labelled radiotracers synthesis. *Curr Med Chem* 2008;**15**:235−77.
291. Goud NS, Bhattacharya A, Joshi RK, Nagaraj C, Bharath RD, Kumar P. Carbon-11: radiochemistry and target-based PET molecular imaging applications in oncology, cardiology, and neurology. *J Med Chem* 2021;**64**:1223−59.
292. Pees A, Chasse M, Lindberg A, Vasdev N. Recent developments in carbon-11 chemistry and applications for first-in-human PET studies. *Molecules* 2023;**28**:931−52.
293. Deng X, Zhang Y, Chen Z, Kumata K, Van R, Rong J, et al. Synthesis and preliminary evaluation of 4-hydroxy-6-(3-[^{11}C]methoxyphenethyl)pyridazin-3(2*H*)-one, a ^{11}C-labeled d-amino acid oxidase (DAAO) inhibitor for PET imaging. *Bioorg Med Chem Lett* 2020;**30**:127326−31.
294. Xiao Z, Sun J, Fujinaga M, Wei H, Zhao C, Haider A, et al. Radiosynthesis and preclinical evaluation of a carbon-11 labeled PDE7 inhibitor for PET neuroimaging. *bioRxiv* 2022. Available from: https://www.biorxiv.org/content/10.1101/2021.06.12.447900v2.
295. Rao Z, Zhang Y, Liu L, Wang M, Zhang C. [^{177}Lu]Lu-FAP-2286 therapy in a case of right lung squamous cell carcinoma with systemic metastases. *Eur J Nucl Med Mol Imag* 2022;**50**:1266−7.
296. Baum RP, Schuchardt C, Singh A, Chantadisai M, Robiller FC, Zhang J, et al. Feasibility, biodistribution, and preliminary dosimetry in peptide-targeted radionuclide therapy of diverse adenocarcinomas using ^{177}Lu-FAP-2286: first-in-Humans Results. *J Nucl Med* 2022;**63**:415−23.